Role of the ubiquitin-like protein Urm1 as a protein modifier

DISSERTATION DER FAKULTÄT FÜR BIOLOGIE
DER LUDWIG-MAXIMILIANS-UNIVERSITÄT MÜNCHEN

vorgelegt von
Diplom-Biologe Sean Lin

August 2017

Eidesstattliche Versicherung und Erklärung

Hiermit erkläre ich an Eides statt, dass ich die vorliegende Dissertation “Role of the ubiquitin-like protein Urm1 as a protein modifier” selbstständig und nur unter Zuhilfenahme der ausgewiesenen Hilfsmittel und der angegebenen Quellen angefertigt habe. Ich habe weder andwerweitig versucht, eine Dissertation einzureichen oder eine Doktorprüfung durchzuführen, noch habe ich diese Dissertation oder Teile derselben einer anderen Prüfungskommission vorgelegt.

München, den 19.12.17 Sean Lin

Promotionsgesuch eingereicht:	29.08.2017
Tag der mündlichen Prüfung:	13.12.2017
Erster Gutachter:	Prof. Dr. Daniel Krappmann
Zweiter Gutachter:	Prof. Dr. Angelika Böttger

Die vorliegende Arbeit wurde zwischen August 2010 und August 2017 unter der Leitung von Prof. Dr. Stefan Jentsch am Max-Planck-Institut für Biochemie in Martinsried durchgeführt.

Table of Contents

1 Summary

Conjugation of ubiquitin-like proteins (UBLs) to target proteins involves an enzymatic cascade. The best-studied member of the UBL family is ubiquitin. In addition to ubiquitin, eukaryotes possess several other UBLs such as SUMO and Rub1/Nedd8. Interestingly, a group of bacterial and archaeal sulphur carriers resemble UBLs structurally, however, these proteins do not form protein conjugates. The eukaryotic protein Urm1 is related to these bacterial sulphur carriers, but also shares functional features of eukaryotic UBLs. Urm1 can act as a sulphur carrier for the thiolation of tRNAs, but also as a protein modifier. Both reactions require the E1-like enzyme Uba4. To date, the only described Urm1 substrate in *S. cerevisiae* is the thioredoxin peroxidase Ahp1. Moreover, it has been shown that the double-glycine motif of Urm1 is required to modify Ahp1, and that Urm1 is covalently attached to a lysine residue of Ahp1. However, until now the functional role of protein urmylation remains unclear.

To gain insights into the function of Urm1 as a posttranslational protein modifier, we use tagged Urm1 to isolate Urm1-substrates and to identify them by mass spectrometry. In this study, we identified putative Urm1-substrates that are part of various cellular processes. In particular, the zinc-responsive activator protein 1 (Zap1), a master zinc regulator in *S. cerevisiae*, emerges as a novel Urm1-substrate. Not only does the transcription factor Zap1 regulate numerous genes in involved, *inter alia*, in zinc homeostasis, ROS defense, sulfate metabolism, phospholipid synthesis, but also *ZAP1* transcription itself. Additionally, Zap1 acts as a zinc sensor by binding zinc ions directly through two zinc fingers (ZFs), which are located at the transactivation domains (ADs) AD1 and AD2. Here, we demonstrate that Zap1 urmylation is restricted to the cytoplasm. Zap1 is urmylated at the lysine residue K871. Intriguingly, lack of Zap1 urmylation seems to promote rapid ubiquitin-dependent degradation, whereas Zap1 is less susceptible to degradation in presence of the urmylation machinery. As a consequence, Zap1 urmylation positively influences Zap1 transcriptional activity and its downstream target Zrt1 *in vivo*. Thus, a possible function of Zap1 urmylation could be to antagonize Zap1 ubiquitination and its subsequent ubiquitin-proteasome system (UPS)-mediated degradation.

2 Introduction

Cellular processes require intricate and multilayered cellular regulation to maintain cellular homeostasis in response to diverse intracellular or extracellular changes. Several cellular strategies such as the regulation of mRNA transcription, mRNA processing, RNA splicing and translational control are employed to induce manifold cellular alterations. Additionally, proteins can undergo a variety of post-translational modifications (PTMs) that can comprise in the conjugation of additional moieties to functional groups (e.g. acetylation, alkylation, methylation, lipidation and glycosylation) or by adding a new functional group to proteins (e.g. phosphorylation). PTMs affect the physical properties of proteins, which in term expand their cellular function and changes the protein dynamics. Proteins are not only modified by small molecules but by entire proteins belonging to the ubiquitin family of modifiers. Ubiquitin-like proteins (UBLs) like ubiquitin, Smt3 (SUMO), Atg8, Rub1 (NEDD8), Hub1, Atg8, Atg12, UFM1, ISG15, FAT10, FUB1, and Urm1 share common features such as the globular β-grasp fold lending UBLs a globular tertiary structure (Hochstrasser, 2000; 2009). Though functionally diverse, the principles of substrate-conjugation of UBLs resemble the mechanism of the best-studied UBL member ubiquitin (Fig. 2-1). Prior to the conjugation to target proteins,

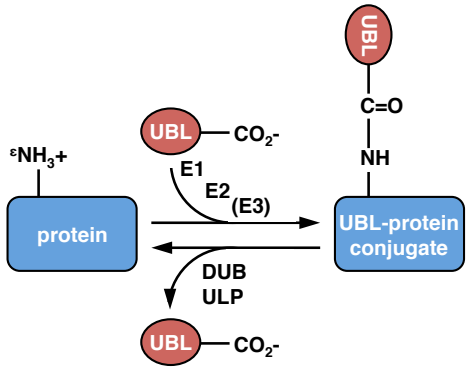

Fig. 2-1. Generalized conjugation system of ubiquitin-like proteins (UBLs).

Activation and conjugation of UBLs usually require an enzymatic cascade involving the E1 activating enzyme, the E2 conjugating enzyme and in some cases an E3 ligase. The C-terminus of the activated UBLs forms an isopeptide bond to the ε-amino group of the target acceptor residue. The UBL-protein modification is reversible through isopeptidases such as ubiquitin-like protein-processing enzymes (ULPs) or deubiquitinating enzymes (DUBs). Adopted from Hochstrasser, 2000.

ubiquitin and UBLs undergo an enzymatic cascade. First, the C- carboxyl group of UBLs' terminal double-glycine motif (GG-motif) is activated by adenylation via the activating enzyme (E1). The E1 attacks the carboxyl-AMP of the UBL via its thiol group resulting in the formation of an UBL-E1 thioester. The activated UBL is transformed from the E1 to the cysteine side chain of the conjugating enzyme (E2), from which the UBL forms a ε-amino bond between the C-terminal carboxylate of the modifier and the lysine side chain of the conjugate. E3 protein ligases are required for the final transfer of the UBL to the substrate. E3s either allosterically activate E2s and/or function as adaptors mediating the UBL-substrate conjugation (e.g. RING E3 ligases). Alternatively, the E2-bound UBL is transferred to the E3 via a thioester bond before the UBL is lastly ligated to the substrate (e.g. HECT E3 ligases).

UBL substrates can be either modified by one UBL moiety or by multiple single UBL moieties at different lysine residues (Geoffrey & Hay, 2009). However, UBLs such as ubiquitin, SUMO, Rub1 (Nedd8) and ISG15 are able to modify target proteins multiple times at the same lysine residue by forming polyUBL-chains based on either linear or branched linkages that can contain the same UBL or a mixture of different UBL moieties (Leidecker *et al.*, 2012; Singh *et al.*, 2012; Ciechanover & Stanhill, 2014; and Fan *et al.*, 2015). Although the function of mixed UBL-chains are not fully understood, chain formation of ubiquitin and its functional implication has been widely studied (Chau *et al.*, 1989; and Pickart, 2001). The best-studied UBL of the UBL family ubiquitin contains seven lysine residues, which all are susceptible to polyubiquitin chain formation (Xu *et al.*, 2009). While polyubiquitination on K48 guides the target protein to the proteasomal degradation, K63-linked polyubiquitin chains are involved in non-proteolytic processes such as endocytosis, translation, DNA repair and signal transduction (Chau *et al.*, 1989; Spence *et al.*, 1995; Kerscher *et al.*, 2006; Chen & Sun, 2009; Hochstrasser, 2009; and Rape, 2010). However, the function of K6-, K27-, K29- and K33-linked polyubiquitination is less known.

Protein modifications are able to play diverse roles in cellular processes (Fig. 2-2). For instance, UBL conjugation to a target protein can provide an additional binding site (Fig. 2-2A). The ubiquitin-binding domain (UBD)-containing

proteasomal receptors such as Rpn13 recognize and strongly bind to polyubiquitin chains that are attached to substrates (Husnjak *et al.*, 2008). Alternatively, UBL conjugation is able to cause conformational changes on the target protein that facilities binding to another protein (Fig. 2-2B). UBL modifications can also act as a molecular switch. The modification of different UBLs to the target protein can result in different fates of the UBL modified protein (Fig. 2-2C). These modifications can happen at the same attachment site and can be mutually exclusive. The proliferating cell nuclear antigen (PCNA), a DNA clamp that is essential for DNA replication and recombination, is modulated by the modification of SUMO or ubiquitin, which recruits distinct cofactors to the modified PCNA (Hoege *et al.*, 2002; Pfander *et al.*, 2005; Moldovan *et al.*, 2006 and Moldovan *et al.*, 2007). Another mechanism of UBL conjugation is the inhibition of protein-protein interaction as a result of UBL modification of the target protein (Fig. 2-2D). For

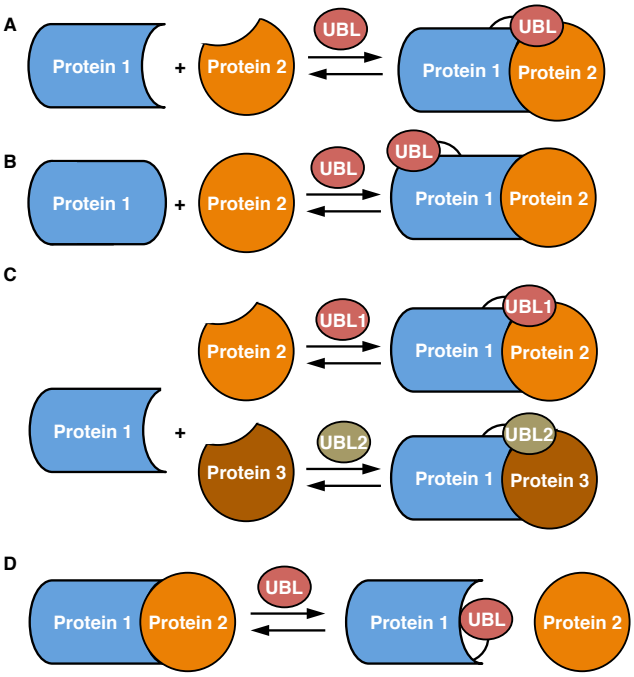

Fig. 2-2. General functions of UBLs.

(A) UBL conjugation to target protein improves protein-protein interaction by providing an additional binding site. **(B)** UBL conjugation enhances protein-protein interaction by triggering a conformational change of the UBL-modified protein. **(C)** Modification by different UBLs acts like a switch enabling the modified protein to interact with different proteins. **(D)** UBL conjugation inhibits the interaction with a potential interaction partner. Adopted from Hochstrasser, 2009.

example, SUMOylation of the transcription factor specificity protein 1 (Sp1) by SUMO-2/3 prevents the interaction of Sp1 with the acetyl transferase p300 during embryonic development (Gong *et al.*, 2014).

Similar to many posttranslational modifications, modifications of proteins by UBLs are mostly reversible (Wilkinson, 1997; Nijman *et al.*, 2005; and Reyes-Turcu *et al.*, 2009). A set of proteases of Deubiquitinating enzymes (DUBs) and ubiquitin-like protein-processing enzymes (ULPs) are capable of removing UBLs from their target proteins. In addition, most UBLs are synthesized as precursors with one or more amino acids following the GG-motif. The free GG-motif at the C-terminal end of UBLs is essential for protein conjugation. Therefore the precursors are processed by DUBs and ULPs, which remove the amino acids C-terminal of the GG-motif. Ubiquitin, for instance, is synthesized as precursor consisting of either a single ubiquitin moiety fused to ribosomal proteins or as polyubiquitin chains, which both require DUBs to yield processed ubiquitin monomers (Wiborg *et al.*, 1985; Baker & Board, 1987; and Ozkaynak *et al.*, 1987). In summary, DUBs are both responsible for the processing of UBL precursors and capable of antagonizing protein modification by UBLs. They are important regulators of the free UBL pool and regulate the amount of UBL-modified proteins and thus influence the fate of the target proteins (Nijman *et al.*, 2005).

2.1 The ubiquitin-related modifier Urm1

Since the discovery of the first prokaryotic UBLs like the bacterial ThiS and MoaD, it has become apparent that UBLs and their activation via an E1-like enzyme seems to be evolutionary highly conserved across the domains of life (Rajagopalan, 1997; Taylor *et al.*, 1998; Iyer *et al.*, 2006; and Maupin-Furlow, 2013). MoaD and ThiS structurally resemble the ubiquitin fold of other UBLs, as both have a β-grasp fold and a functional GG-motif (Rajagopalan, 1997; Taylor *et al.*, 1998; Lake *et al.*, 2001; Rudolph *et al.*, 2001; and Wang *et al.*, 2001). In 2000, the eukaryotic ubiquitin-related modifier 1 (Urm1) was discovered by a PSI BLAST search using the sequences of ThiS and MoaD, which were analyzed for proteins with high sequence similarity in *S. cerevisiae* database (Furukawa *et al.*, 2000). The 99 amino acids (aa) long and β-grasp fold containing Urm1 protein shows

high identify to ThiS (20%) and MoaD (23%), particularly in the C-terminal region (Furukawa *et al.*, 2000). ThiS, MoaD and the eukaryotic Urm1 are activated by adenylation at their C-terminal GG-motif by the E1-like enzymes ThiF, MoeB or Uba4 (MOCS3 in *H. sapiens*), respectively. It is believed that MoaB, ThiF and Uba4/MOCS3 most closely resemble the antecedent of the E1 superfamily (Taylor *et al.*, 1998; Leimkühler *et al.*, 2001; and Burroughs *et al.*, 2009). Unlike most adenylated UBLs that form a thioester bond between the UBL and its E1, ThiS and MoaD are bound to ThiF and MoeB via an acyl disulphide, respectively (Fig. 2-3A) (Leimkühler *et al.*, 2001; Xi *et al.*, 2001; and Lehmann *et al.*, 2006). In contrast to most UBLs, ThiS and MoaD do not conjugate to proteins, but serve as sulphur carriers in the thiamine and in the molybdenum-cofactor (MoCo) biosynthesis pathway, respectively (Pitterle *et al.*, 1993; Taylor *et al.*, 1998; Begley *et al.*, 1999; Lake *et al.*, 2001; Leimkühler *et al.*, 2001; Wang *et al.*, 2001). Remarkably, Urm1 possesses a MoaD-related fold and is therefore structurally more similar to the prokaryotic sulphur carriers MoaD and ThiS than the eukaryotic UBLs (Xu *et al.*, 2006). Unlike most UBLs that are expressed as precursors, Urm1 is synthesized without any C-terminal extension preceding its functional GG-motif. It remains unclear how free Urm1 proteins are regulated. Notably, Urm1 is shown to dimerize *in vitro* resulting in the formation of a homodimer via its C-terminal ends that results in the internalization of the GG-motifs and potentially serves as a regulation for Urm1 conjugation activity (Yu & Zhou, 2008). Urm1 is highly conserved from *S. cerevisiae* to *H. sapiens* and contains a β-grasp fold (Furukawa *et al.*, 2000; Xu *et al.*, 2006).

2.1.1 The Urm1 pathway

A yeast-two hybrid (Y2H) screen using Urm1 as a bait led to the identification of the E1-like ubiquitin activating enzyme 4 (Uba4, MOCS3 in *H. sapiens*), whose N-terminal region contains a MoeB-like domain showing high similarities to the E1 domain of the eukaryotic Uba1, but also to the prokaryotic ThiF and MoeB (Furukawa *et al.*, 2000; and Burroughs *et al.*, 2009). Additionally, Uba4 contains a C-terminal rhodanese-like domain (RLD) that is present in many prokaryotic and in

all eukaryotic MoeB homologs (Hochstrasser, 2000; Mendel & Schwarz, 2002; Matthies *et al.*, 2004; Krempinsky & Leimkühler, 2007; Schmitz *et al.*, 2008; and Burroughs *et al.*, 2009). Analogous to the activation of ubiquitin or ThiS/MoaD, Urm1 is first activated through the adenylation at its GG-motif by Uba4 (Fig. 2-3B). Adenylated Urm1 forms a covalent acyl-disulphide with Uba4 and is then released from Uba4 as a thiocarboxylated Urm1 intermediate (Fig. 2-3AB) (Pedrioli *et al.*, 2008; Schmitz *et al.*, 2008; Schlieker *et al.*, 2008; Nakai *et al.*, 2008; Noma *et al.*, 2009; Hochstrasser, 2009; Leidel *et al.*, 2009; Van der Veen *et al.*, 2011 Wang *et al.*, 2011). Interestingly, the two small archaeal modifiers (SAMP1 and SAMP2) function as protein modifiers and as sulphur carriers in tRNA thiolation and MoCo biosynthesis in a similar manner as the Urm1 system (Humbard *et al.*, 2010; Miranda *et al.*, 2011; and Anjum *et al.*, 2015). Therefore, it is believed that Urm1 is a molecular fossil of the UBL family that is derived from its archaeal ancestors SAMP1/2 (Xu *et al.*, 2006; Maupin-Furlow, 2013; and Anjum *et al.*, 2015).

Uba4 has two conserved cysteine residues that are vital for the thiocarboxylate formation of Urm1 and Urm1 function: C225 in the MoeB-like domain and C397 in the RLD (Furukawa *et al.*, 2000; Matthies *et al.*, 2005; Schmitz *et al.,* 2008; Nakai *et al.*, 2008; Leidel *et al.*, 2009; Hochstrasser, 2009; Noma *et al.*, 2009; Van der Veen *et al.*, 2011; and Jüdes *et al.*, 2016). To uphold Uba4 activity, Uba4 receives sulphur from the cysteine desulfurase Nfs1 and the RLD-containing sulfur transferase Tum1 (YOR251C) (Nakai *et al*, 2008; Leidel *et al.*, 2009; Noma *et al.*, 2009; Huang *et al*., 2008; and Jüdes *et al*., 2016). To date no Urm1-specific E2, E3 or deurmylating enzyme has been identified. It has been speculated that Uba4 might function as an E1- and E2-like hybrid (Hochstrasser, 2000), however this hypothesis has been challenged by the discovery of Urm1-Uba4 acyl-disulphide bond formation and of Urm1 thioester intermediates, since thioester bond formation are typically found in UBL-E2 conjugation (Pedrioli *et al.*, 2008; Van der Veen *et al.*, 2011; Wang *et al.*, 2011).

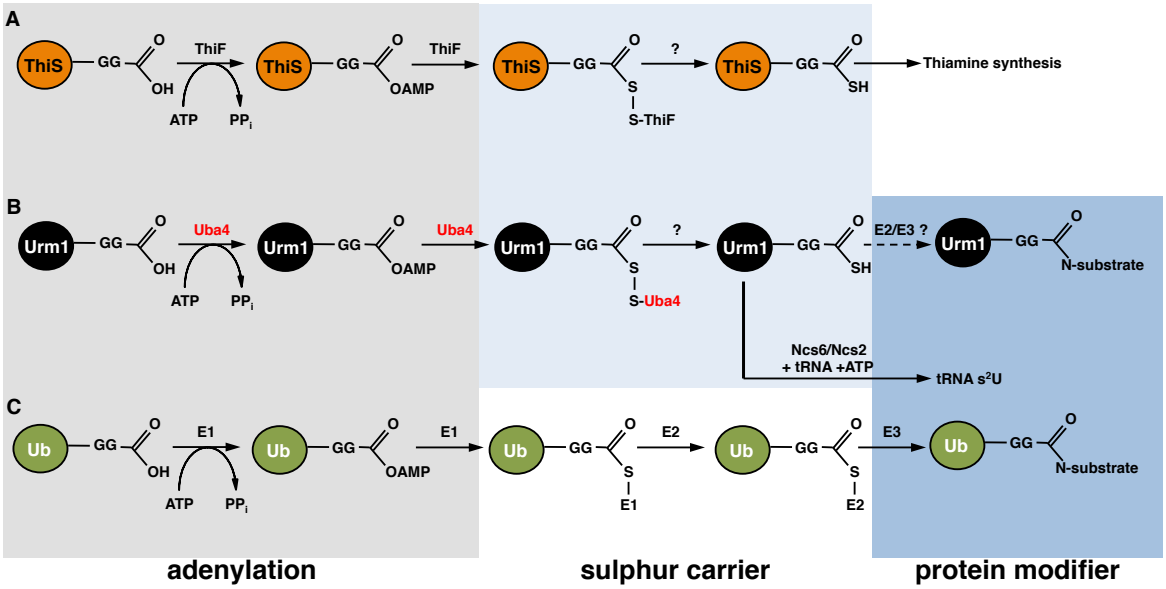

Fig. 2-3. Analogies between the ubiquitin, Urm1 and ThiS pathways.

(A) The thiocarboxylated ThiS functions as a sulphur carrier in the biosynthesis of thiamine. **(B)** Urm1 acts as a sulphur carrier and as a protein modifier. Analogous to ubiquitin and ThiS, Urm1 is activated at its carboxyl terminus by acyl-adenylation via the E1-like enzyme Uba4. The adenylated Urm1 covalently binds to Uba4 forms a covalent Urm1-Uba4 binding. Through a series of enzymatic reactions, C-terminus of Urm1 is thiocarboxylated that is able to function as a sulphur donor in transfer RNA (tRNA) modification or as a protein modifier by an unknown mechanism. **(C)** Ubiquitin modifies proteins via an enzymatic cascade involving the enzymes E1, E2 and E3. Adopted from Pedrioli *et al.*, 2008 and Wang *et al.*, 2011.

2.1.2 The role of Urm1 as sulphur carrier

So far 144 different RNA modifications have been identified in all kingdoms of life of which an array of PTMs are found in transfer RNAs (tRNAs) that enhances translational fidelity, structural stability, codon recognition and decoding accuracy (El Yacoubi *et* al., 2012; Jackman & Alfonzo, 2013; Machnicka *et al.*, 2013; Hopper, 2013; Nakai *et al.*, 2017). One of tRNA modifications is found at wobble uridine U_{34} of $tRNA^{Lys(UUU)}$, $tRNA^{Glu(UUC)}$ and $tRNA^{Gln(UUG)}$. Wobble U_{34} of tRNAs are commonly subjected to methoxycarbonylmethyl modification (mcm^5U_{34}) at the 5' position by the Elongator complex and/or to the addition of a thiocarbonyl group (s^2U_{34}) at the uracil ring by the Urm1 pathway (Machnicka *et al.*, 2013; Nakai *et al.*, 2017). Thiocarboxylated Urm1 together with the thiouridylase Ncs6 ("Needs Cla4 to Survive 6" or cytosolic thiouridylase 1 (CTU1/ATPBD3) in *H. sapiens*) and Ncs2 (CTU2 in *H. sapiens*) are likely to transfer the sulphur from the Urm1 C-terminus to

thiolate U_{34} and modify U_{34} to s^2U_{34} (Fig. 2-3B) (Nakai *et al.*, 2008; Dewez *et al.*, 2008; Leidel *et al.*, 2009; Schlieker *et al.*, 2008; and Noma *et al.*, 2009).

Modification of $mcm^5s^2U_{34}$ helps codon-anticodon interaction necessary for efficient mRNA decoding and enhances translational fidelity (Jablonowski *et al.*, 2006; Johansson *et al.*, 2008; Laxman *et al.*, 2013; Rezgui *et al.*, 2013; Tükenmez *et al.*, 2015; and Nedialkova *et al.*, 2015). Lack thereof in Elongator and Urm1 pathway mutants result in a complete loss or strong reduction in $mcm^5s^2U_{34}$ of $tRNA^{Lys(UUU)}$, $tRNA^{Glu(UUC)}$ and $tRNA^{Gln(UUG)}$ and result in translational defects such as slower mRNA decoding, ribosomal stalling and subsequently protein aggregation (Nakai *et al.*, 2004; Bjork *et al.*, 2007; Dewez *et al.*, 2008; Leidel *et al.*, 2008; Schlieker *et al.*, 2008; Nakai *et al.*, 2008; Noma *et al.*, 2009; Nedialkova *et al.*, 2015). Consequently protein abundance of ~260 proteins is decreased in *S. cerevisiae* due to inefficient translation of long mRNAs containing a high amount of codons for K, Q and E (Fig. 2-4) (Laxman *et al.*, 2013; and Rezgui *et al.*, 2013). While lack of mcm^5U_{34} modification pathway has no effects on cell viability, the cells lacking components of the Urm1 pathway for s^2U_{34} modification pathway have reduced or no viability under stress conditions such as oxidative stress, high temperatures, nutrient starvation and DNA damage (Furukawa *et al.*, 2000; Goehring *et al.*, 2003ab; Chen *et al.*, 2009; Khoshnood et al., 2016; Damon *et al.*, 2015; and Schorpp, 2011). Lack of both mcm^5U_{34} and of s^2U_{34} causes lethality in *S. cerevisiae* and in *C. elegans* during embryogenesis at elevated temperatures (Bjork *et al.*, 2007; Chen *et al.*, 2009). Conversely, yeast lacking Urm1, Uba4 and Ncs6 are resistant to the *Kluyveromyces lactis* toxin γ-toxin that exclusively cleaves mcm^5s^2-modified tRNAs and causes G1 cell cycle arrest to WT cells (Fichtner *et al.*, 2003; Lu *et al.*, 2005; Huang *et al.*, 2008; Jüdes *et al.*, 2016). Urm1 pathway mutants share certain phenotypes with target of rapamycin complex 1 (TORC1) mutants such as rapamycin and caffeine sensitivity. Moreover, cells lacking Urm1 and Uba4 cause the mislocalization of the TORC1- and nutrient-regulated transcription factors Gln3 and Gat1, which causes the misregulation of the TORC1-regulated target genes GAP1 and CIT2 and indicates the importance of the Urm1 pathway in nutrient sensing (Rubio-Texeira, 2007). Remarkably, sensitivity of rapamycin, caffeine and the oxidative stress inducing agent diamide

of Urm1-pathway mutants can be rescued by overexpression of unmodified $tRNA^{Lys(UUU)}$, $tRNA^{Glu(UUC)}$ and $tRNA^{Gln(UUG)}$ indicating that these phenotypes together with the resistance towards to *K. lactis* γ-toxin and temperature sensitivity can be attributed to the absence of tRNA thiolation (Huang *et al.*, 2008; Leidel *et al.*, 2009; and Damon *et al.*, 2015).

2.1.3 Urm1, the protein modifier

In contrast to the well-studied role of Urm1 as a sulphur carrier in tRNA thiolation, the function of Urm1 as a protein modifier remains enigmatic. Until now, the mechanism of Urm1 protein-modification pathway and the function of urmylation are as yet unclear. Previous works have shown the presence of higher migrating Urm1 adducts under steady state conditions, which massively increases under oxidative stress in *S. cerevisiae*, and cells from *D. melanogaster* and *H. sapiens* (Furukawa *et al.*, 2000; Goehring *et al.*, 2003a; Van der Veen *et al.*, 2011; and Khoshnood *et al.*, 2016). However, Urm1 adducts were absent in absence of Uba4, the catalytically inactive uba4 variants (*uba4 C225S/A*, *uba4 C397S/A*, *uba4 C225, C397S*), or yeast expressing *urm1ΔG* and *urm1ΔGG* truncations. This clearly indicates the existence of Urm1-modified substrates, whose Urm1 modification requires an ATP-dependent activation of its C-terminal glycine by the enzymatic activity of Uba4. Since no Urm1-specific E2, E3 have been identified, it remains unclear how substrate recognition and specificity is achieved. In terms of protein modification by Urm1, Van der Veen *et al.* have demonstrated that Urm1 is covalently conjugated to Urm1 substrates via a covalent isopeptide bond, as Urm1 conjugates are fairly resistant to reducing agents such as hydroxylamine Dithiothreitol (DTT) or hydroxylamine (NH_2OH) (Van der Veen *et al.*, 2011). In contrast to ubiquitination, urmylation requires a thiocarboxylated Urm1 intermediate, but also an Urm1 thioester intermediate, which is commonly observed in canonical UBL modifiers, as well. Through a series of site-directed mutagenesis of the only known yeast Urm1-substrate Ahp1, it could be demonstrated that the Urm1 conjugation machinery recognizes and conjugates Urm1 to lysine (K) 32 of Ahp1 (Van der Veen *et al.*, 2011). Whether all Urm1-

substrates are conjugated at their acceptor lysine has yet to be determined. All known Urm1 substrates are modified by a single Urm1 moiety and no polyurmylation has been observed in all known Urm1 substrates (Goehring *et al.*, 2003a; Van der Veen *et al.*, 2011; Khoshnood et al., 2016). Though no deurmylation enzymes have been identified in eukaryotes, Urm1 substrates seem to accumulate by the addition of the irreversible cysteine peptidase inhibitor N-ethylmaleimide (NEM), which is commonly used as an inhibitor of deubiquitination and deSUMOylation, suggesting the possible existence of a deurmylation enzyme in eukaryotes (Goehring *et al.*, 2003a; Van der Veen *et al.*, 2011; and Schorpp, 2011). Previous studies show a reduction of putative urmylated substrates in cells lacking Ncs2 and Ncs6 indicating a potential crosstalk between the Urm1 protein modification and sulphur carrier pathway (Goehring *et al.*, 2003b). However, this finding could not be reproduced in later studies, which showed no influence of urmylation in *Δncs2* or in human cells that have significantly reduced levels of ATPBD3/Ctu1 (Ncs6 in *S. cerevisiae*) (Schorpp, 2011; and Van der Veen *et al.*, 2011). Interestingly, components of the Urm1 pathway, such as Uba4/MOCS3, ATPBD3/Ctu1 and Ctu2 (Ncs2 in *S. cerevisiae*), among with the deubiquitinating enzyme USP15, the nucleocytoplasmic shuttling factor CAS (cellular apoptosis susceptibility protein), the peroxiredoxin Ahp1 that plays an essential role in cellular response to reactive oxygen species (ROS) in yeast and its ortholog Prx5 in *D. melanogaster* are confirmed Urm1 substrates *in vivo* (Jeong *et al.*, 1999; Lee *et al.*, 1999; Van der Veen *et al.,* 2011; and Khoshnood et al., 2016). Moreover, Van der Veen *et al.* identified a small set of potential Urm1 substrates via MS/MS, which are involved in various cellular pathways such as ubiquitination, tRNA modification, nuclear transport, RNA regulation and oxidative stress (Fig. 2-4) (Van der Veen *et al.*, 2011). Urmylation is present under steady state conditions and is significantly elevated under oxidative stress (Furukawa *et al.*, 2000; Goehring *et al.*, 2003; and Van der Veen *et al.*, 2011). Intriguingly, the Urm1 pathway distinctively responses to different oxidative stressors, as treatment with hydrogen peroxide (H_2O_2), diamide and *tert*-Butyl hydroperoxide (t-BOOH) induces the formation of specific sets of Urm1 adducts (Van der Veen *et al.*, 2011; and Schorpp, 2011). Indeed, while Ahp1 is urmylated under steady state conditions

and under diamide treatment, Urm1 does not modify Ahp1 under t-BOOH treatment (Goehring *et al.*, 2003a).

Though the function of urmylation remains unclear, urmylation might play a detrimental role in oxidative stress tolerance, as oxidative stress has been shown to be a strong inducer of urmylation. In concordant to these findings, cells deficient of Ahp1, Urm1 and Uba4 show sensitivity towards various oxidative stress-inducing drugs (Goehring *et al.*, 2003a). Since *Δahp1* cells do not share many phenotypes with Urm1-pathway mutants that result in pleiotropic phenotypes, Urm1 might function and modify additional proteins in other cellular process (Goehring *et al.*, 2003ab). Indeed, urmylation plays an important role during embryogenesis and improves overall fitness of *D. melanogaster* (Khoshnood *et al.*, 2016). Urm1 expression and protein conjugation by Urm1 are highly elevated during early embryonic stages and during larval/pupal transition. Concordantly to the appearance of urmylation during embryogenesis, loss of Urm1 causes a high lethality rate among flies homozygous for *urm1* either during embryogenesis or at late pupal stages, raising the question what proteins are modified by Urm1 (Khoshnood *et al.*, 2016). Around 20% of flies homozygous for *urm1* reach adulthood, but display a significantly reduced lifespan compared to wild type and Urm1 revertant flies. Recent *in vitro* studies have shown that the archaeal Urm1/SAMP homologue of *S. solfataricus* modify proteins, which are in turn recognized by the 20S proteasome and by the ATPase proteasome-activating nucleotidase (PAN) (Anjum *et al.*, 2015). Furthermore, *in vitro* experiments using N-terminal fusion of the archaeal Urm1 to GFP, mimicking Urm1-modified GFP species, showed the degradation of Urm1-GFP in presence of an active 20S proteasome suggesting that protein stability in *S. solfataricus* might be regulated by Urm1 and would therefore resemble the eukaryotic UPS. Unlike archaeal Urm1, Urm1-modified substrates in yeast and human were not subjected to protein degradation (Goehring *et al.*, 2003; and Van der Veen *et al.*, 2011).

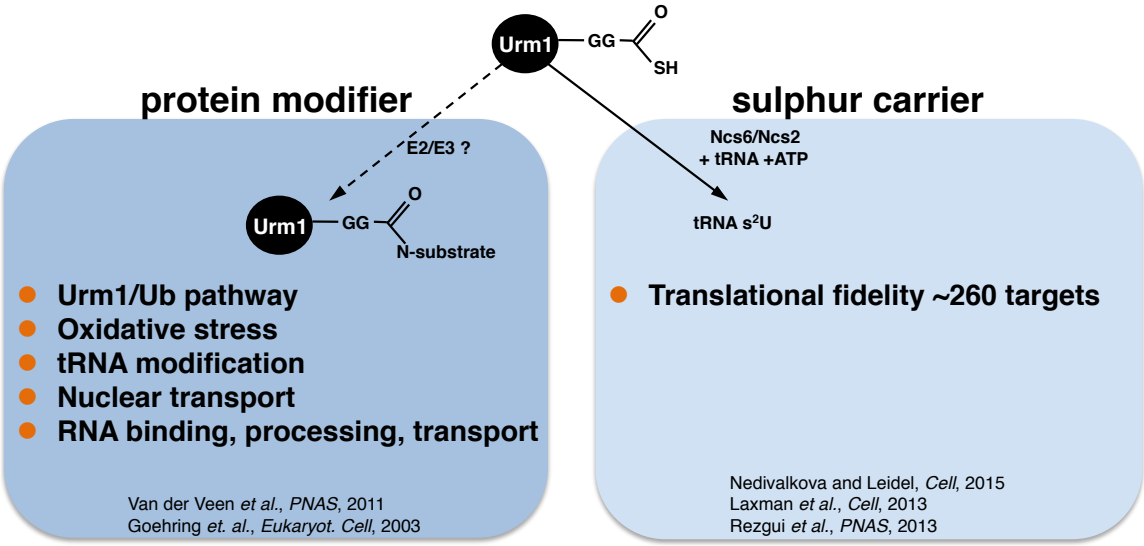

Fig. 2-4. Dual function of Urm1 as a protein modifier and a sulphur carrier.

2.2 Zinc Regulation in Yeast

Zinc (Zn) is an indispensible trace element for all organisms and serves as cofactors in around 10% of all proteins in humans ranging from enzymes, receptors, and growth factors to transcription factors (Sugarman, 1983; Andreini *et al.*, 2006; Broadley, 2007; Prasad, 2008; and Plum *et al.*, 2010). Since metalloproteins and Zn-binding proteins are as ubiquitous as their role in biological processes such as oogenesis, embryogenesis, conception, immune response, and regulation of the central nervous system, a tight control of the intracellular zinc levels is therefore a requirement for cell survivability (Hambidge & Krebs, 2007; Prakash *et al.*, 2015). Excess of intracellular zinc levels are toxic and can compete with other metal ions for the binding to transporter proteins, enzymes, and ligands. The regulation of zinc homeostasis is mediated by a multilayered regulatory mechanism including RNA expression, RNA stability, translation, degradation, zinc storage/conservation, zinc sensors such as metallothioneins and zinc trafficking via anterograde and retrograde zinc transporters (Hamer, 1986; Palmiter & Findley, 1995; Eide, 2003; Rutherford & Bird, 2004; Krezel & Maret, 2007; Fukada *et al.*, 2011; and Bird, 2015). The expression of the zinc-regulatory proteins and zinc-transporters are controlled by metal-responsive transcription factors such as the metal-responsive transcription factor 1 (MTF-1) in insects, fish, reptiles and mammals (Brugnera *et al.*, 1994; and Choi & Bird, 2014). While MTF-1 regulates

cupper, iron and zinc homeostasis in higher eukaryotes, *S. cerevisiae* possess three metal-responsive transcription factors each specialized in either regulating cupper, iron and zinc, respectively (Rutherford & Bird, 2004). The zinc homeostasis in yeast is controlled by the zinc-responsive activator protein 1 (Zap1) (Zhao *et al.*, 1997; Eide, 2009; and Wilson & Bird, 2016). Functional homologs of Zap1 have been identified in *Cryptococcus gattii*, *Candida albicans*, *Candida dubliniensis* and *Aspergillus fumigatus*, suggesting that the mechanism to regulate zinc homeostasis by Zap1 homologs might be a common mechanism among the fungal kingdom (Moreno *et al.*, 2007; Kim *et al.*, 2008; Schneider *et al.*, 2012; and Choi & Bird, 2014, Böttcher *et al.* 2015).

In response to zinc deficiency, Zap1 activates genes, which either play roles in zinc homeostasis or survivability under zinc starvation (Fig. 2-5A) (De Nicola *et al.*, 2007; Wu *et al.*, 2008; North *et al.*, 2012; MacDiarmid *et al.*, 2013). Under zinc-limiting conditions Zap1 mediates the expression of *FET4*, which transports Zn^{2+}, Cu^{2+} and Fe^{2+}, and two high affinity Zn^{2+}-specific ZIP-family transporters *ZRT1* and *ZRT2*, whose homologs play a detrimental role in metal transport among all kingdoms (Fig. 2-5A) (Zhao & Eide, 1996ab; Gaither & Eide, 2001; Waters & Eide, 2002; Kambe *et al.*, 2006; and Choi & Bird, 2014). Zap1 activates target genes expression by binding to one or more zinc-responsive elements (ZREs) located within the target genes' promoter region (Fig. 2-5B) (Zhao *et al.*, 1998; and Wu *et al.*, 2008). Moreover, Zap1 activates its own expression by binding to a single ZRE conserved among Zap1-like homologs (Fig. 2-5B) (Zhao *et al.*, 1998; Moreno *et al.*, 2007; Schneider *et al.*, 2012; Böttcher *et al.*, 2015). Under zinc-replete conditions, binding of Zn^{2+} to the transactivation domains (ADs) AD1 and AD2 of Zap1, which in turn inactivates the transcriptional activity of Zap1 under a yet unknown mechanism. (Fig. 2-5B) (Bird *et al.*, 2000; Bird *et al.*, 2003; Qiao *et al.*, 2006; Wang *et al.*, 2006; and Frey & Eide, 2011). Even though the Zap1 zinc-sensing ability is important to suppress Zap1 target genes, expression of the C-terminal DNA-binding domain (DBD) of Zap1 enables binding to ZREs, which activates Zap1 target genes in a zinc-independent fashion, indicating an additional post-translational mechanism to control Zap1 expression (Frey *et al.*, 2011; and

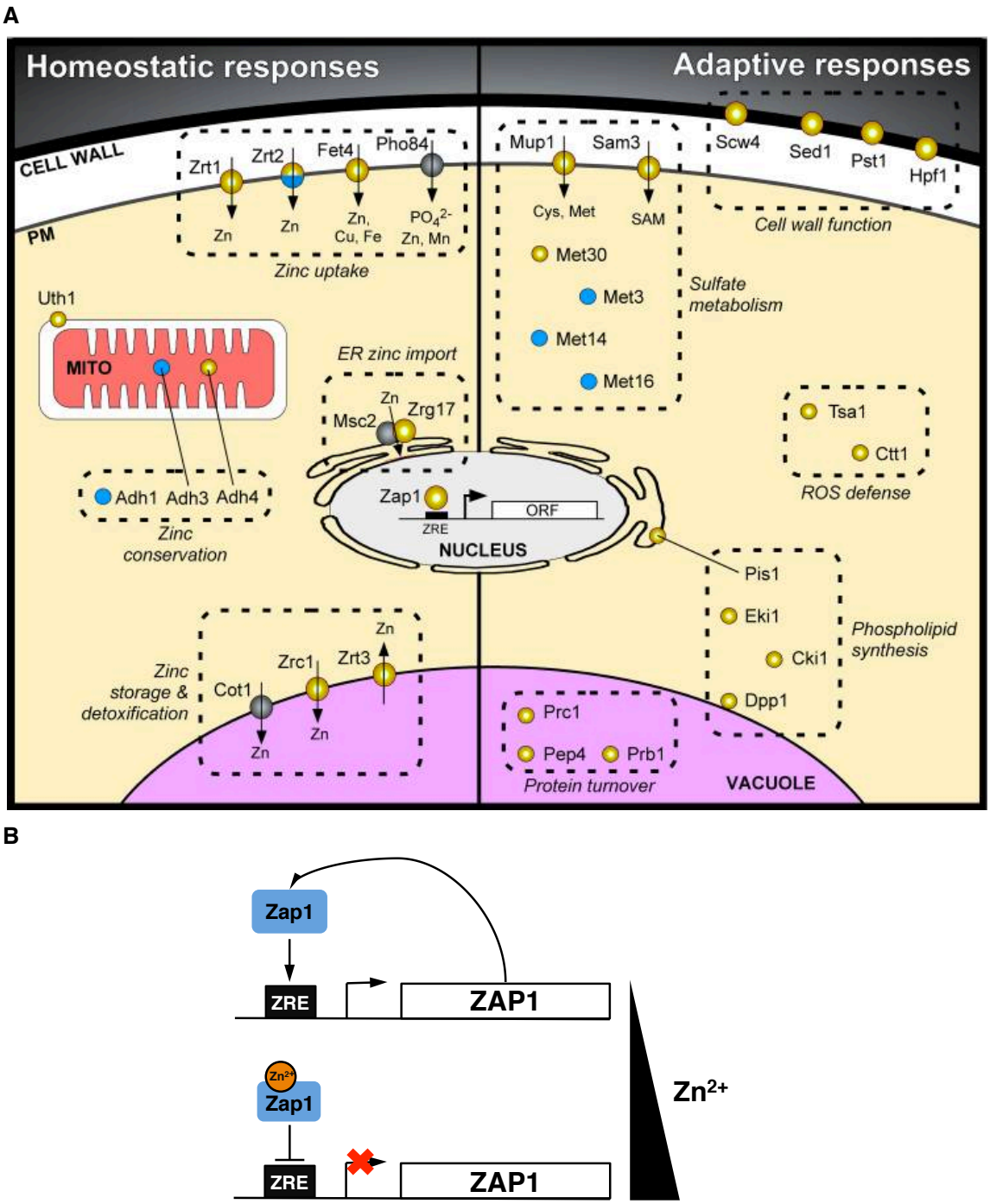

Fig. 2-5. Zap1 target genes and zinc-dependent autoregulatory mechanism of Zap1.

(A) Functional role of known or putative Zap1 target genes in yeast. Upregulated genes are depicted in yellow and down-regulated genes are depicted in blue. Since ZRT2 is activated and repressed by Zap1 depending to the intracellular zinc concentration, ZRT2 is depicted in blue and yellow. Genes, depicted as grey circles, are not regulated by Zap1. MITO: mitochondria; PM: plasma membrane; ORF: open reading frame. Fig. 2-5A is adapted from Eide, 2009. **(B)** Zinc-dependent autoregulatory mechanism of Zap1. Under zinc-depleted conditions Zap1 is transcriptional active and activates ZAP1 transcription by binding to the zinc-responsive element (ZRE) of upstream ZAP1 ORF. Zn^{2+} binding to Zap1 transcriptionally inactivates Zap1 and hence represses ZAP1 transcription.

Wilson & Bird, 2016). Zap1 not only controls zinc-dependent homeostatic responses, but also targets genes in sulfate metabolism, cell wall function, phospholipid synthesis, protein turnover and ROS defense (Fig. 2-5A) (Eide, 2009). Previous studies showed an increase of intracellular ROS levels under zinc-limiting conditions, which, in turn, leads to DNA damage, and to protein and lipid oxidation (Powell, 2000; Ho, 2004; Wu *et al.*, 2007). As a protective mechanism from zinc deficiency-induced oxidative stress, Zap1 activates the expression of the cytosolic peroxiredoxin Tsa1 and the cytosolic catalase Ctt1 under low zinc conditions (Wu *et al.*, 2008). Intriguingly, deletion of *URM1* and *ZRT1* shows a significantly slower growth indicating a possible connection between the Urm1 pathway and the Zap1 signaling pathway (Costanzo *et al.*, 2010).

Aim of this work

The dual role of Urm1 as a sulphur carrier and protein modifier combines seemingly unrelated features of the prokaryotic sulphur carrier system and the eukaryotic protein modification system, suggesting that Urm1 may be an evolutionary fossil of the UBL family. While the sulphur carrier function of Urm1 in tRNA thiolation has been revealed, the protein modifier function of Urm1 remains largely unclear. Aside from this, only few proteins have been identified as Urm1-substrates. Although numerous Urm1 adducts are present under regular growth conditions and upon oxidative stress, the peroxiredoxin Ahp1 is the only known Urm1 substrate in yeast, raising the question whether more proteins are modified by Urm1. Since Urm1 targets a specific lysine residue of Ahp1, it is conceivable that Urm1 may conjugate more proteins in a similar fashion. Despite extensive research on Ahp1 and its function in ROS defense, the role of Ahp1 urmylation continues to be ambiguous.

In this study, we aimed to elucidate the function of protein urmylation *in vivo*. To address this question, an unbiased tandem mass spectrometry (MS/MS) screen was conducted to identify novel lysine-directed Urm1 substrates. Candidates were verified by biochemical methods and thus served as model substrates in investigating the mechanistic and cellular consequences of urmylation.

3 Results

3.1 Identification of novel Urm1-substrates

Although the role of Urm1 as a sulfur carrier in tRNA modification is adequately described (Leidel *et al.*, 2009, Rezgui *et al.*, 2013, Laxman *et al.*, 2013 and Nedialkova & Leidel, 2015) the function of Urm1 as a protein modifier remains unknown. To date only few urmylated substrates are identified, such as MOCS3 (Uba4 in *S. cerevisiae*), ATPBD3, CTU2, USP15 and CAS in mammalian cells (Van der Veen *et al.*, 2011), Uba4 and the thiol-specific peroxiredoxin Ahp1 in *S. cerevisiae*, respectively (Goehring *et al.*, 2003ab, Schorpp, 2011). To date, no functional relevance of Urm1 modification has been assigned to any of the above-mentioned Urm1 substrates.

Urm1 conjugation to Ahp1 is covalent and requires the ε-amino group of acceptor lysine (K) residues of Ahp1 and the enzymatic activity of the E1-like enzyme Uba4 (Van der Veen *et al.*, 2011 and Schorpp, 2011). In this work a SILAC-based mass spectrometry approach was performed to screen for novel Urm1-substrates and to identify urmylation sites, which would allow a greater understanding of the functional consequences of urmylation (Ong *et al.*, 2002, Mann, 2006; Andersen *et al.*, 2009, Matic *et al.* 2010; and Psakhye & Jentsch, 2012). Tryptic-digestion of Urm1 conjugated proteins produces branched peptides in which the C-terminal fragment of Urm1 is attached to a lysine residue within the target peptide. Thus, a proteomic search for specific peptides derived from trypsin-digested Urm1-substrate branched conjugates (i.e. Urm1 branched peptides) could allow mapping of so far unknown urmylation sites. Detection of Urm1 branched peptides is challenging using wild type (WT) Urm1, as tryptic digestion of WT Urm1 results in very long Urm1 branched peptides (K/R…$^{\text{KDYILEDGDIISFTSTLHGG-ε-}}$**K**…K/R). These masses would generate complex LC-MS/MS spectra making the identification of such Urm1 branched peptides demanding (Matic *et al.*, 2008; and Matic & Hay, 2012). To increase the probability of identifying Urm1-substrate branched peptides, a modified yeast strain expressing an Urm1 variant was constructed that would generate shorter Urm1 branched peptides (*Δurm1* ^{HisHA}*urm1-L96R*) (Fig. 3-1A). Tryptic digestion of *urm1-L96R* with its covalently attached target protein

would yield in K/R…$^{HGG\text{-}\varepsilon\text{-}}$**K**…K/R (HGG-ε-K) Urm1 branched peptides and ought to improve the detection of urmylation sites via mass spectrometry. To determine whether the ^{HisHA}*urm1-L96R* variant can function as a WT version of Urm1, zeocin sensitivity of different *Δurm1* mutant strains (as described in Schorpp, 2011) was tested (Fig. 3-1B). *Δurm1* cells show high sensitivity at already low concentrations of zeocin, whereas *Δurm1* cells expressing ^{HisHA}*urm1-L96R* could rescue the sensitivity of the *Δurm1* strain entirely. *Δurm1* ^{HisHA}*urm1-L96R cells* with an additional deletion of the E1 enzyme Uba4 were once again sensitive to zeocin. Moreover the conjugation of ^{HisHA}*urm1-L96R* to protein substrates was also investigated (Fig. 3-1C). As previously shown, N-ethylmaleimide (NEM) enhances Urm1-conjugation (Van der Veen *et al.*, 2011 and Schorpp, 2011). Both ^{HisHA}Urm1 and ^{HisHA}*urm1-L96R* showed a comparable urmylation pattern in cells treated with and without NEM. Thus, the ^{HisHA}*urm1-L96R* strain appears to be suitable to

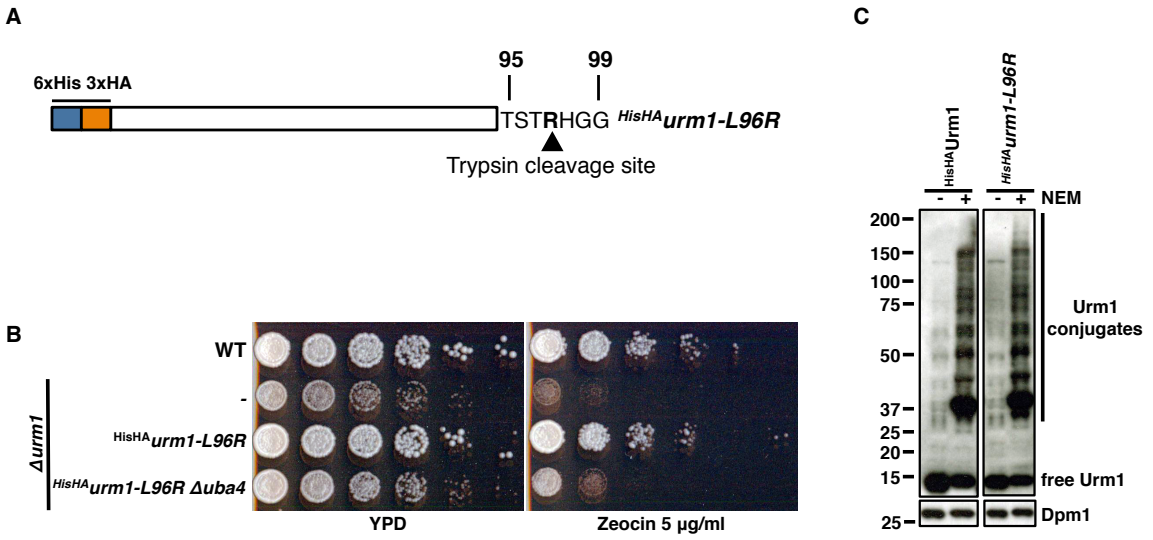

Figure 3-1. Construction of a modified yeast strain to identify lysine-directed Urm1 substrates. (A) Schematic of the Urm1 expression constructs. Tryptic digestion of ^{HisHA}*urm1-L96R* gives rise to a short HGG-ε-K branched peptide. ^{HisHA}*urm1-L96R* was integrated at the *LEU2* locus of *Δurm1* cells (^{HisHA}*urm1-L96R*). The arrow indicates the tryptic cleavage site. **(B)** ^{HisHA}*urm1-L96R* is able to rescue the zeocin-induced sensitivity of *Δurm1* cells, indicating that this variant does not interfere with Urm1 functions in yeast cells. Cells were plated in 5-fold dilutions on YPD with or without zeocin and incubated for 3 days at 30°C. ^{HisHA}*urm1-L96R* was integrated at the *LEU2* locus of *Δurm1* (^{HisHA}*urm1-L96R*) and of *Δurm1 Δuba4* (^{HisHA}*urm1-L96R Δuba4*). **(C)** Urm1 conjugation pattern in yeast strains expressing ^{HisHA}Urm1 and ^{HisHA}*urm1-L96R*. Cells were grown at 30°C either with (+) or without (-) 1h of 10 mM NEM incubation. Samples were collected and subjected to immunoblotting using anti-HA antibodies to detect ^{HisHA}Urm1. Dpm1 levels serve as a loading control.

screen for novel Urm1-substrates (Fig. 3-2A). To this end, the *HisHA*urm1-L96R strain was used to first enrich Urm1 and Urm1-conjugates in a denaturing Ni-NTA pull-down followed by a SILAC-based LC-MS/MS method that allows the quantitative detection of changes in protein abundance among differentially treated samples. Subsequently, isolated Urm1-conjugates from untreated and NEM-treated cells were analyzed using the LC-MS/MS method. The LC-MS/MS screen identified 547 potential Urm1 substrates in total, of which a small subset of 21 Urm1-substrates were significantly enriched upon NEM-treatment (H/L ratio of >1 and a p-value of <0.05, Fig. 3-2B). Among these candidates, proteins are found associated with various cellular processes such as glycolysis (Pyk1, Tdh2 and Tdh3), sterol metabolism (Nsg2), protein biosynthesis (Ses1), RAS-cAMP pathway

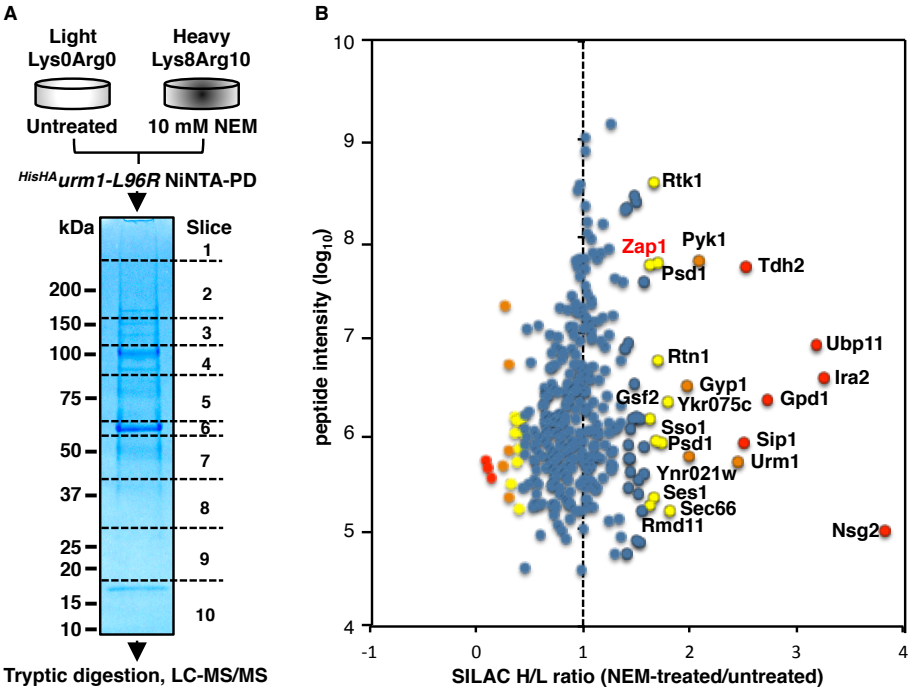

C

Gene	Peptide Sequence	HGG (K) Site Positions	SILAC I Ratio H/L Normalized	SILAC II Ratio L/H Normalized
ZAP1	VKCALER	K871	1.64	1.88

Figure 3-2. Purification and identification of urmylated substrates.

(A) Overview of the experimental workflow for the purification and identification of Urm1-modified substrates with HGG-ε-K linkages using the mutant variant *HisHA*urm1-L96R. **(B)** Scatter plot of normalized SILAC H/L ratios (NEM-treated versus untreated) for 547 quantified proteins were plotted against the sum of the respective peptide intensities. Proteins are color-coded according to their respective p-values, with red circles having values <0.001, orange circles between 0.001 and 0.01, yellow circles between 0.01 and 0.05 and blue circles >0.05. **(C)** A single Urm1-conjugation site of Zap1 was identified at K871. Following Ni-NTA pull-down, HisHAUrm1-conjugates were digested with trypsin. Branched peptides with HGG-ε-K linkages were detected and identified by LC-MS/MS and MaxQuant, respectively.

(Ira2), ubiquitin pathway (Ubp11), and zinc metabolism (Zap1) (Tab. 3-1). Together with the previously described Urm1-substrate Ahp1, proteins of the Urm1 pathway (Nfs1 and Uba4) were identified among the targets. Unlike previous studies, Ahp1 urmylation was not increased upon NEM treatment (Van der Veen *et al.*, 2011; and Schorpp, 2011).

Common quantification errors in SILAC experiments are due to an incomplete incorporation of isotopic amino acids and arginine-to-proline conversions that lead to reduced ion intensities of the 'heavy' labeled peptides that results in a reduced H/L ratio (Ong *et al.*, 2003; and Park *et al.*, 2012). Previous studies have shown that a reciprocal label-swap replication experiment would reduce the preceding technical errors (Park *et al.*, 2012). For this reason, a label-swap replication experiment was performed in parallel. The LC-MS/MS analysis of the label-swap experiment revealed that 17 proteins of the 21 identified proteins had a negative H/L ratio, strongly indicating that these proteins were urmylated upon NEM treatment (Tab. 3-1). In order to ensure reproducibility and comparability of the generated data, we repeated the experiments twice using ^{HisStrep}*urm1-L96R* in label-free LC-MS/MS analysis. Most proteins that were identified from the previous SILAC experiment were identified once or twice in the above-mentioned replication experiments (Tab. 3-1). Furthermore, to demonstrate that the *urm1-L96R* variant modifies the same set of proteins as WT Urm1 upon NEM-treatment, a yeast strain expressing ^{HisHA}Urm1 and ^{HisStrep}Urm1 was generated and used in following denaturing purification experiments: (1) SILAC with ^{HisHA}Urm1 without NEM vs. ^{HisHA}Urm1 with NEM; (2) SILAC with ^{HisHA}Urm1 *Δuba4* with NEM vs. ^{HisHA}Urm1 with NEM and (3) two label-free LC-MS/MS experiments with ^{HisStrep}Urm1 in presence of NEM (Tab. 3-1). In summary, all of the highly accumulated substrates that were previously found in ^{HisStrep}*urm1-L96R* could be identified in the experiments conducted with WT ^{HisStrep}Urm1. In addition the *urm1-L96R* variant allows prediction of protein urmylation sites by identifying HGG-ε-K branched peptides. In total, 59 proteins with their respective HGG-ε-K branched peptides were detected in the entirety of all purification experiments using the *urm1-L96R* variant. In one of the label-free experiment, we were able to identify three tryptic branched peptides of Urm1-Ahp1 at K41, K107 and K32, which was previously identified as the

urmylation site of Ahp1 (data not shown, Van der Veen *et al.*, 2011). Out of the 21 highly accumulated substrates, we were able to find HGG-ε-K branched peptides, which could be assigned to 5 proteins (Tab. 3-1). Importantly, the zinc-responsive activator protein (Zap1) was identified as Urm1-substrate in several repetition experiments using ^{HisHA}*urm1-L96R* variant and wild type Urm1 with NEM-treated cells. Moreover, an Urm1-Zap1 branched peptide at K871 was identified, signifying a likely acceptor lysine residue for Zap1 urmylation (Fig. 3-2C, Tab. 3-1). Additionally, we could confirm Zap1 with a negative H/L ratio in a reciprocal label-swap replication experiment, confirming NEM-induction (Fig. 3-2C).

Systematic name	Standard name	Protein description	Urm1	*urm1-L96R*	HGG-K Site Positions
YNL156C	NSG2	sterol biosynthesis	yes	yes	
YOL081W	IRA2	GTPase-activator protein for Ras-like GTPase	yes	no	
YKR098C	UBP11	Ubiquitin carboxyl-terminal hydrolase	yes	yes	
YJR009C	TDH2	Glyceraldehyde 3-phosphate dehydrogenase	yes	yes	331*
YGR192C	TDH3	Glyceraldehyde 3-phosphate dehydrogenase	yes	yes	331*
YDR422C	SIP1	5'-AMP-activated protein kinase	yes	yes	
YIL008W	URM1		yes	yes	
YAL038W	PYK1	Pyruvate kinase	yes	yes	135;233;236*
YNR021W	YNR021W	Protein of unknown function	yes	yes	
YOR070C	GYP1	Cis-golgi GTPase-activating protein (GAP) for yeast Rabs	yes	yes	
YBR171W	SEC66	Preprotein translocase subunit Sec66	yes	yes	
YKR075C	YKR075C	Unknown function	yes	yes	
YNL169C	PSD1	Phosphatidylserine decarboxylase	yes	no	
YPL224C	MMT2	Cation efflux family	yes	yes	
YDR233C	RTN1	Reticulon	yes	yes	
YMR183C	SSO2	SNARE domain;Syntaxin	yes	yes	
YDR023W	SES1	Cytosolic seryl-tRNA synthetase	yes	no	
YDL025C	RTK1	Putative protein kinase	yes	yes	177*
YML048W	GSF2	Endoplasmic reticulum (ER) localized integral membrane protein	yes	yes	
YJL056C	ZAP1	Zinc-responsive activator protein 1	yes	yes	871
YHL023C	RMD11	Subunit of the Iml1p/SEACIT complex	yes	yes	

Table 3-1. List of ^{HisHA}*urm1-L96R* modified proteins significantly enriched in NEM-treated cells.

Proteins are color-marked according to their respective p-values, with red having values <0.001, orange between 0.001 and 0.01, and yellow between 0.01 and 0.05. Experiments in which the respective proteins are detected using WT Urm1: (1) ^{HisHA}Urm1 (-NEM; 'light' medium) vs. ^{HisHA}Urm1 (+NEM, 'heavy' medium); (2) ^{HisHA}Urm1 *Δuba4* (+NEM; 'light' medium) vs. ^{HisHA}Urm1 (+NEM; 'heavy' medium); (3) label-free experiments LC-MS/MS analysis of ^{HisStrep}Urm1 and ^{HisHA}*urm1-L96R*: (1) label-swap replication experiment (+NEM; 'light' medium) vs. (-NEM, 'heavy' medium); (2) label-free experiment LC-MS/MS analysis of ^{HisHA}*urm1-L96R*. *Urm1-substrate branched peptide detected in replicates using ^{HisStrep}*urm1-L96R.*

3.2 Zap1 – a novel Urm1-substrate

3.2.1 Urm1 modifies Zap1

Zap1 is a zinc-regulated transcription factor (Zhao & Eide, 1997), which is not only the master regulator of zinc uptake, homeostasis (Zhao & Eide, 1996ab), conservation (Lyons *et al.* 2000), storage (MacDiarmid *et al.*, 2000) and detoxification (Miyabe *et al.*, 2000 and MacDiarmid *et al.*, 2003), but is involved in various adaptive processes such as sulfate metabolism (De Nicola *et al.* 2007 and Wu *et al.*, 2008), cell wall function, phospholipid synthesis, protein turnover and ROS defense (Wu *et al.*, 2007 and Wu *et al.,* 2008). Zap1 also regulates its own expression via a positive auto-regulatory mechanism (Zhao & Eide, 1997). This transcriptional auto-regulation is controlled through the binding of Zap1 to a short DNA sequence called zinc-responsive element (ZRE), which is located upstream at the *ZAP1* promoter. Zap1 binding to *ZRE* occurs under zinc-deficient conditions and thus potentiates the transcriptional activity of Zap1. Zap1 acts as a zinc sensor by directly binding to Zn^{2+} ions.

To confirm Zap1 as *bona fide* Urm1-substrate, ^{HisStrep}Urm1 was first purified using a denaturing tandem affinity purification (TAP) method (adapted from Tagwerker *et al.*, 2006; and Maine *et al.*, 2010) and immunoblotted against urmylated Zap1 using anti-HA antibodies (Fig. 3-3). A slower-migrating Zap1^{HA}-species was detected in cells expressing Zap1^{HA} and ^{HisStrep}Urm1, corresponding to an Urm1-modified Zap1 variant.

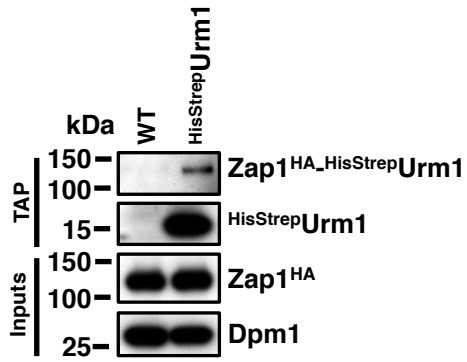

Figure 3-3. Zap1 is a novel Urm1 substrate.

Detection of urmylated Zap1^{HA} using tandem affinity purification of ^{HisStrep}Urm1. Zap1 urmylation was verified by a denaturing Ni-NTA pull-down of ^{HisStrep}Urm1 followed by denaturing Strep-tag purification (TAP). Prior to

TAP, cells were treated with 10 mM NEM for 1h at 30°C. Samples were subjected to immunoblotting using anti-Urm1 antibodies to detect ^{HisStrep}Urm1 and anti-HA antibodies to detect Zap1^{HA}. Dpm1 levels serve as a loading control. The C-terminal HA-tag was integrated at the endogenous *ZAP1* locus. ^{HisStrep}Urm1 was integrated at the *LEU2* locus of *Δurm1*.

3.2.2 Urm1 influences the transcriptional activity of Zap1

Initial experiments have shown that Zap1 levels were significantly decreased in *Δuba4* and cells expressing *zap1-K871R* (*KR)* that no longer has the predicted lysine residue for Zap1 urmylation (data not shown). We therefore wondered if the decrease of Zap1 levels was dependent on intracellular zinc concentrations. To this end, we constructed yeast strains that contain a C-terminally HA-tagged Zap1 variant expressed from its endogenous locus. WT, *Δurm1* cells expressing Zap1^{HA} or *zap1-K871R^{HA}* were grown in either zinc-limiting (-Zn) or zinc-replete (+Zn) conditions. As expected, addition of zinc drastically reduces the expression of Zap1^{HA}, but Zap1^{HA} levels were decreased in *Δurm1*, *KR* and *Δurm1 KR* independent of zinc abundance when compared with WT (Fig 3-4A). We therefore checked whether the *ZAP1* expression was affected by lack of urmylation. To this end, we quantified mRNA levels via the real time RT-qPCR method. Absolute amounts of *ZAP1* mRNA were quantified in WT, *Δurm1* cells expressing WT Zap1 or WT cells expressing *zap1-K871R^{HA}* that were grown in zinc-replete (+Zn) and zinc-deficient conditions (-Zn). While expression of *ZAP1* mRNA levels were downregulated under zinc-replete conditions, *ZAP1* expression was upregulated under zinc-limiting conditions (Fig. 3-4B). Compared to WT, *ZAP1* expression was reduced by approximately two-fold in *Δurm1*, *zap1-K871R^{HA}* and *Δurm1 zap1-K871R^{HA}* under zinc-limiting conditions. Consequently, we investigated, if the expression of the Zap1 downstream target Zrt1 is affected by the absence of urmylation. Indeed, *ZRT1* expression was slightly downregulated in *Δurm1,* in *zap1-K871R^{HA}* and *Δurm1 zap1-K871R^{HA}* (Fig. 3-4C).

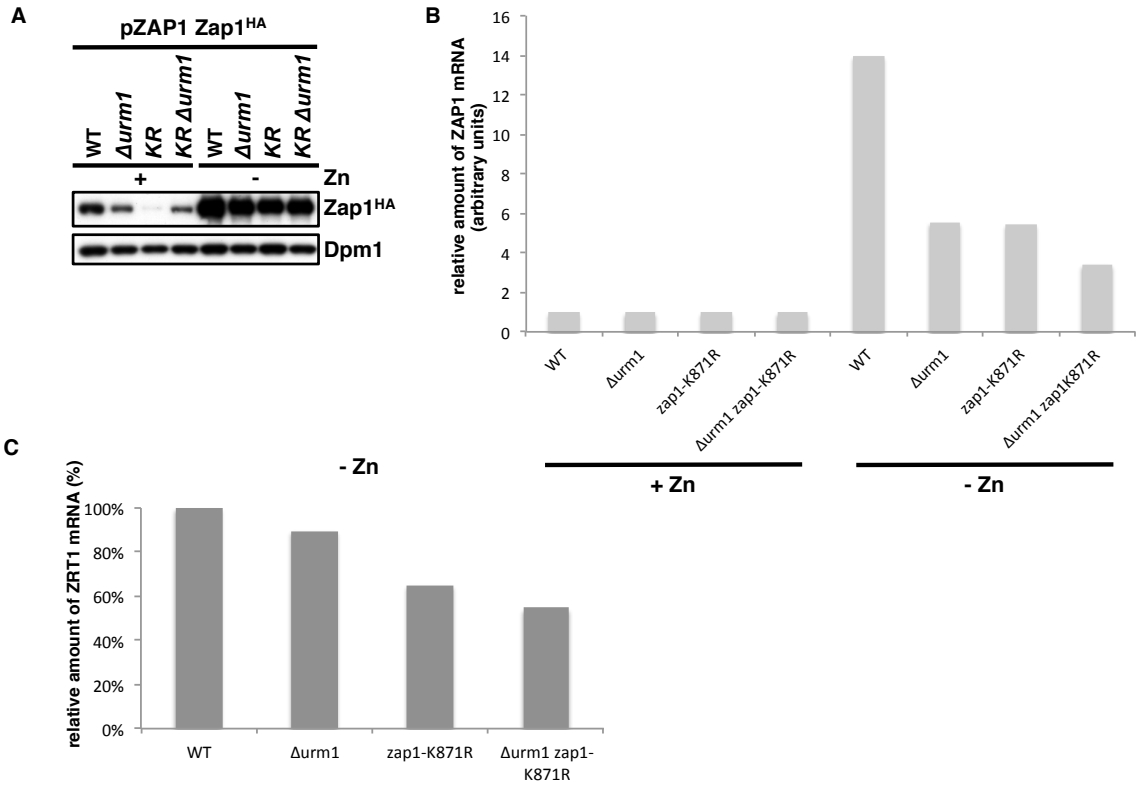

Figure 3-4. Loss of Zap1 urmylation results in decreased Zap1 level and reduced transcriptional activity of Zap1.

(A) Zap1 levels are reduced in absence of Zap1 urmylation. WT, *Δurm1* expressing endogenous $Zap1^{HA}$ or *zap1-K871R*^{HA} were grown exponentially in either LZM containing 1 mM (+) or 3 µM (-) $ZnCl_2$ at 30°C. Samples were subjected to immunoblotting using anti-HA antibodies to detect $Zap1^{HA}$. Dpm1 levels serve as a loading control. **(B)** Real-time RT-qPCR analysis of *ZAP1* gene expression of cells WT, *Δurm1*, *zap1 K871R* and combinations grown to log phase in zinc-abundant 1mM $ZnCl_2$ LZM (+Zn) and switched to zinc limiting conditions in 3 µM $ZnCl_2$ LZM (-Zn) at 30°C for 4.5h. Fold change was calculated relative to -Zn/+Zn ratio. Transcripts were normalized to the housekeeping gene *ACT1*. Normalized *ZAP1* mRNA of cells grown in +Zn were set to 1. Values are mean for n=2. **(C)** Quantitative reverse transcription PCR (RT-qPCR) of ZRT1 mRNA under zinc-limiting conditions. WT, *Δurm1* cells, cells expressing *zap1 K871R* or combinations were grown to log phase in LZM containing either 1000 µM or 3 µM $ZnCl_2$ at 30°C for 4.5h. mRNA was extracted from cells and cDNA was generated by using the RT-PCR method. Shown are the relative *ZRT1* mRNA levels normalized to the housekeeping gene *ACT1*. Normalized *ZRT1* mRNA signal were set to 1. Values are mean for n=2.

3.2.3 Urmylation in response to zinc-deficiency

Prior studies have shown that zinc deficiency increases intracellular levels of reactive oxygen species (ROS) (Powell *et al.*, 2000; and Ho, 2004), which in turn leads to DNA damage and to protein and lipid peroxidation. Since both Urm1 and Zap1 play a vital role in ROS defense (Goehring *et al.*, 2003a; Khoshnood *et al.*,

2016; Wu *et al.*, 2007, 2009; and MacDiarmid *et al.*, 2013), we wondered if urmylation is changed under zinc-limiting condition. Therefore, *Δurm1* cells expressing ^{HisStrep}Urm1 under the constitutive *ADH1* promoter were grown with NEM, the oxidizing reagent tert-Butyl hydroperoxide (t-BOOH) or with a limiting zinc medium (LZM) (Fig. 3-5). Even though Zap1 urmylation does not seem to be increased by zinc-deficiency (data not shown), more substrates are urmylated upon zinc-deficient conditions. While cells grown in YPD show few urmylated substrates, cells grown in LZM showed increased amounts of Urm1-conjugates indicating that zinc deficiency might be an additional trigger for urmylation. NEM and t-BOOH served as controls as it is known that these substances strongly induce urmylation.

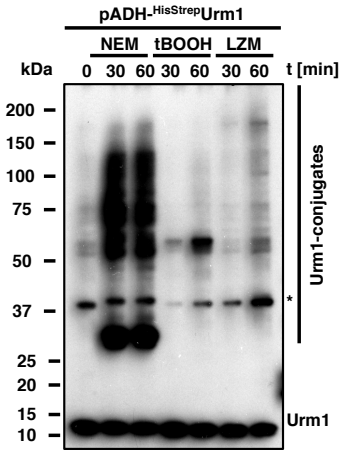

Figure 3-5. Effects of oxidative stress and low zinc conditions on Urm1 conjugation.
Cells expressing ^{HisStrep}Urm1 under the control of the constitutive *ADH1* promoter were grown in YPD and switched to 10 mM NEM, 1.5 mM t-BOOH or zinc-limiting LZM containing 3 µM $ZnCl_2$. Samples were then taken after the indicated time points and subjected to immunoblotting using Urm1-specific antibodies to detect Urm1. Asterisk indicates cross-reactive bands.

3.2.4 Role of Urm1 in zinc-deficiency

Since several urmylated substrates accumulate under zinc-limiting conditions, we next investigated, if cells lacking Urm1 or Uba4 were sensitive under zinc deficiency. Therefore, cells were grown on either zinc-replete (+Zn) or zinc-limiting (-Zn) medium (Fig. 3-6A). Cells lacking either Urm1 or Uba4 show a strong sensitivity towards zinc-limiting conditions. *zap1-K871R*^{HA} however showed no sensitivity towards zinc-limiting conditions. As previously shown, Zap1 levels are

lower in absence of Urm1 and in cells expressing *zap1-K871R* under zinc-replete and –limiting conditions potentially caused by a decrease in transcriptional activity of Zap1 and/or due to a destabilization of Zap1 caused by lack of Zap1 urmylation (Fig. 3-4A). Hence, we wondered whether constitutively urmylated Zap1 in *Δurm1*, *Δuba4* and *zap1-K871R* improves the stability Zap1, which in turn reverts the sensitivity of cells lacking Urm1, Uba4 and cells expressing *zap1-K871R*. To mimic a constitutively urmylated Zap1 species, the fusion protein *zap1-urm1ΔGG*^{HisHA} was constructed and integrated into the endogenous *ZAP1* locus (or *ZAP1-K871R* locus) in WT, *Δurm1* and *Δuba4* cells. To assess the expression of *zap1-urm1ΔGG*^{HisHA} in WT, *Δurm1*, *Δuba4* and *zap1-K871R*, protein levels of *zap1-urm1ΔGG*^{HisHA} are evaluated (Fig. 3-6B). In contrast to the lowered levels of Zap1^{HA} in *Δurm1* and in *zap1-K871R*^{HA} expressed in WT (Fig. 3-4A), *zap1-urm1ΔGG*^{HisHA} levels are comparable between WT, *zap1-K871R* and *Δurm1* cells. However, *zap1-urm1ΔGG*^{HisHA} levels are lower in *Δuba4* cells compared to WT. Cell-growth of the above-mentioned strains expressing *zap1-urm1ΔGG*^{HisHA} are subsequently tested on zinc-replete and -limiting conditions (Fig. 3-6A). In contrast to the zinc sensitivity of *Δurm1* and *Δuba4*, *Δurm1* and *Δuba4* expressing of *zap1-urm1ΔGG*^{HisHA} show no or slight sensitivity to zinc-limiting conditions, respectively. This finding suggests that Urm1-modification of Zap1 is vital for cell survival under zinc deficiency. Previous studies indicate that Zap1 plays a role in oxidative stress tolerance by activating the thioredoxin peroxidase Tsa1 and the cytosolic catalase Ctt1 (Wu *et al*., 2007, 2009). To test whether Zap1 and Zap1 urmylation protect cells under oxidative stress, we spotted cells in serial dilution on YPD and on YPD containing t-BOOH (Fig 3-6C). Cells lacking Zap1 show an equivalent sensitivity to t-BOOH seen in *Δurm1*, *Δuba4* and *Δzap1 Δurm1*. Yet, *zap1-K871R*^{HA} showed no sensitivity to t-BOOH. Expression of *zap1-urm1ΔGG*^{HisHA} could partially rescue the sensitivity of *Δurm1*, but not in cells lacking Uba4, suggesting that Urm1-modification of Zap1 plays a vital role in the cell survivability under zinc-limiting conditions, but to a lesser extent under oxidative stress. Though the expression of *zap1-urm1ΔGG*^{HisHA} in *Δurm1* fully or partially reverts the sensitivity to zinc deficiency and oxidative stress, respectively, cells lacking Uba4 expressing *zap1-urm1ΔGG*^{HisHA} are partially sensitive to zinc-limiting conditions and strongly

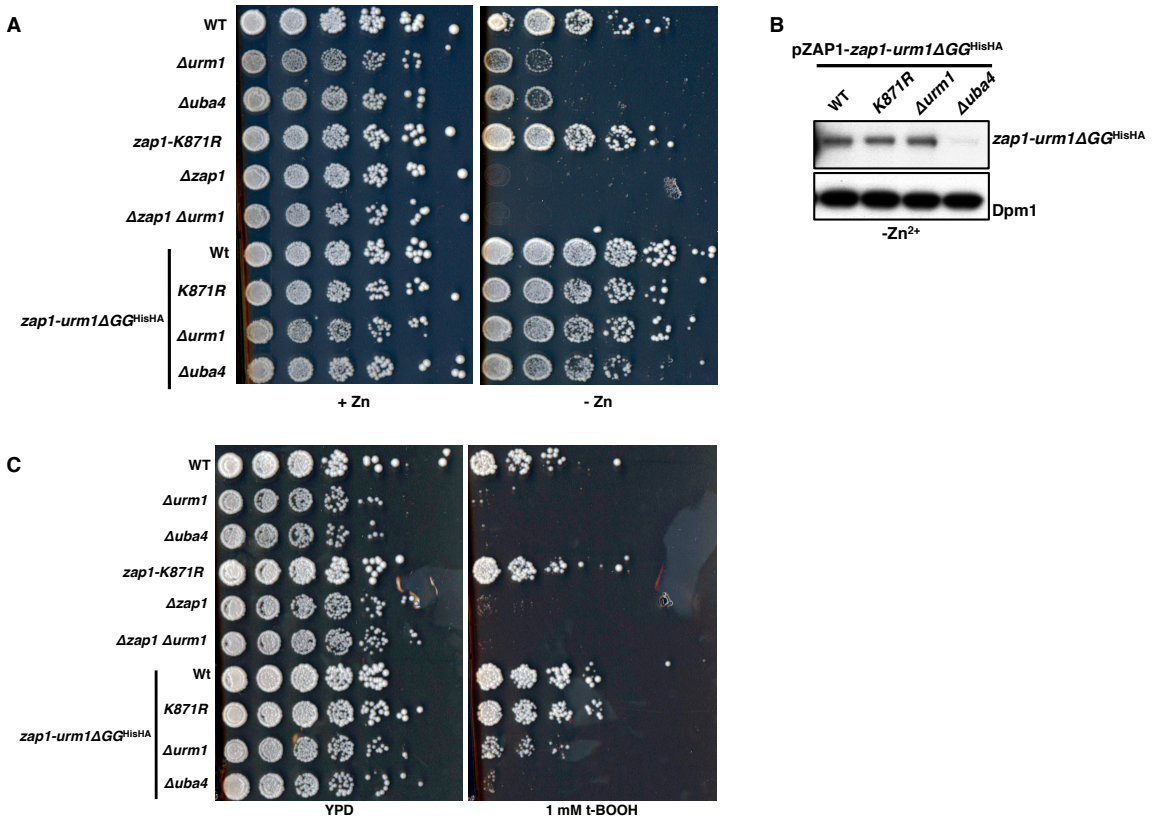

Figure 3-6. Epistatic analysis of *Δurm1*, *Δuba4*, *Δzap1*, zap1 K871R and *zap1-urm1ΔGG*^{HisHA} under zinc-limiting and oxidative stress-induced conditions.

(A) WT strain or strains lacking Urm1, Uba4, Zap1 or combinations expressing either Zap1 or *zap1-urm1ΔGG*^{HisHA} under the endogenous *ZAP1* promoter were grown over night. To create *zap1-urm1ΔGG*^{HisHA}, *urm1ΔGG*^{HisHA}::*LEU2* was integrated to the C-terminal *ZAP1* locus. Five-fold serial dilutions of cells (adjusted to OD600 = 0.5) were spotted on LZM plates either containing 1 mM (+Zn) or 3 µM $ZnCl_2$ (-Zn). Plates were incubated at 30°C for 3 days. **(B)** WT, *Δurm1* and *Δuba4* cells expressing either *zap1-urm1ΔGG*^{HisHA} or *zap1 K871R-urm1ΔGG*^{HisHA} under the endogenous *ZAP1* promoter were grown in LZM with 3 µM $ZnCl_2$ (- Zn) at 30°C. Samples were subjected to immunoblotting using anti-HA antibodies to detect *zap1-urm1ΔGG*^{HisHA} or *zap1 K871R-urm1ΔGG*^{HisHA}, respectively. **(C)** WT strain or strains lacking Urm1, Uba4, Zap1 or combinations expressing either Zap1 or *zap1-urm1ΔGG*^{HisHA} under the endogenous *ZAP1* promoter were grown over night. Five-fold serial dilutions of cells (adjusted to OD600 = 0.5) were spotted on YPD plates and on YPD plates containing 1 mM t-BOOH. Plates were incubated at 30°C for 3 days.

sensitive to oxidative stress (Fig. 3-6AC). This sensitivity might stem from the significantly lower *zap1-urm1ΔGG*^{HisHA} levels *Δuba4* compared with the *zap1-urm1ΔGG*^{HisHA} levels in WT and *Δurm1*, and *zap1-K871R-urm1ΔGG*^{HisHA} expressed in WT (Fig. 3-6B).

3.2.5 Prerequisites for Zap1 urmylation

Due to the multi-layered Zap1 regulation through its own transcriptional activation via a positive auto-regulatory mechanism and as a zinc sensor, we examined the zinc-dependency of Zap1 urmylation. In zinc-replete conditions, zinc ions are able to bind residues embedded in the transactivation domains AD1 and AD2 (Fig. 3-7A, red and orange box), which in terms inhibit the transcriptional activity of Zap1. Prior studies have shown that the Zap1 truncation *zap1*$^{552\text{-}880}$ (zap1-AD2) is transcriptionally impaired, as it lacks AD1 (Bird *et al.*, 2000ab, Fig. 3-7A). Similarly, the N-terminal truncation *zap1*$^{\Delta 17\text{-}700}$ (zap1-DBD), that lacks both transactivation domains AD1 and AD2, shows no transcriptionally activity. Importantly, however, both truncations are able to bind to ZREs (Frey & Eide, 2011). To investigate whether the transcriptional activation domains are necessary for Zap1 urmylation, we constructed the zap1 truncations zap1-AD2^{HA} and zap1-DBD^{HA} using the constitutive *CYC1* promoter to bypass the transcriptional positive feedback loop (Fig. 3-7A). To see whether zap1-AD2^{HA} or zap1-DBD^{HA} were urmylated the denaturing Ni-NTA pull-down method was used to purify ^{HisStrep}Urm1 and potentially urmylated zap1-AD2^{HA} or zap1-DBD^{HA} (Fig. 3-7B). Indeed, a slower migrating urmylated species of zap1-AD2^{HA} and zap1-DBD^{HA} could be detected indicating that the activation domains AD1 and AD2 are not required for Zap1 urmylation. Since both Zap1 truncations are shown to bind to ZREs via the DNA-binding domain (DBD), we examined whether Urm1-modification of Zap1 depends on the presence of the DBD domain. Therefore, a Green fluorescent protein (GFP)-tagged C-terminal Zap1 variant under the control of *CYC1* promoter, containing the last 64 aa of Zap1 C-terminus, was integrated in WT and in *Δuba4* expressing ^{HisStrep}Urm1 (zap1-C, Fig. 3-7C). Compared to endogenous expressed

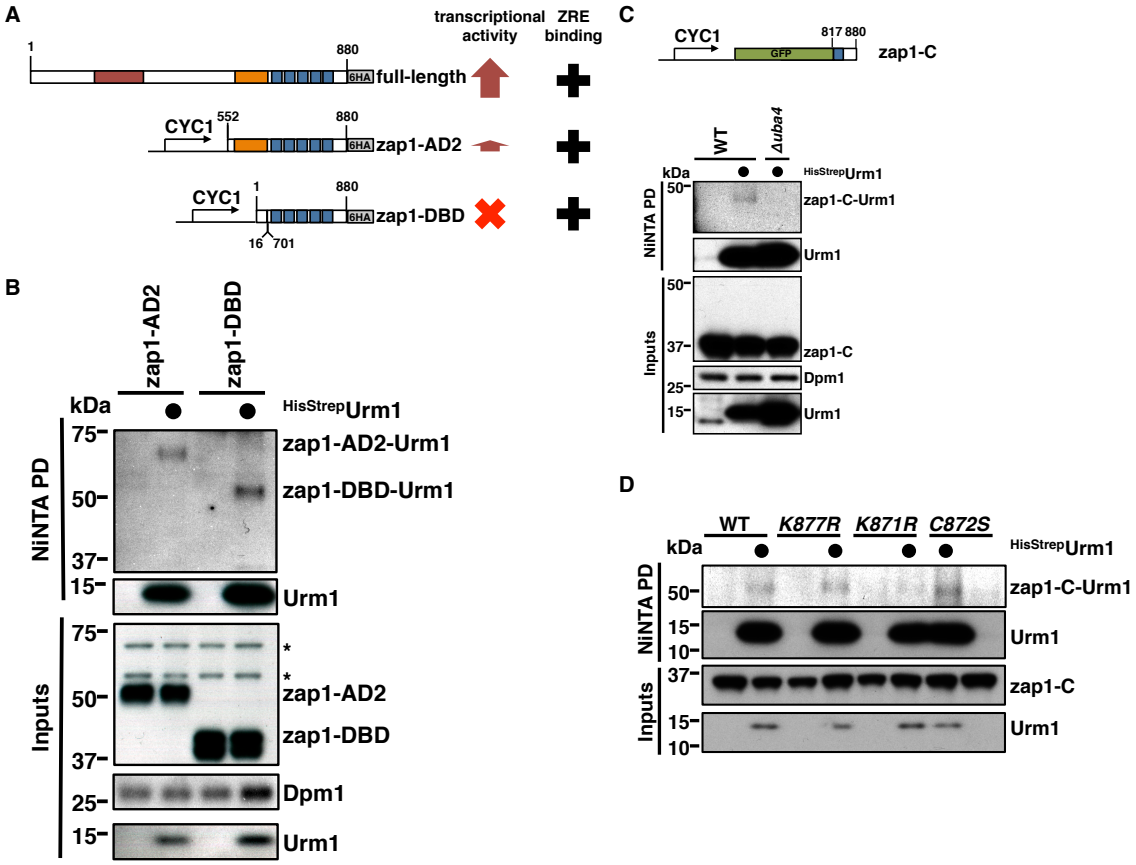

Figure 3-7. Urm1 modifies Zap1 at K871.

(A) Schematic diagram of full-length Zap1 and truncated Zap1-fragments lacking AD1 (zap1-AD2) or both activation domains (zap1-DBD). Both truncations are able to bind ZREs. However, zap1-AD2 displays low transcription activity, while zap1-DBD shows no transcriptional activity. Both constructs are expressed under the *CYC1* promoter, possess a C-terminal HA-tag and are integrated into the *LEU2* locus. Transactivation domains AD1 and AD2 are shown as red and orange boxes, respectively, while the DNA-binding domain DBD, consisting of five zinc fingers, is marked in blue boxes. **(B)** Cells expressing zap1-AD2 or zap1-DBD with His-Strep-tagged or untagged Urm1 under the control of the constitutive *ADH1* promoter were treated with 10 mM NEM for 1h at 30°C. ^{HisStrep}Urm1 was purified using a denaturing Ni-NTA pull-down to detect urmylated truncated Zap1-fragments. Samples were subjected to immunoblotting using Urm1-specific antibodies to detect ^{HisStrep}Urm1 and anti-HA antibodies to detect HA-tagged zap1-variants. Dpm1 levels serve as a loading control. **(C)** The 64 aa long C-terminal fragment zap1-C, which lacks both activation domains and the DNA-binding domain, was expressed under the *CYC1* promoter. zap1-C was N-terminally GFP-tagged and integrated into the *LEU2* locus. Urmylated zap1-C species was detected by Ni-NTA pull-down of either HisStrep-tagged or untagged Urm1. Prior to Ni-NTA pull-down, cells were treated with 10 mM NEM for 1h at 30°C. Samples were subjected to immunoblotting using Urm1-specific antibodies to detect ^{HisStrep}Urm1 and anti-GFP antibodies to detect zap1-C. Dpm1 levels serve as a loading control. **(D)** Urm1 modifies zap1-C at K871. A lysine to arginine mutation of the neighboring lysine residue *zap1-C-K877R* or a cysteine to serine substitution of *zap1-C-C872S* did not abolish urmylation. However, *zap1-C-K871R* was no longer urmylated.

full-length Zap1, ^{GFP}zap1-C fragment protein levels are higher and affected from the presence or absence of Uba4. Thus, we were able to use these novel strains and test the influence of Uba4 on urmylation of Zap1. Using the denaturing Ni-NTA pull-down method to purify ^{HisStrep}Urm1, a slower migrating urmylated ^{GFP}zap1-C species was detected in WT cells expressing ^{GFP}zap1-C and ^{HisStrep}Urm1, but not in cells lacking Uba4, indicating that Zap1 urmylation is Uba4-dependent (Fig. 3-7C). According to previous experiments we generated ^{GFP}zap1-C variants, which possess lysine to arginine substitutions at either K871, the neighboring K877 or a cysteine to serine substitution at C872 (Fig. 3-7D). ^{GFP}zap1-C and all ^{GFP}zap1-C variants, but ^{GFP}*zap1-C K871R*, were urmylated. This result implies that the Urm1-conjugation machinery is able to specifically recognize and urmylate the predicted acceptor lysine residue K871 in the zap1-C fragment and possibly urmylate full-length Zap1 at K871.

3.2.6 Zap1 urmylation occurs in the cytoplasm

Next we investigated whether Zap1 urmylation occurs in specific compartments (e.g. nucleus or cytoplasm) or in the entire cell. Previous microscopic and subcellular fractionation assays show that the localization of overexpressed Zap1 under the inducible *GAL* promoter is nuclear (Bird *et al.*, 2000, Frey *et al.,* 2011). However, overexpression of Zap1 results in zinc-independent transcriptional activation of target genes such as *ZRT1* due to the zinc-independent and constitutive binding of Zap1 to the chromatin via the ZREs (Frey *et al.*, 2011). To examine the localization of endogenous Zap1, we integrated a GFP-tag at the C-terminus of the *ZAP1* locus (Fig. 3-8A). Zap1^{GFP} was predominantly localized at the cytoplasm as speckled dots and only a fraction of Zap1^{GFP} was found in the nucleus. As previously demonstrated, zap1-AD2 also localized in the cytoplasm as speckled dots and to the nucleus (Bird *et al.*, 2000). We therefore speculated if a nuclear localization signal (NLS) is localized within the C-terminus of Zap1. Using NLS-Mapper (http://nls-mapper.iab.keio.ac.jp/, Kosugi *et al.*, 2009), we were able to identify a putative bipartite NLS at 847-876 aa within Zap1. Consequently, we

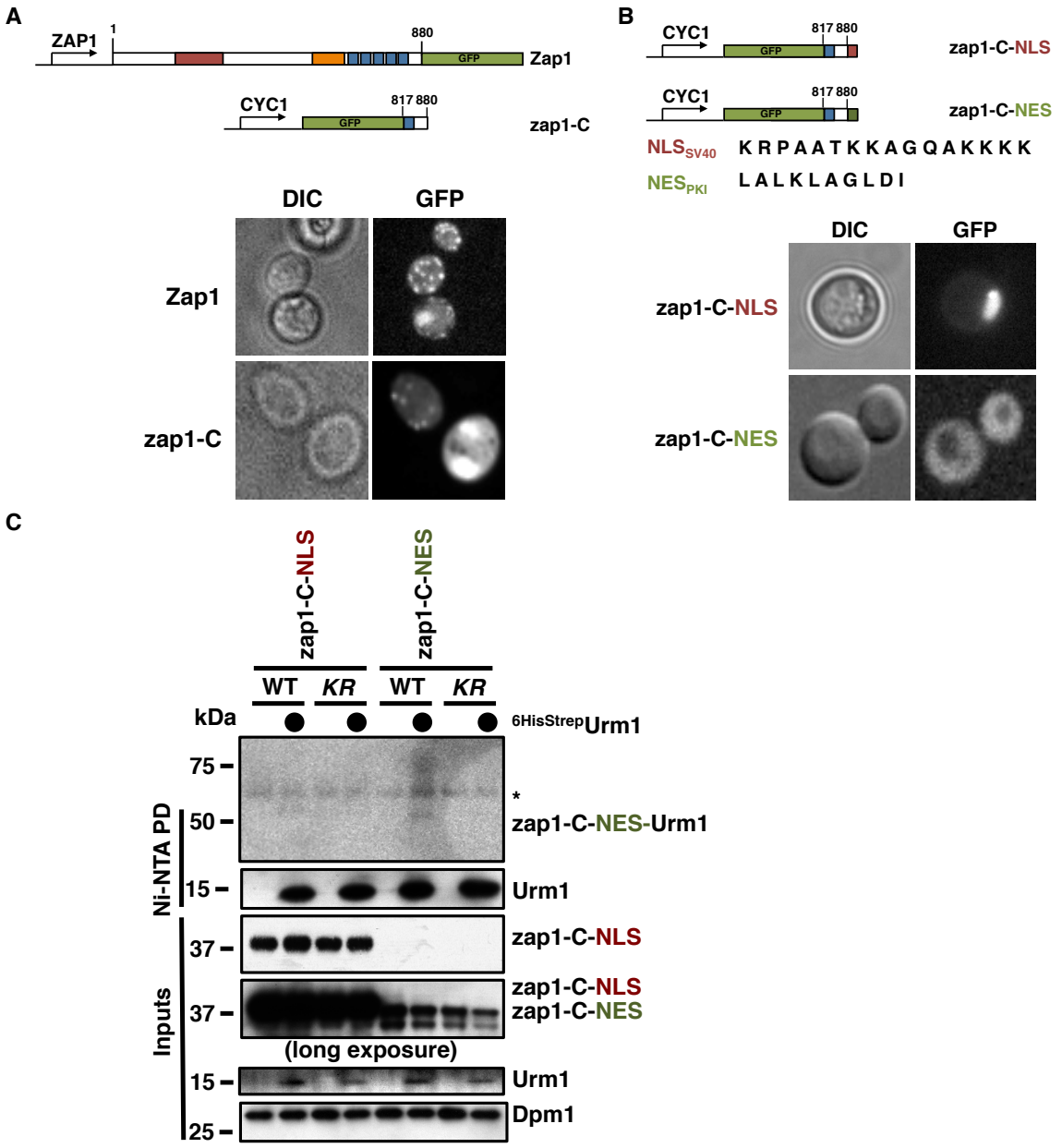

Figure 3-8. Zap1 urmylation occurs in the cytoplasm.

(A) Live cell fluorescence microscopy of yeast cells expressing either C-terminal GFP-tagged Zap1 with *ZAP1* promoter or N-terminal GFP-tagged zap1-C with *CYC1* promoter. Cells were grown exponentially in SC medium at 30°C and images were taken using a fluorescence microscopy. **(B)** Localization of nuclear or cytoplasmic zap1-C. zap1-C under the control of the *CYC1* promoter was fused to the SV40 bipartite NLS (zap1-C-NLS, KRPAATKKAGQAKKKK) or to the PKI NES (zap1-C-NES, LALKLAGLDI) and integrated to the *LEU2* locus. Cells were grown exponentially in SC medium at 30°C and images were taken using a fluorescence microscopy. **(C)** Cells expressing either the nuclear zap1-C-NLS or cytoplasmic zap1-C-NES with His-Strep-tagged or untagged Urm1 were treated with 10 mM NEM for 1h at 30°C. ^{HisStrep}Urm1 was purified using a denaturing Ni-NTA pull-down to detect urmylated zap1-C variants. zap1-C-NLS *KR* and zap1-C-NES *KR* possess a K871R mutation. Samples were subjected to immunoblotting using Urm1-specific antibodies to detect ^{HisStrep}Urm1 and anti-GFP antibodies to detect zap1-C. Dpm1 levels serve as a loading control. The asterisk denotes a cross-reactive band.

looked for the localization of the ^{GFP}zap1-C (Fig. 3-8A). Similar to full-length Zap1^{GFP}, ^{GFP}zap1-C was predominantly localized in the cytoplasm as speckled dots and was rarely found in the nucleus. This finding coincided with recent screens for subcellular localization of proteins (Chong et al., 2015 and Koh et al., 2015). In these studies, Zap1 was predominantly localized in the cytoplasm under steady-state conditions. Since Zap1^{HA} and ^{GFP}zap1-C share an analogous nucleocytoplasmic localization, we wondered whether urmylation takes place in the nucleus, cytoplasm or in both compartments. To this end zap1-C variants were constructed that would be exclusively localized to the nucleus or in the cytosol. Therefore we fused SV40 bipartite nuclear localization signal (NLS_{SV40}, KRPAATKKAGQAKKKK) or the protein kinase inhibitor nuclear export signal (NES_{PKI}, LALKLAGLDI) to the C-terminus of zap1-C (Fig. 3-8B). All these reporter constructs were under the control of the *CYC1* promoter and were integrated to the *LEU2* locus. While ^{GFP}zap1-C-NLS was largely localized to the nucleus, ^{GFP}zap1-C-NES was homogenously distributed throughout the cells (Fig. 3-8C). To evaluate whether the nuclear or cytoplasmic ^{GFP}zap1-C variant was urmylated, cells expressing ^{HisStrep}Urm1 and ^{GFP}zap1-C-NLS or ^{GFP}zap1-C-NES were subjected to denaturing Ni-NTA pull-down of ^{HisStrep}Urm1. Both cytoplasmic ^{GFP}zap1-C-NES and nuclear ^{GFP}zap1-C-NLS were urmylated (Fig. 3-8C).

3.3 Function of Zap1 urmylation

3.3.1 Zap1 stability is increased in the presence of Zap1 urmylation

After showing that Urm1 covalently modifies Zap1 in the cytoplasm we studied the cellular consequence of Zap1 urmylation. Initially, we could observe that Zap1 urmylation correlates with Zap1 protein levels. We already showed that this was partially due to increased transcription activity (Fig. 3-3B and Fig. 3-4AB). We now analyzed whether urmylation could have an additional effect on protein stability. To this end, we constructed yeast strains that express Zap1^{HA} under the control of the constitutive *CYC1* promoter that lacked the *ZAP1* ZRE in the sequence upstream of the *CYC1* promoter and that were integrated to the *LEU2* locus. To test whether urmylation stabilizes Zap1, we first investigated degradation kinetics of full-length

Zap1^{HA} under the control of the *CYC1* promoter by utilizing the cycloheximide (CHX) shut-off method in WT, *Δurm1 and Δuba4* cells (Fig. 3-10A). In contrast to WT cells, Zap1^{HA} was degraded with slightly faster kinetics in cells lacking Urm1 and Uba4. Since GFP is a very stable protein that is resistant to proteases and ubiquitin-dependent degradation, putative degrons were frequently fused to GFP in order to destabilize the GFP-fusion protein (Chalfie *et al.*, 1994 and Li *et al.*, 1998). Therefore, we examined the degradation kinetics of GFP and ^{GFP}zap1-C. Since ^{GFP}zap1-C was urmylated at K871, the degradation kinetics of ^{GFP}*zap1-C-K871R* was tested as well (Fig. 3-10B). Though, ^{GFP}zap1-C was degraded over time, ^{GFP}zap1-C degradation kinetics was slower than full-length Zap1^{HA}. In absence of urmylation (^{GFP}zap1-C *Δurm1* and ^{GFP}*zap1-K871R*) ^{GFP}zap1-C was degraded with faster kinetics. Since the Zap1^{HA} and zap1-C^{GFP} degradation in absence of urmylation was marginally faster, we wondered if the non-urmylated nuclear Zap1 pool masks the urmylated cytoplasmic pool of Zap1.

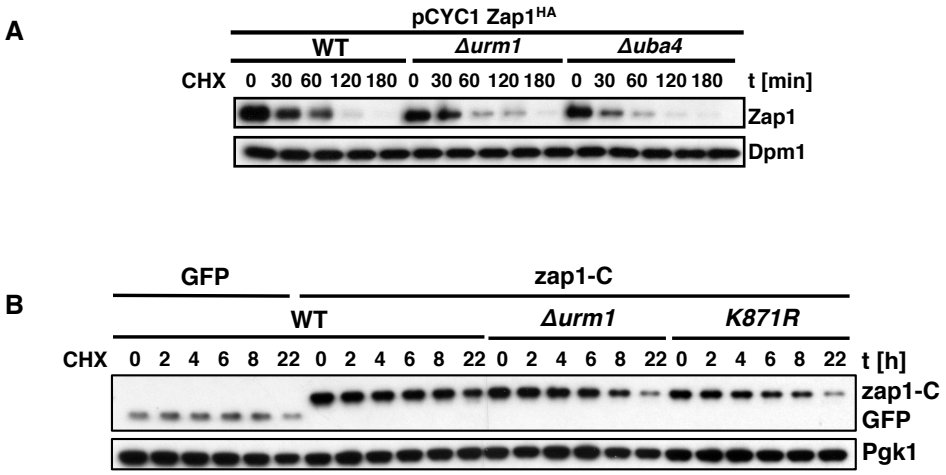

Figure 3-10. Zap1 is degraded with faster kinetics in absence of urmylation.

(A) Degradation kinetics of *Δurm1* and *Δuba4* cells expressing Zap1^{HA} under the control of the constitutive *CYC1* promoter. Exponentially grown cells incubated in YPD at 30°C were treated with CHX to inhibit translation. Samples were then taken after the indicated time points and subjected to immunoblotting using anti-HA antibodies to detect Zap1^{HA}. Dpm1 levels serve as a loading control. **(B)** WT and *Δurm1* expressing GFP, ^{GFP}zap1-C or ^{GFP}*zap1-C-K871R* under the control of the constitutive *CYC1* promoter were incubated in YPD at 30°C. CHX was added to the cultures to inhibit translation. Samples were then taken after the indicated time points and subjected to immunoblotting using anti-GFP antibodies to detect GFP, ^{GFP}zap1-C and ^{GFP}*zap1-C-K871R*, respectively. Pgk1 levels serve as a loading control.

To investigate the degradation kinetics of the non-urmylated nuclear pool and the urmylated cytoplasmic Zap1 pool, we utilized the CHX shut-off experiment to study the degradation kinetics of ^{GFP}zap1-C-NLS (Fig. 3-11A) and ^{GFP}zap1-C-NES (Fig. 3-11B). Initial experiments show that ^{GFP}zap1-C-NLS and ^{GFP}*zap1-C-K871R-NLS* were stable over a period of ≥4h in all cell lines (data not shown). Cells expressing ^{GFP}zap1-C-NES and ^{GFP}*zap1-C-NES K871R* were rapidly degraded within 30 min. We therefore shortened the CHX shut-off experiment and examined the degradation kinetics of both constructs within 25 min. While ^{GFP}zap1-C-NLS was stable over time, full-length ^{GFP}zap1-C-NES was rapidly and completely degraded into a shorter N-terminal degradation intermediate at 25 min. Remarkably, ^{GFP}*zap1-C-NES K871R* degraded even faster than ^{GFP}zap1-C-NES indicating that Zap1 urmylation enhances Zap1 stability.

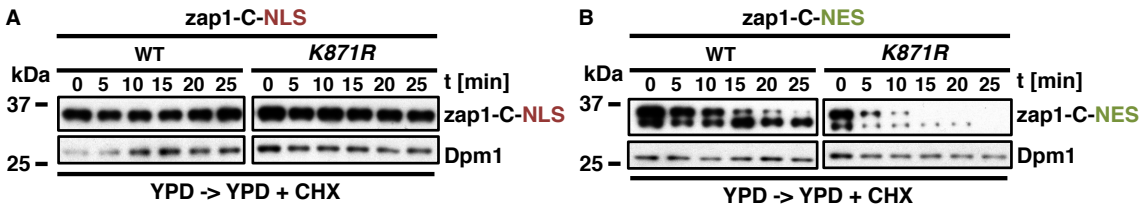

Figure 3-11. Zap1 C-terminus contains a cytoplasmic, Urm1-dependent degron.
(A) Cells expressing ^{GFP}zap1-C-NLS and ^{GFP}zap1-C-NLS *K871R* under the control of the constitutive *CYC1* promoter were incubated in YPD at 30°C. CHX was added to the cultures to inhibit translation. Samples were then taken after the indicated time points and subjected to immunoblotting using anti-GFP antibodies to detect ^{GFP}zap1-C-NLS and ^{GFP}zap1-C-NLS *K871R*, respectively. Dpm1 levels serve as a loading control. **(B)** Cells expressing ^{GFP}zap1-C-NES and ^{GFP}zap1-C-NES *K871R* under the control of the constitutive *CYC1* promoter were incubated in YPD at 30°C. CHX was added to the cultures to inhibit translation. Samples were then taken after the indicated time points and subjected to immunoblotting using anti-GFP antibodies to detect ^{GFP}zap1-C-NES and ^{GFP}*zap1-C-NES K871R*. Dpm1 levels serve as a loading control.

Prior experiments showed that overexpression of Urm1 not only leads to an increase in free Urm1, but also an overall increase in Urm1-conjugates (data not shown). Urmylation significantly increased when replacing the endogenous *URM1* promoter to the inducible *GAL1* promoter (Fig. 3-12A). We therefore asked whether a pulse of galactose-induced Urm1 would increase the overall Zap1^{HA} by putatively increasing the urmylated Zap1 pool. To this end, we utilized cells expressing Zap1^{HA} under the *CYC1* promoter together with the inducible Urm1 under the *GAL1* promoter (Fig. 3-12A). Remarkably, overall Zap1^{HA} level was

elevated in galactose-induced cells (Fig. 3-12A). Hence, we speculated that the elevated Zap1^{HA} level was due to Zap1 urmylation triggered by a burst of galactose-induced Urm1 expression. To exclude that the elevated Zap1^{HA} level in presence of galactose-induced Urm1 was due to improved Zap1 transcription or translation, we utilized the CHX shut-off experiment to determine Zap1^{HA} degradation kinetic of cells, which were grown either with (+) or without (-) galactose for 3h at 30°C (Fig. 3-12B). Intriguingly, while Zap1^{HA} was entirely

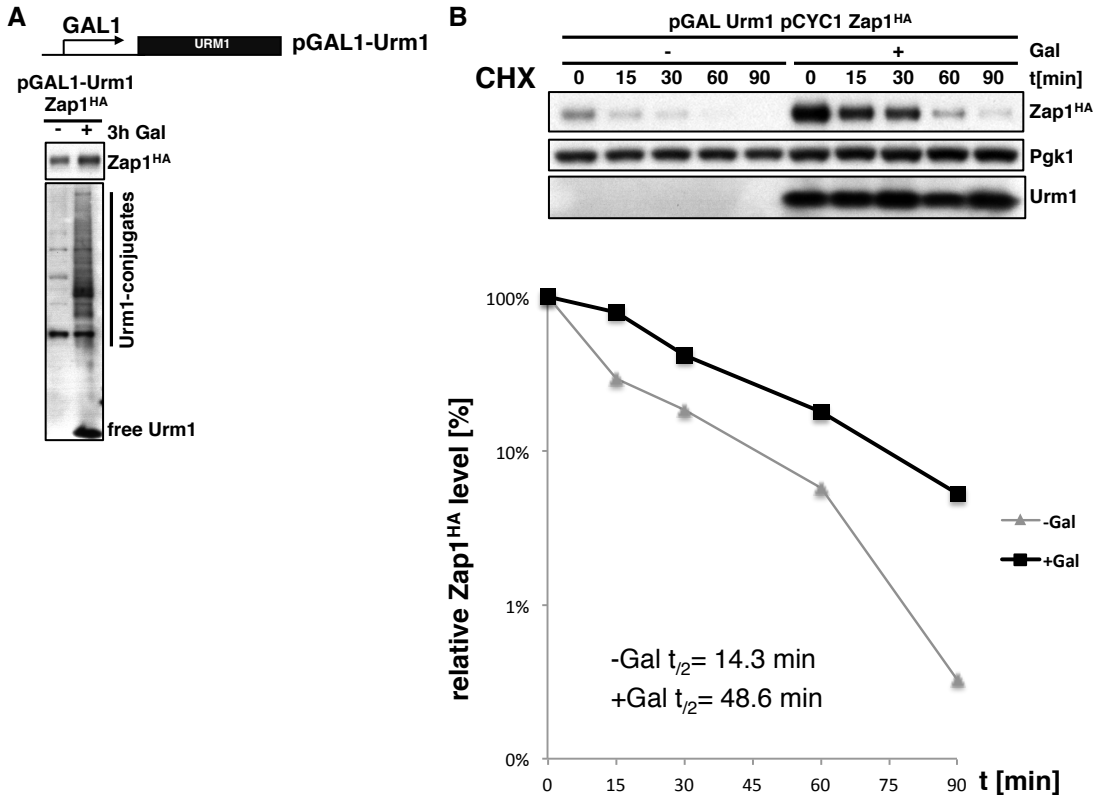

Figure 3-12. Elevated Urm1 levels lead to Zap1 stabilization.

(A) Overview of Urm1 under the control of the inducible *GAL1* promoter. Upon galactose-induced overexpression of Urm1 Zap1^{HA} protein levels are elevated. Cells expressing Zap1^{HA} and Urm1 under the control of the inducible *GAL1* promoter were grown exponentially in YPR for 4.5h. Galactose was added to the medium and incubated for 3h to induce Urm1. Samples were collected and subjected to immunoblotting using anti-HA antibodies and Urm1-specific antibodies to detect Zap1^{HA} and Urm1, respectively. **(B)** Zap1 degradation rate is decreased in presence of elevated Urm1 levels. Cells expressing Zap1^{HA} and Urm1 under the control of the inducible *GAL1* promoter were grown exponentially in YPR for 4.5h. Galactose was added to the medium and incubated for 3h to induce Urm1. CHX was then added to the cultures to inhibit translation. Samples were then taken after the indicated time points and subjected to immunoblotting using anti-HA antibodies and Urm1-specific antibodies to detect Zap1^{HA} and Urm1, respectively. Pgk1 levels serve as a loading control. Quantification of Zap1 degradation kinetics and half-life are shown below. Values are mean for n=2.

degraded after 90 min in cells grown without galactose (-Gal half-life $t_{1/2}$=14.3 min), Urm1-inducing cells showed a notable delay in Zap1^{HA} degradation kinetics (+ Gal half-life $t_{1/2}$=48.6 min) (Fig. 3-12B). This finding suggests that a short overexpression of Urm1 was able to protect Zap1^{HA} from degradation.

3.3.2 Ubiquitin proteasome-dependent degradation of Zap1

As shown previously, Zap1 is a highly unstable protein that is rapidly degraded in an Urm1-dependent manner. We therefore investigated the nature of Zap1 degradation in order to understand how Zap1 urmylation could positively influence Zap1 stability. Earlier studies showed that yeast cells carrying the heat-sensitive, proteasomal mutant *cim3-1* grown under restrictive temperatures caused a cell cycle arrest at G2/M and an accumulation of proteasomal substrates (Ghislain *et al.*, 1993). To investigate if degradation of Zap1 is proteasomal dependent, the degradation kinetics of Zap1^{HA} under the constitutive *CYC1* promoter were tested in WT, *cim3-1* and *Δurm1 cim3-1* cells (Fig 3-13). Zap1^{HA} expressed in *cim3-1* and *cim3-1 Δurm1* was strongly stabilized. We therefore conclude that degradation of Zap1 is mediated via the proteasome. To assess, if the proteasomal degradation of Zap1 was mediated by Zap1 ubiquitination, we examined whether the C-terminus of Zap1 was polyubiquitinated. Using an immunoprecipitation (IP) method to purify GFP and ^{GFP}zap1-C, the eluates were probed with anti-ubiquitin antibodies (Fig. 3-14A). We could detect faint bands of ubiquitin in mock and GFP samples, whereas several higher migrating bands corresponding to ubiquitinated

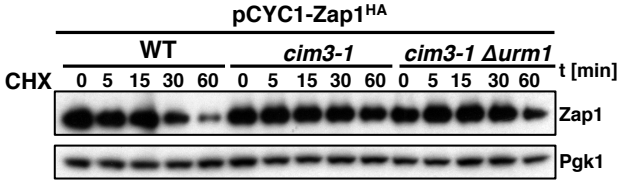

Figure 3-13. Zap1 is degraded via the ubiquitin-proteasome system.

WT, *cim3-1* and *cim3-1 Δurm1* expressing Zap1^{HA} under the control of the constitutive *CYC1* promoter were first grown to log phase at 25°C and incubated under the non-permissive temperature of 37°C for 1.5h to functionally inactivate the proteasome in *cim3-1* cells. CHX was added to the cultures to inhibit translation.

Samples were then taken after the indicated time points and subjected to immunoblotting using anti-HA antibodies to detect Zap1^{HA}. Pgk1 levels serve as a loading control.

species were detected in the immunoprecipitated ^{GFP}zap1-C sample indicating that the C-terminus of Zap1 is ubiquitinated. Next, ^{GFP}zap1-C-NLS and ^{GFP}zap1-C-NES were immunoprecipitated under denaturing conditions and probed for ubiquitin using anti-ubiquitin antibodies (Fig. 3-14B). Compared to ^{GFP}zap1-C-NLS, a high amount of ubiquitin was co-immunoprecipitated with ^{GFP}zap1-C-NES. Since we could not IP ^{GFP}zap1-C-NES in equimolar amounts among all strains, we were unable to conclusively discern whether Zap1 urmylation influences Zap1 ubiquitination in this experimental setup.

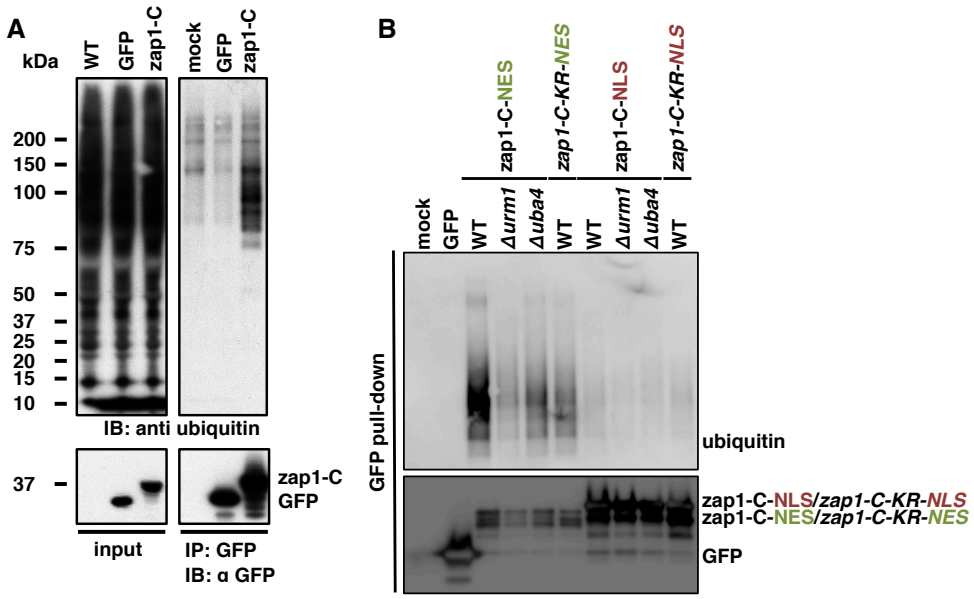

Figure 3-14. ^{GFP}zap1-C and the cytoplasmic ^{GFP}zap1-C-NES are strongly ubiquitylated.

(A) WT cells (mock) and cells expressing GFP or GFP-tagged zap1-C were grown exponentially in YPD at 30°C and subjugated to immunoprecipitation of GFP and ^{GFP}zap1-C using GFP-Trap. Samples were subjected to immunoblotting using anti-GFP antibodies to detect GFP and ^{GFP}zap1-C and anti-ubiquitin antibodies to detect ubiquitinated substrates. **(B)** Cytoplasmic ^{GFP}zap1-C-NES is strongly ubiquitylated, but not the nuclear ^{GFP}zap1-C-NLS. WT cells (mock) and WT, *Δurm1*, *Δuba4*, *cells* expressing either GFP, ^{GFP}zap1-C-NES, ^{GFP}zap1-C-NLS or their respective KR mutant counterparts, were grown exponentially in YPD at 30°C and subjugated to immunoprecipitation of GFP and ^{GFP}zap1-C using GFP-Trap. Samples were subjected to immunoblotting using anti-GFP antibodies to detect GFP, ^{GFP}zap1-C-NES and ^{GFP}zap1-C-NLS. Anti-ubiquitin antibodies were used to detect ubiquitinated substrates.

3.3.3 Identification of a Zap1-specific E3 ligase

As ^{GFP}zap1-C and the cytoplasmic ^{GFP}zap1-C-NES were shown to be highly ubiquitinated, we sought to identify the responsible E3 ligase. For this reason, we immunoprecipitated ^{GFP}zap1-C and ^{GFP}*zap1-C-K871R* (Fig 3-15, left) and investigated samples by LC-MS/MS analysis (Fig 3-15, right). Due to a contamination of the ^{GFP}*zap1-C-K871R* sample with ^{GFP}zap1-C proteins possibly during sample preparation, an examination on the differences between both samples was not possible. Nonetheless, the interaction partners of ^{GFP}zap1-C could be analyzed using immunoprecipitated ^{GFP}zap1-C samples after a LC-MS/MS analysis. Alongside the identification of Urm1 and Uba4, we could co-purify most of the Doa10 complex (i.e. Doa10, Cue1, Rad23, Ubx2, Ufd2, Npl4 and Cdc48) in the ^{GFP}zap1-C samples. Interestingly, it was previously shown that the E3 ligase Doa10 together with the ER-associated intramembrane protease Ypf1 and the ERAD-factor Dfm1 could recognize and degrade the Zap1-target gene *ZRT1* in a zinc-dependent manner (Avci *et al.*, 2014). In order to verify that the

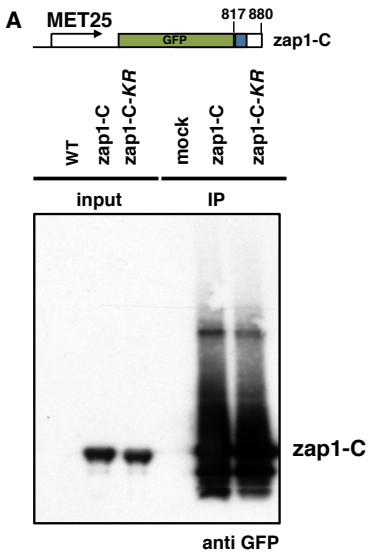

Gene names	Protein names	Intensity
PMA1;PMA2	Plasma membrane ATPase 1;Plasma membrane ATPase 2	2,14E+10
zap1-C		**1,93E+10**
ADH1	Alcohol dehydrogenase 1	3,89E+09
SSA2	Heat shock protein SSA2	2,27E+09
FOL2	GTP cyclohydrolase 1	1,38E+09
TEF1	Elongation factor 1-alpha	1,21E+09
SSB2	Heat shock protein SSB2	9,64E+08
TIF1	ATP-dependent RNA helicase eIF4A	9,20E+08
URA2	Protein URA2	9,06E+08
CDC48	**Cell division control protein 48**	**3,16E+08**
UFD2	**E4 ubiquitin-protein ligase UFD2**	**1,89E+06**
UBX2	**UBX domain-containing protein 2**	**2,23E+06**
UBR1	**E3 ubiquitin-protein ligase UBR1**	**6,00E+06**
RAD23	**UV excision repair protein RAD23**	**9,76E+06**
NPL4	**Nuclear protein localization protein 4**	**9,30E+05**
DOA10	**ERAD-associated E3 ubiquitin-protein ligase DOA10**	**2,93E+06**
CUE1	**Coupling of ubiquitin conjugation to ER degradation protein 1**	**1,41E+05**
UBA4	**Adenylyltransferase and sulfurtransferase UBA4**	**2,35E+06**
URM1	**Ubiquitin-related modifier 1**	**5,24E+05**

Figure 3-15. Putative interaction partners of zap1-C.

WT cells (mock) and cells expressing GFP-tagged zap1-C or *zap1-C-KR* under the control of *MET25* promoter were immunoprecipitated using GFP-Trap to immunoprecipitate zap1-C or *zap1-C-KR* (left panel). Samples were collected and a fraction was subjected to immunoblotting using anti-GFP antibodies to detect zap1-C. The remaining sample was subjected to LC-MS/MS analysis. A list of selected, putative zap1-C interaction partners were listed with their respective peptide intensities (right).

Doa10 complex was responsible for mediating the ubiquitin-dependent degradation of Zap1; we examined the degradation kinetics of WT, *Δdoa10* and *cdc48-3* cells expressing Zap1 under the control of the constitutive *CYC1* promoter using the CHX shut-off method (Fig. 3-16A). Degradation of $Zap1^{HA}$ in cells lacking Doa10 and in *cdc48-3* cells was either delayed or completely abolished, respectively. Analogously, we tested if the delay in $Zap1^{HA}$ degradation in *Δdoa10* and *cdc48-3* cells could be attributed to defective degradation of the cytoplasmic Zap1 pool. We therefore utilized the CHX shut-off experiment to monitor the degradation kinetic of ^{GFP}zap1-C-NES in WT, *Δdoa10* and *cdc48-3* cells (Fig. 3-16B). ^{GFP}zap1-C-NES degradation was completely blocked in *Δdoa10* and strongly delayed in *cdc48-3* cells. Intriguingly, ^{GFP}zap1-C-NES was completely stabilized in *Δdoa10* cells. These data clearly indicate that the degradation process of cytoplasmic Zap1 works via a Doa10 and Cdc48 dependent pathway.

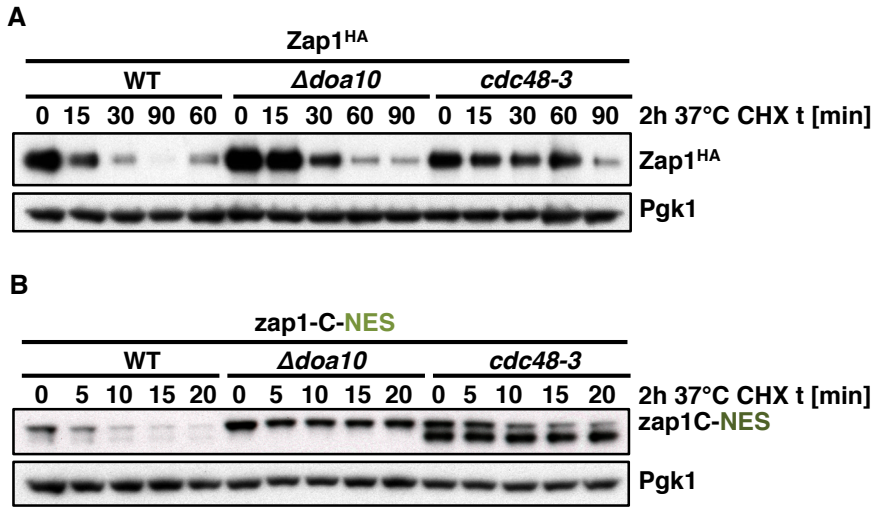

Figure 3-16. Doa10 and Cdc48 mediate the degradation of Zap1 and zap1-C.

(A) WT, *Δdoa10*, *cdc48-3* cells expressing $Zap1^{HA}$ under the control of the constitutive *CYC1* promoter were first grown at room temperature to reach logarithmic phase of growth. Prior CHX addition, the cells were incubated for 2h at non-permissive temperature (37 °C). Samples were then taken after the indicated time points and subjected to immunoblotting using anti-HA antibodies to detect $Zap1^{HA}$. Pgk1 levels serve as a loading control. **(B)** WT, *Δdoa10*, *cdc48-3* cells expressing ^{GFP}zap1-C under the control of the constitutive *CYC1* promoter were first grown at room temperature to reach logarithmic phase of growth. Prior CHX addition, the cells were incubated for 2h at non-permissive temperature (37 °C). Samples were then taken after the indicated time points and were prepared by the TCA method and subjected to immunoblotting using anti-GFP antibodies to detect ^{GFP}zap1-C. Pgk1 levels serve as a loading control.

4 Discussion

Despite recent studies about the importance of Urm1 as a sulphur carrier by thiolating U_{34} in wobble $tRNA^{Lys(UUU)}$, $tRNA^{Gln(UUG)}$, and $tRNA^{Glu(UUC)}$, little is known about Urm1 as a post-translational protein modifier. Though a few Urm1 substrates have been identified, the precise role of urmylation on these Urm1-modified substrates have yet to be elucidated.

In this thesis, we developed a quantitative proteomic approach to identify novel Urm1 substrates. We could reproducibly recognize a set of so far unknown Urm1 protein substrates. Importantly, with this strategy we were able to detect known Urm1 target proteins such as Ahp1 and Uba4, and several previously unidentified Urm1-substrates, indicating that our MS-based protocol is a potent method for the detection of Urm1 target proteins. Moreover, for the first time we could detect respective Urm1-attachment sites in a proteomic approach confirming that Urm1 is indeed a lysine-directed modifier. Among this set of proteins, we could identify and verify the zinc-dependent transcription-activator Zap1, a master zinc regulator in *S. cerevisiae,* as a lysine-directed Urm1-substrate. Urm1 modifies Zap1 at the very C-terminus (even in absence of the transcriptional-activation and chromatin-binding domain of Zap1) and seems to stabilize Zap1. Accordingly, absence of Zap1 urmylation made Zap1 more susceptible to ubiquitin-dependent degradation. While cells lacking Urm1 and Uba4 show an impaired growth under zinc-depleted conditions, these cells can be rescued by expressing a linearly fused *zap1-urm1ΔGG*, indicating that Zap1 urmylation plays an important role under zinc deficiency. In line with the zinc sensitivity of cells lacking Urm1, *ZAP1* expression and the expression of the Zap1 target gene *ZRT1* are downregulated. The following findings and their implications will be discussed below.

4.1 Strategy for the identification of novel Urm1-substrates

Deletion of the Urm1 pathway displays a plethora of stress-induced phenotypes in *S. cerevisiae* suggesting an essential role of Urm1 in stress tolerance (Furukawa *et al.*, 2000; Goehring *et al.*, 2003ab; Chen *et al.*, 2009; Khoshnood et al., 2016;

Damon *et al.*, 2015; and Schorpp, 2011). Due to the dual function of Urm1 as a protein modifier and its role in Urm1 tRNA thiolation it is difficult to connect a new identified stress-induced phenotype with a specific Urm1 activity. Many Urm1-deficient phenotypes correlate with lack of U_{34} thiolation and there are no known phenotypes that are attributed to a lack in substrate urmylation (Leidel *et al.*, 2009; data not shown). Moreover, it remains unclear, if the urmylation and sulphur donor function of Urm1 are functionally connected (Goehring *et al.*, 2003b; Schorpp, 2011; data not shown). Previous studies in *S. cerevisiae*, mammalian cells and *D. melanogaster* described very few urmylated substrates under steady-state conditions, but various oxidizing agents such as diamide, H_2O_2, *tert*-butyl hydroperoxide (t-BOOH) enhanced protein urmylation (Furukawa *et al.*, 2000; Goehring *et al.*, 2003a; Van der Veen *et al.*, 2011; and Khoshnood *et al.*, 2016). Treatment with diamide, H_2O_2 and t-BOOH yielded disparate and distinct urmylation patterns suggesting that these oxidizing agents trigger specific Urm1 conjugates. An even more potent stimulant of Urm1 conjugation is N-ethylmaleimide (NEM), which causes irreversible alkylation of free thiols (Gregory, 1955). This in turn affects all thiol-containing proteins such as the alkylation and inactivation of cysteine peptidases that are able to resolve UBLs and possibly deurmylases.

To understand the cellular functions of Urm1 and to maximize the amount of urmylated proteins in an unbiased manner, a SILAC-based quantitative proteomics approach was conducted in the presence of NEM, as it would potentially deactivate deurmylases, trapping urmylated proteins and eventually leading to the accumulation of Urm1-substrates. To exclude Urm1 interactors and to increase the amount of urmylated proteins, a denaturing Nickel-nitrilotriacetic acid (Ni-NTA) purification method or a denaturing tandem affinity purification (TAP) method was utilized. By the nature of LC-MS/MS-based sample preparation, branched peptides, among other things, are generated by tryptic digestion. These branched peptides are derived from covalently modified proteins and enable the identification of potential Urm1-targeted acceptor lysine residues. Since WT Urm1 would generate Urm1 branched peptides of considerable length, the ^{HisHA}*urm1-L96R* variant was used in order to generate Urm1-specific HGG-ε-K signature

branched peptides in a LC-MS/MS approach, which allows the recognition of urmylation sites (Fig. 3-2A). A total of 547 putative Urm1-substrates were identified in the screen using NEM-treated and untreated cells expressing ^{HisHA}*urm1-L96R*, which included the known Urm1-substrates Ahp1 and Uba4 indicating the overall reliability of the LC-MS/MS. Even though Urm1 and the Urm1-modified substrates were purified under denaturing conditions, it is still possible for high-affinity binders and contaminants to be co-purified (Lüders *et al.*, 2003; and Tagwerker *et al.*, 2006). Since both samples contain approximately equimolar amounts of high-affinity binders and contaminants, proteins with a H/L ratio of >1 and a p-value of <0.05 were inquired in order to exclude false-positives. Indeed, 21 proteins met the above-mentioned criteria and were significantly enriched in NEM-treated cells (Fig. 3-2B, Tab. 3-1). The majority of these proteins was additionally found in at least one of two confirmation experiments using *urm1-L96R* variants and was also identified in at least one of three experiments using WT Urm1, suggesting that these proteins are very likely to be true covalently modified Urm1-substrates (Tab. 3-1). Utilizing the *urm1-L96R* variants proved to be advantageous, as it allowed the identification of Urm1-specific HGG-ε-K signature peptides, which in turn lead to the recognition and characterization of Urm1-attachment sites. Thus, we were able to identify a total of 59 Urm1-attachment sites using the *urm1-L96R* variant in the total sum of three denaturing purification experiments. Consistent with previous results, we were able to identify the lysine residue K32 of the peroxiredoxin Ahp1 as the Urm1-attachment site and K41 and K107 as additional acceptor lysine (Van der Veen *et al.*, 2011, data not shown). Whether urmylation of Ahp1 at K41 and/or K107 plays a physiological role in regulating Ahp1, remains to be shown in future studies. Among the Urm1-attachment sites, we were able to discover the lysine residue 871 of the zinc-responsive transcription factor Zap1 as Urm1 acceptor site and could confirm Zap1 urmylation at K871 in western blot experiments (Tab. 3-1, Fig, 3-7D).

Altogether, the ^{HisHA}*urm1-L96R* variant appears to be an excellent tool to identify unknown Urm1-substrates under various conditions in a mass spectrometry approach. The His-tag enables Urm1-conjugates to be purified under denaturing conditions by preserving protein modifications, while non-covalent protein-protein

interactions are unstable under these conditions. In addition the L to R conversion of the *urm1-L96R* variant allows the identification of Urm1-attachment sites by trypsin digestion and creating tryptic branched peptides of Urm1-substrates that can be measured by LC-MS/MS. We were able to identify several unknown Urm1-substrates and a set of Urm1-modified proteins with their respective Urm1-attachment sites. This data could provide new insights into the role of Urm1 as a protein modifier. It remains to be seen if more proteins can be validated as *bona fide* Urm1-substrates and how these urmylated proteins impact cells *in vivo*.

4.2 Urm1 modifies Zap1

In this work, we identified the zinc-responsive transcription factor Zap1 as a novel lysine-directed Urm1-substrate using LC-MS/MS and validated Zap1 urmylation by the denaturing tandem affinity purification (TAP) method. As previously shown, substrate urmylation requires the presence of the E1-like enzyme Uba4 and an acceptor lysine within the target protein (Furukawa *et al.*, 2000; and Van der Veen *et al.*, 2011). To investigate whether Zap1 urmylation is dependent on the enzymatic activity of Uba4 and requires the acceptor lysine K871, *Δuba4* $Zap1^{HA}$ and *zap1 K871R*^{HA} strains were created in ^{HisStrep}Urm1 background. However, $Zap1^{HA}$ was unstable in these strains compared to $Zap1^{HA}$ in Wt cells making it challenging to investigate Zap1 urmylation in these strain backgrounds. To examine whether the decrease in Zap1 levels stems from the influence of Zap1 urmylation on the transcriptional activity of Zap1, the endogenous *ZAP1* promoter was replaced to various constitutive (*CYC1*, *ADH1*) and inducible promoters (*MET25*, *GAL1*) in order to discontinue Zap1 binding to *ZAP1* ZRE and hence uncoupling the autoregulatory Zap1 mechanism. Yet, Zap1 levels remained decreased in absence of Urm1, Uba4 or in cells expressing *zap1-K871R*^{HA} indicating that Urm1-conjugation to Zap1 does not influence the transcriptional activity of Zap1, but may improve Zap1 stability (data not shown). By fusing the last 64 aa of Zap1 ($zap1^{817-880}$, zap1-C) to GFP, we were able to obtain a GFP reporter that was more stable than $Zap1^{HA}$ and thus could be used in *Δuba4* strains and in cells expressing ^{GFP}*zap1-C-K871R*. Remarkably, the Urm1

conjugation machinery was able to recognize the short Zap1-specific sequence of ^{GFP}zap1-C and urmylate ^{GFP}zap1-C in an Uba4-dependent manner. Moreover, urmylation clearly depends on presence of lysine K871 of Zap1, as *^{GFP}zap1-C-K871R* was no longer urmylated. Zap1 seems to be specifically mono-urmylated at K871 although the C-terminal part of Zap1 and zap1-C contains multiple lysine residues. Zap1 (and zap1-C variant) urmylation only affects a small fraction of the total Zap1 pool independent of Zap1 expression and intracellular zinc concentrations (data not shown). This observation is especially peculiar, as the zap1-C variants are overexpressed under constitutive promoters like *CYC1* and *ADH1* indicating that the urmylated Zap1 pool is being tightly regulated. Whether this observation stems from a transient Zap1 urmylation and subsequent deurmylation or from an unknown trigger that potentiates or down regulates Zap1 urmylation is unclear.

4.2.1 Localization of Zap1-Urm1

To gain more insights into the function of Zap1 urmylation, we studied the cellular localization of urmylated Zap1. Unlike previous publications showing ^{myc}Zap1 under the control of *GAL1* promoter to be localized to the nucleus, we showed that endogenously expressed Zap1^{GFP} was predominantly localized to the cytoplasm and was rarely observed in the nucleus under zinc-replete conditions (Bird *et al.*, 2000, Fig. 3-8A). The discrepancy in localization of overexpressed ^{myc}Zap1 and endogenously expressed Zap1^{GFP} could be explained by preceding studies that showed that overexpressed Zap1 was constitutively bound to *ZRT1* ZREs, (and possibly other ZREs), independent of the cellular zinc concentration (Frey *et al.*, 2011). The constitutive binding of ^{myc}Zap1 to the chromatin could explain prior observations of a predominant nuclear ^{myc}Zap1, as overexpression of Zap1 seems to bypass the zinc-sensing ability of Zap1 and possibly enabling the translocation of Zap1. As our data concurred with recent screens for subcellular localization of yeast proteins, in which endogenous Zap1^{GFP} showed a predominantly cytoplasmic localization under zinc-replete conditions (Chong *et al.*, 2015; and Koh *et al.*, 2015), it is likely that Zap1 is retained in the cytoplasm under zinc-replete

conditions and translocated to the nucleus under zinc deficiency; a regulatory mechanism commonly observed with conditional transcription factors that are retained in the cytoplasm, but translocated to the nucleus in response to external stimuli (Johnson *et al.*, 1999; Yamaguchi-Iwai *et al.*, 2002; Cox *et al.*, 2004; and Lindert *et al.*, 2009). In fact, a recent study demonstrated that zinc-starvation promoted the gradual nuclear translocation of Zap1 over time (Kawamata *et al.*, 2017). Since ^{GFP}zap1-C is recognized by the Urm1 conjugation machinery and shows a similar cellular localization of full-length Zap1, we used this ^{GFP}zap1-C version to fuse it to sequences targeting ^{GFP}zap1-C either to the nucleus via a nuclear localization signal (NLS) or cytoplasm via a nuclear export signal (NES). Both ^{GFP}zap1-C-NES and ^{GFP}zap1-C-NLS predominantly localized into their intended cellular compartments. We could demonstrate that the cytoplasmic ^{GFP}zap1-C-NES and nuclear ^{GFP}zap1-C-NLS was urmylated. While ScUrm1 and hUrm1 are localized ubiquitously distributed within cells, ScUba4 and hUba4 are strictly located at the cytoplasm (Chowdhury *et al.*, 2012; Chong *et al.*, 2015 and Koh *et al.*, 2015). However, subcellular fractionation of human cells showed that free hUrm1 and conjugated hUrm1-substrates alike are solely found in the cytoplasm (Van der Veen *et al.*, 2011). In line with this finding, *Drosophila* Urm1 is exclusively localized at the cytoplasm (Khoshnood *et al.*, 2016). How is the predominantly nuclear ^{GFP}zap1-C-NLS still being recognized and urmylated by the cytoplasmic-localized Urm1-conjugation machinery? The urmylation machinery might target the newly translated and cytoplasmic ^{GFP}zap1-C-NLS pool. Thus, a small fraction of ^{GFP}zap1-C-NLS is being urmylated. Together, the localization studies done on the Urm1 machinery and the Urm1 conjugates as well as our data on ^{GFP}zap1-C-NES/NLS urmylation point to the urmylation of the cytoplasmic Zap1 pool.

4.2.2 Role of Zap1 urmylation

Thus far, accumulation of Urm1-modified proteins was observed upon oxidative stress implying a contribution of protein urmylation in the defense against reactive oxygen species (ROS). Another contributor for preserving the intracellular redox

homeostasis is zinc (Powell, 2000). It is believed that zinc exerts its antioxidant properties by complexation with sulfhydryl groups, which prevents ROS-induced oxidation and thus preventing formation of aberrant disulfide bonds (Eide, 2011; and Jarosz *et al.* 2017). Consequently, zinc deficiency elevates the intracellular ROS level, resulting in a higher susceptibility to ROS-induced cellular damages (Oteiza *et al.*, 2000; Ho & Ames, 2002; Wu *et al.*, 2007; and Wu *et al.*, 2009). The zinc-dependent transcription factor Zap1 is able to counteract zinc deficiency by activating zinc transporters that facilitate zinc influx (Zhao & Eide, 1996, 1997). Additionally, Zap1 activates the expression of the thioredoxin peroxidase Tsa1 and the cytosolic catalase Ctt1 (Wu *et al.*, 2007, 2009). These two proteins play a pivotal role in protecting cells from ROS under low zinc conditions. In zinc limiting conditions, sulphur assimilation is repressed in a Zap1-dependent manner (Wu *et al.*, 2009). Since both sulphur assimilation and combating oxidative stress require large amounts of NADPH, Zap1-dependent repression of the sulphur assimilation pathway results in a higher availability of NADPH to combat oxidative stress (Slekar *et al.*, 1996; and Eide, 2009). Consequently, we investigated the role of the Urm1 pathway under zinc deficiency. Remarkably, lack of Urm1 and/or Uba4 caused sensitivity towards cells grown under zinc-limiting conditions, whereas supplementing the medium with zinc reversed the growth defects. These data suggest that the observed growth defects are linked to zinc deficiency and/or its subsequent induction of oxidative stress. In addition, Urm1 adducts appeared in response to zinc deficiency, indicating that the protein-conjugation branch of Urm1 might play an important role in combating the adversary effects of zinc deficiency. Which proteins are urmylated, how urmylation of these substrates benefit cells under zinc-limiting conditions and whether the sulphur-donor branch of Urm1 acts synergistically under low zinc remains an open question.

Under zinc-limiting condition, *ZAP1* expression was significantly reduced in cells lacking urmylation, as both cells expressing *Δurm1* and *zap1-K871R* showed a comparable reduction in *ZAP1* mRNA*,* indicating that Zap1 urmylation improves the transcriptional fidelity of Zap1 and is therefore detrimental in maintaining the transcriptional autoregulation of *ZAP1*. As a consequence of the decreased *ZAP1* expression, protein levels of Zap1 were reduced in both *Δurm1* and *zap1-K871R.*

Furthermore, the reduction in *ZAP1* expression resulted in a mild reduction of the downstream target *ZRT1*, which is the primary zinc transporter in *S. cerevisiae* that is activated upon zinc deficiency. As this reduced *ZRT1* expression is most likely a secondary effect caused by a reduced *ZAP1* transcription in absence of Zap1 urmylation, it is likely that more *ZAP1* downstream targets are negatively affected by loss of Zap1 urmylation. As Zrt1 levels were reduced in *Δurm1* and *Δuba4* cells, loss of Zap1 urmylation may impair Zap1's function in zinc homeostasis (data not shown). To test whether Zap1 urmylation improves cell growth on zinc-limiting conditions, we also tested growth of cells that did not express endogenous Zap1, but the linear fused *zap1-urm1ΔGG*. This variant was used to mimic a constitutively urmylated Zap1 variant. Intriguingly, cells expressing a *zap1-urm1ΔGG* fusion, but lacking Urm1 or Uba4, were able to grow like or perhaps even slightly better than WT cells expressing *zap1-urm1ΔGG* or under zinc-limiting conditions. However, cells expressing *zap1-urm1ΔGG* lacking Urm1 and Uba4 showed growth impairment or no growth under t-BOOH induced oxidative stress. This result implies that Zap1 urmylation seems to be vital in restoring Zap1 function in zinc homeostasis, but does not contribute in ROS defense. In contrast, cells expressing *zap1-K871R* showed no growth defects under the above-mentioned conditions. How *zap1-K871R* is able to grow on zinc-limiting conditions, but *Δurm1* does not, remains ambiguous. A possible explanation for this discrepancy is that Urm1 could conjugate to neighboring lysine residues of Zap1, though no urmylation could be observed with cells expressing ^{GFP}*zap1-C-K871R* and ^{GFP}*zap1-C-NES-K871R*. Another possible explanation is that Urm1 modifies additional target proteins that are involved in zinc homeostasis, enabling these urmylated substrates to compensate the reduced functionality of unmodified Zap1/*zap1-K871R* (Fig. 3-5). Conversely, the rescue of cells lacking Urm1 and Uba4 with the expression of the Zap1-Urm1 fusion *zap1-urm1ΔGG* could stem from the fact that the entire Zap1 pool is constitutively urmylated, which might drastically enhance overall activity of Zap1 that in turn allows a more efficient response to zinc deficiency. In addition, *zap1-urm1ΔGG* could even carry out additional cellular functions that are advantageous during low zinc conditions. Prior studies showed that fusion of ubiquitin-like proteins (UBLs) such as SUMO or

ubiquitin to proteins could indeed mimic a UBL-modified form of the target protein and therefore results in a change of the target protein's properties, such as an increase in stability and solubility (SUMO, Malakhov *et al.*, 2004; and Wang *et al.*, 2010) or in the destabilization of the fused protein (ubiquitin, Bachmair *et al.*, 1986; and Cadima-Couto *et al.*, 2009). Indeed, *zap1-urm1ΔGG* levels and *zap1-K871R-urm1ΔGG* between WT and *Δurm1*, but not *Δuba4*, were comparable and could indicate to a more stabilized Zap1 variant than WT Zap1 (Fig. 3-6B). However, further studies are required to assess whether *zap1-urm1ΔGG* is indeed more stable than Zap1.

Concordant to the observed reduction of *ZAP1* mRNA in cells lacking the ability to urmylate Zap1, we could consistently observe noticeable reduction in Zap1 levels in cells lacking urmylation. This phenomenon persisted in cells lacking Urm1, Uba4 expressing Zap1 or in cells expressing *zap1-K871R* under constitutive promoters such as *CYC1*, which uncouples the autoregulatory mechanism of Zap1 and enables Zap1-indepdendent, constitutive *ZAP1* expression (Fig. 3-10A, data not shown). These findings indicate that Zap1 urmylation positively affects Zap1 stability, but not the transcriptional activity of Zap1. Since *zap1-K871R* protein levels were reduced as well and is unlikely to alter the activity of the URM1 pathway, it is improbable that the Urm1-dependent tRNA modification branch has an effect on Zap1 translation and consequently on Zap1 protein level. Since the translation of a subset of genes enriched for AAA, CAA and GAA codons is impaired in absence of Urm1- and ELP-dependent tRNA modification of tK^{UUU}, tQ^{UUG}, tE^{UUC} (Rezgui *et al.*, 2013 and Laxman *et al.*, 2013), we examined if *ZAP1* mRNA is enriched with these above-mentioned codons. *In silico* analyses done by Rezgui *et al.* show that *ZAP1* is not significantly enriched in the codons AAA, CAA and GAA, indicating that the translation of Zap1 is probably not impaired in absence of Urm1-dependent tRNA modification (Rezgui *et al.*, 2013).

Since Zap1 urmylation positively influences Zap1 levels, it is possible that Urm1-modified Zap1 species are less prone to degradation compared to unmodified Zap1. Thus, the role of Zap1 urmylation could be to maintain a constant pool of Zap1 that is able to rapidly respond to Zap1-dependent environmental stressors. Intriguingly, degradation of full-length Zap1 was not dramatically accelerated in

absence of Zap1 urmylation, even though the overall protein levels of Zap1 were largely reduced. This observation might be blurred by the fact that only a small percentage of the overall Zap1 is urmylated. A way to potentiate urmylation would be to increase Urm1 expression, as Urm1 is low abundant under steady-state conditions (Ghaemmaghami *et al.*, 2003; and Chong *et al.*, 2015). Indeed, free Urm1 and Urm1 adducts increased when Urm1 was expressed under the *GAL1* promoter than Urm1 expressed under the constitutive *ADH1* promoter (Fig. 3-12A). Consequently, strong overexpression of Urm1 could be used to increase the urmylated Zap1 pool, which in turn would facilitate to study the effect of elevated Zap1 urmylation in cells. Indeed, when Urm1 was overexpressed using the galactose-inducing system, we could observe a markedly increase in $Zap1^{HA}$ level and slowed $Zap1^{HA}$ degradation compared to the accelerated Zap1 degradation kinetics in cells, which had no galactose-induction and consequently no Urm1 expression (Fig. 3-12B). Even though these findings suggest that Zap1 urmylation antagonizes Zap1 degradation, it has yet to be assessed whether there is indeed an increase in Zap1 urmylation under the *GAL* induction system than in WT cells. Since Zap1 urmylation exclusively occurs in the cytoplasm under zinc-replete conditions, a way to monitor a larger pool of urmylated Zap1 would be to examine the degradation kinetics of cytoplasmic Zap1. Consequently, we looked for the degradation kinetics of the cytoplasmic ^{GFP}zap1-C-NES, which we have shown to be recognized by the Urm1 conjugation machinery and urmylated at the acceptor lysine K871, and compared the degradation kinetics to the non-urmylated nuclear ^{GFP}zap1-C-NLS. While the nuclear ^{GFP}zap1-C-NLS was very stable, ^{GFP}zap1-C-NES was rapidly degraded (Fig. 3-11). Compared to ^{GFP}zap1-C-NES, degradation of the non-urmylated *^{GFP}zap1-C-NES-K871R* variant was highly accelerated; indicating that Zap1 urmylation positively influences the stability of cytoplasmic Zap1 (Fig. 3-11B). A way to further verify the positive effect of Urm1 on Zap1 stability would be to examine the degradation kinetics of full-length Zap1 in the cytoplasm and compare it to the stability of nuclear Zap1. Despite these findings, the exact mechanism by which Urm1 is able to antagonize Zap1 degradation is not entirely clear. Prior studies have shown that the otherwise stable GFP can be susceptible to degradation by fusing GFP to a degron (Li *et al.*, 1998). Various

degrons consist of a short amino-acid sequence such as the Deg1 of Matα2 or CL1 and are able to destabilize various reporter proteins (Hochstrasser & Varshavsky, 1990, Hochstrasser *et al.*, 1991, Chen *et al.*, 1993 and Gilon *et al.*, 1998). Peculiarly, only cytoplasmic Zap1 seems to be highly susceptible to degradation, suggesting that the C-terminus sequence of Zap1 contains a degron, which is exclusively recognized in the cytoplasm. While various degrons are degraded independent to their respective subcellular localization, the ubiquitously localized Cdc5 appears to be efficiently degraded in the nucleus (Bennett *et al.*, 2005; and Arnold *et al.*, 2015). Similarly, the C-terminal Zap1 degron seems to be solely recognized in the cytoplasm. We have shown that ^{GFP}zap1-C and the cytoplasmic ^{GFP}zap1-C-NES as well as ^{GFP}*zap1-C-K871R-NES*, but not ^{GFP}zap1-C-NLS and ^{GFP}*zap1-C-K871R-NLS*, were highly ubiquitinated and that full-length Zap1 degradation was halted in the proteasomal mutant *cim3-1* (Fig. 3-14AB, Fig. 3-13). Moreover, ^{GFP}zap1, ^{GFP}zap1-C-NES and ^{GFP}*zap1-C-K871R-NES* were highly ubiquitinated, whereas ^{GFP}zap1-C-NLS and ^{GFP}*zap1-C-K871R-NLS* were not modified by ubiquitin (Fig. 3-14AB). As ^{GFP}*zap1-C-K871R-NES* was more susceptible to proteasomal degradation than ^{GFP}zap1-C-NES, non-urmylated ^{GFP}zap1-C-NES in cells lacking Urm1 and Uba4 and ^{GFP}*zap1-C-K871R-NES* should be ubiquitinated more. However, the comparison of ubiquitination between ^{GFP}zap1-C-NES expressed in WT, *Δurm1* and *Δuba4*, as well as ^{GFP}*zap1-C-K871R-NES* expressed in WT, was no possible as overall protein levels and pull-down efficiency of ^{GFP}zap1-C-NES and ^{GFP}*zap1-C-K871R-NES* in cells lacking urmylation were significantly lower than ^{GFP}zap1-C-NES expressed in WT (Fig. 3-11, 3-14B). Therefore, further ubiquitination experiments using equimolar amounts of purified ^{GFP}zap1-C-NES and ^{GFP}*zap1-C-K871R-NES* are needed to assess Zap1 ubiquitination in presence and absence of urmylation.

Taken together, these findings suggest Zap1 is degraded via the proteasome and indicate that the C-terminus contains an ubiquitin-dependent cytoplasmic degron. As the ubiquitin-dependent Zap1 degradation occurs in the cytoplasm, we searched for potential E3 ligases that could be responsible for the ubiquitination of Zap1. We were able to identify most of the E3 ubiquitin ligase complex Doa10 as interaction partners in a mass spectrometry approach. Furthermore we could show

that the degradation of Zap1 is slowed down or completely halted in *Δdoa10* and *cdcd48-3* cells expressing $Zap1^{HA}$ or zap1-C-NES, respectively. It remains to be seen, whether the binding of Doa10 to Zap1 and its consequent ubiquitination is countered by Zap1 urmylation. Taken together our data suggest that urmylation and ubiquitination of Zap1 are interconnected and serve as disparate mechanisms in regulating Zap1 – and also Zap1 transcription – on a posttranslational level. Urm1 might function as an antagonist of ubiquitin and ubiquitination of Zap1, similar to the proposed role of IκBα SUMOylation (Desterro *et al.*, 1998). In this study, the authors showed that SUMOylation and ubiquitination of IκBα occur at the same acceptor lysine (K21) and that SUMOylated IκBα is resistant to TNFα-induced degradation, suggesting that SUMO1 functions as a direct antagonist of ubiquitin and ubiquitin-dependent degradation of IκBα. Unlike SUMOylation and ubiquitination of IκBα that target the same acceptor lysine, Zap1 appears to be urmylated and ubiquitinated at different lysine residues, as *zap1-K871R-NES* is still being degraded (Fig. 3-11B).

4.2.3 Working model and outlook

Zap1 is urmylated at K871 in the cytoplasm (Fig. 4-1). In contrast to the nuclear pool of Zap1, cytoplasmic Zap1 is highly unstable. In presence of the urmylation machinery, Zap1 is less prone to degradation by the UPS, but is highly destabilized in absence of Zap1 urmylation. Therefore, Urm1 conjugation to Zap1 could sterically hinder the interaction of the ubiquitin conjugation machinery by blocking the interaction of an ubiquitin E3 ligase such as Doa10 and consequently obstruct the degradation of Zap1. Stabilization of urmylated Zap1 could also be caused indirectly, such as facilitating the nucleocytoplasmic shuttling of Zap1 (as implicated by Van der Veen and colleagues), which in turn leaves less Zap1 to be localized in the cytoplasm that might consequently be degraded by the UPS machinery (Van der Veen *et al.*, 2011). Either way, Zap1 urmylation seems to be detrimental in stabilizing Zap1, which in turn improves *ZAP1* expression and expression of target genes under zinc-limiting conditions. Future studies are needed to elucidate the mechanism on how Zap1 urmylation antagonizes Zap1

degradation and whether this protective mechanism of Urm1 affects additional Urm1-substrates.

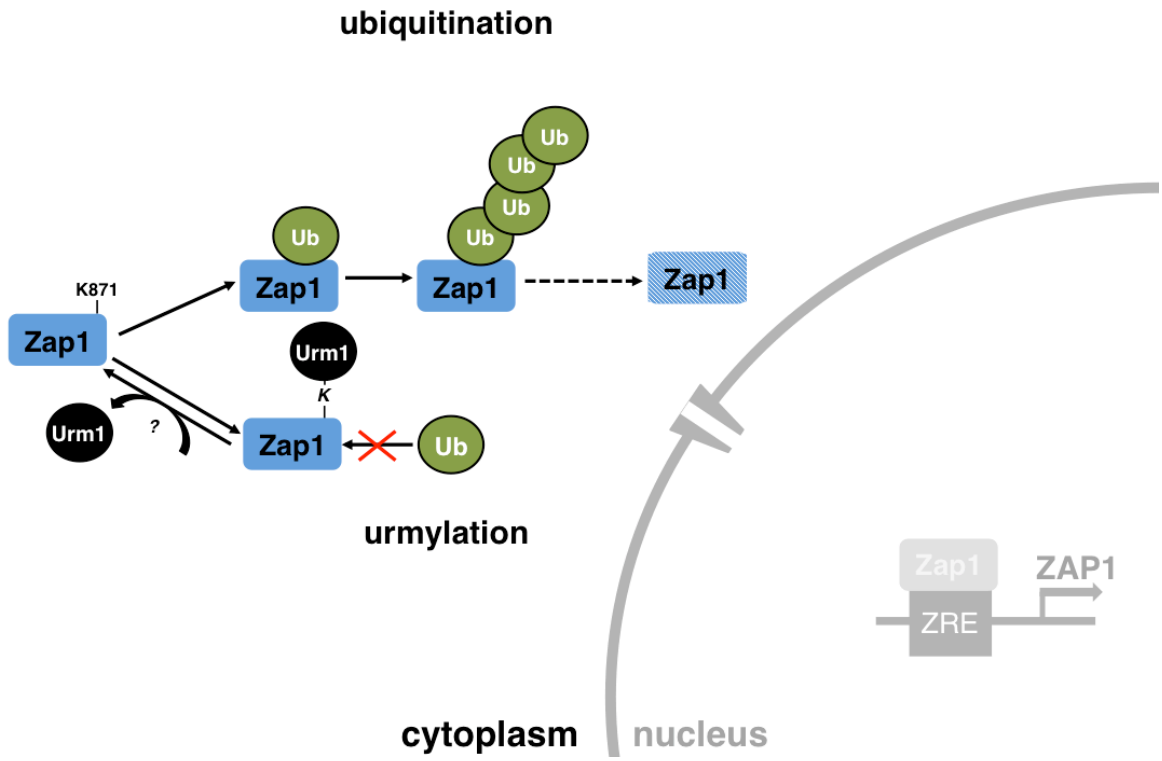

Figure 4-1. Model for the role of Zap1 urmylation.

Cytoplasmic Zap1 is recognized by the Urm1 conjugation machinery and modified at C-terminus of Zap1 at K871. Unmodified or deurmylated Zap1 are ubiquitinated at the C-terminus of Zap1 and consequently degraded by the UPS. On the other hand, Zap1 modification by Urm1 sterically hinders the binding of the ubiquitination machinery to Zap1. Conversely, urmylated Zap1 inhibits Zap1 ubiquitination and is therefore resistant to the targeting and consequent degradation via the ubiquitin-proteasome system.

5 Materials and methods

5.1 Materials

5.1.1 Chemicals and reagents

Unless otherwise mentioned, chemicals and reagents were obtained from Abcam, Applied Biosystems, Becton Dickinson, Biomol, Biorad, Biozym, Carl Roth, Chromotek, GE Healthcare, Invitrogen, Merck, New England Biolabs, Promega, Roche or Sigma-Aldrich. For all the methods described, sterile solutions, sterile flasks and deionized water were used.

5.1.2 Antibodies

The following antibodies were used for protein detection by immunoblotting, for intracellular localization studies by immunofluorescence microscopy and for studying protein-protein interactions by immunoprecipitation.

Primary antibodies	**Source**
Monoclonal anti-c-myc (9E10)	Santa Cruz
Polyclonal anti-c-myc (A-14)	Santa Cruz
Monoclonal anti-Dpm1	Invitrogen
Monoclonal anti-GFP (B-2)	Santa Cruz
Monoclonal anti-HA (F-7)	Santa Cruz
Polyclonal anti-HA (Y-11)	Santa Cruz
Monoclonal anti-Pgk1	Invitrogen
Polyclonal anti-Urm1	This study
Secondary antibodies	
HRP-coupled anti-mouse IgG	Dianova
HRP-coupled anti-rabbit IgG	Dianova
Alexa Fluor 488 anti-rabbit IgG	Molecular Probes

5.2 Microbiological and genetic techniques

5.2.1 *E. coli techniques*

E. coli strains

Strain name	Genotype	Source
Rosetta (DE3)	F⁻ *ompT hsdS$_B$(r_B^- m_B^-) gal dcm* (DE3) pRARE (Cam^R)	Novagen
Rosetta 2	F⁻ *ompT hsdS$_B$(r_B^- m_B^-) gal dcm* lacY1 pRARE (Cam^R)	Novagen
Stellar	*F–, endA1, supE44, thi-1, recA1, relA1, gyrA96, phoA, Φ80d lacZΔ M15, Δ (lacZYA - argF) U169, Δ (mrr - hsdRMS - mcrBC), ΔmcrA, λ–*	Clontech
XL1-Blue	*recA1 endA1 gyrA96 thi-1 hsdR17 supE44 relA1 lac* [F´ *proAB lacI^q ZΔM15* Tn*10* (Tet^r)]	Stratagene

E. coli vectors

Vector name	Epitope tag	Selection marker	Source
pGEX-4T1	GST	ampicillin	Sigma-Aldrich
pQE30	6xHis	ampicillin	Clontech

E. coli media

LB-medium/[plates]

1% (w/v)	tryptone peptone
0.5% (w/v)	yeast extract
0.5% (w/v)	NaCl
[2% (w/v)	agar]
adjust volume with ddH_2O	
sterilize by autoclaving	

optional: add antibiotics after autoclaving and cooling down to 60°C.

SOB

2.5% (w/v)	tryptone peptone
0.625% (w/v)	yeast extract
10 mM	NaCl
2.5 mM	KCl
adjust volume with ddH_2O	
10 mM $MgCl_2$ and 10 mM $MgSO_4$	

SOC SOB containing 10 mM glucose

Transformation buffer 1 (TB 1) 10 mM MOPS, pH 6.5 adjusted with KOH

100 mM KCl
45 mM $MnCl_2$
10 mM $CaCl_2$
10 mM KAc, pH 7.5 adjusted with HCl
adjust volume with ddH_2O

Transformation buffer 2 (TB 2) TB 1 with 10% glycerol

Transformation buffer 3 (TB 3) 100 mM $CaCl_2$
50 mM $MgCl_2$

Cultivation and storage of *E. coli*

Liquid cultures were grown on LB media at 37°C (or at 25°C for recombinant protein expression) with constant shaking. Cells grown on agar plates were incubated at 37°C. Bacteria transformed with plasmid DNA were grown on media containing the appropriate antibiotic (50 µg/ml ampicillin and 50 µg/ml kanamycin). The cell culture density was determined by measuring the absorbance at a wavelength of 600 nm (OD_{600}). Cultures were either stored temporarily at 4°C or were put in 15% (v/v) glycerol solution at -80°C for long-term storage.

Preparation of chemically competent *E. coli*

Fresh cells were streaked out from a frozen glycerol stock on a LB agar plate and grown overnight. A single colony was picked and incubated in 5 ml LB medium overnight. 2 ml of the overnight culture was inoculated in 200 ml pre-warmed SOB and grown to ~0.5 OD_{600}. The culture was then cooled on ice for 10 min were harvested by centrifugation (10 min, 2500 rpm, 4°C). The cell pellet was resuspended in 100 ml TB 1 and cooled on ice for 10 min. The resuspended cells were pelleted by centrifugation and resuspended in a solution containing 16 ml TB

2 and 560 µl DMSO and incubated on ice for 15 min. Finally, the competent cells were stored in 150 µl aliquots at -80°C.

Transformation of plasmid DNA into competent *E. coli*

Competent *E. coli* cells were thawed on ice and 50 µl of chemically competent cells were mixed with 10 ng plasmid DNA. Subsequently, the solution was incubated on ice for 30 min, incubated at 42°C for 45 s. After the heat shock, the cells were incubated on ice for 2 min and were incubated in 1 ml LB at 37°C for 30-45 min under constant shaking. The transformed cells were harvested (3 min, 800 g, room temperature), plated on ampicillin-containing LB agar plates and incubated overnight at 37°C.

Recombinant protein expression in *E. coli*

For the expression recombinant proteins in *E. coli*, competent Rosetta (DE3) and Rosetta 2 were used. Cells transformed with the desired plasmid DNA were directly transferred and incubated in 25 ml LB medium containing the appropriate antibiotic overnight at 37°C. The overnight culture was transferred to 1 l ampicillin-containing LB medium. Once the cells reach 0.6 OD, the protein expression was induced by the addition of 0.5 M IPTG for at least 4 h at 25°C. Lastly, the cells were harvested by centrifugation (5 min, 800 g, 4°C) and stored in -80°C.

5.2.2 *S. cerevisiae* techniques

S. cerevisiae strains

Strain name	Genotype	Reference
DF5 MATa (WT)	*MATa his3-200, LEU2-3, 2-112, lys2-801, trp1-1, ura3-52*	(Finley *et al.*, 1987)
IP541	*MATa lys1::natNT2 arg4::hphNT1*	I. Psakhye
W303	*MATa eu2-3,112 trp1-1 can1-100 ura3-1 ade2-1 his3-11,15*	E. Schwob, K. Nasymth
PJ69-7a	*MATa trp1-901 LEU2-3,112 ura3-53 his3-200 gal4 gal80 GAL1-HIS3 GAL2-ADE2 met2::GAL7-lacZ*	Warf
RH448a	*MATa LEU2 his4 lys2 ura3 bar1-1*	M. Knop
RC757α	*MATα his6 met1 sst2-1 cyh2 can1*	M. Knop
ySL_333	DF5, *MATa pCYC1-GFP-zap1-C::LEU2*	this work
ySL_334	DF5, *MATa urm1::natNT2 pADH1-6His-Strep-URM1-tADH::URA3 pCYC1-GFP-zap1-C::LEU2*	this work
ySL_335	DF5, *MATa uba4::kanMX6 urm1::natNT2 pADH1-6His-Strep-URM1-tADH::URA3 pCYC1-GFP-zap1-C::LEU2*	this work
ySL_336	DF5, *MATa urm1::natNT2 pCYC1-GFP-zap1-C::LEU2*	this work

ySL_337	DF5, *MATa uba4::kanMX6 urm1::natNT2 pCYC1-GFP-zap1-C::LEU2*	this work
ySL_010	DF5, *MATa lys1::natNT2 arg4::hphNT1 uba4::HIS3MX6 urm1::kanMX6 pADH1-6His-3HA-URM1L96R-tADH::URA3*	this work
ySL_018	DF5, *MATa lys1::natNT2 arg4::hphNT1 urm1::kanMX6 pADH1-6His-Strep-URM1-tADH::URA3*	this work
ySL_021	DF5, *MATa urm1::natNT2 pADH1-6His-Strep-URM1-tADH::URA3*	this work
ySL_022	DF5, *MATa lys1::natNT2 arg4::hphNT1 urm1::natNT2 pADH1-6His-Strep-URM1-L96R-tADH::URA3*	this work
ySL_026	DF5, *MATa ZAP1-6HA::klTRP1*	this work
ySL_030	DF5, *MATa uba4::kanMX6 urm1::natNT2 pADH1-6His-Strep-URM1-tADH::URA3 ZAP1-6HA::klTRP1*	this work
ySL_031	DF5, *MATa urm1::natNT2 pADH1-6His-Strep-URM1-tADH::URA3 ZAP1-6HA::klTRP1*	this work
ySL_061	DF5, *MATa ZRT1-3myc::klTRP1*	this work
ySL_062	DF5, *MATa ZRT1-3myc::klTRP1 urm1::natNT2*	this work
ySL_063	DF5, *MATa uba4::kanMX6 urm1::natNT2 pADH1-6HisFlag-URM1 tADH::URA3 ZRT1-3myc::klTRP1*	this work
ySL_065	DF5, *MATa urm1::kanMX6 zap1-K871R-6HA:TRP*	this work
ySL_073	DF5, *MATa zap1::hphNT1*	this work
ySL_075	DF5, *MATa urm1::natNT2 pADH1-6His-Strep-URM1-tADH::URA3 zap1-K871R-6HA::klTRP1*	this work
ySL_081	DF5, *MATa uba4::kanMX6 ZAP1-6HA::klTRP1*	this work
ySL_105	DF5, *MATa urm1::natNT2 zap1::hphNT1*	this work
ySL_105	DF5, *MATa urm1::natNT2 zap1::hphNT1NT1*	this work
ySL_107	DF5, *MATa ZAP1-GFP::klTRP1*	this work
ySL_117	DF5, *MATa pMET25-GFP-zap1-C::URA3*	this work
ySL_132	DF5, *MATa pMET25-GFP-zap1-C-K871R::URA3*	this work
ySL_249	DF5, *MATa ZAP1-urm1ΔGG-6His-3HA::LEU2*	this work
ySL_250	DF5, *MATa zap1-K871R-urm1ΔGG-6His-3HA::LEU2*	this work
ySL_251	DF5, *MATa ZAP1-urm1ΔGG-6His-3HA::LEU2 urm1::natNT2*	this work
ySL_252	DF5, *MATa ZAP1-urm1ΔGG-6His-3HA::LEU2 uba4::kanMX6*	this work
ySL_255	DF5, *MATa zap1-K871R-6HA::klTRP1*	this work
ySL_256	DF5, *MATa pCYC1-ZAP1-6HA::LEU2*	this work
ySL_259	*DF5, MATa pCYC1-zap1-AD2-6HA::LEU2*	this work
ySL_260	DF5, *MATa urm1::natNT2 pADH1-6His-Strep-URM1-tADH::URA3 pCYC1-zap1-AD2 6HA::LEU2*	this work
ySL_262	DF5, *MATa pCYC1-zap1-DBD-6HA::LEU2*	this work
ySL_263	DF5, *MATa urm1::natNT2 pADH1-6His-Strep-URM1-tADH::URA3 pCYC1-zap1-DBD 6HA::LEU2*	this work
ySL_274	DF5, *MATa uba4::kanMX6 pCYC1-ZAP1-6HA::klTRP1*	this work
ySL_363	DF5, *MATa pCYC1-GFP-zap1-C K877R::LEU2*	this work
ySL_364	DF5, *MATa urm1::natNT2 pADH1-6His-Strep-URM1-tADH::URA3 pCYC1-GFP-zap1-C-K877R::LEU2*	this work
ySL_365	DF5, *MATa pCYC1-GFP-zap1-C-K871R::LEU2*	this work
ySL_366	DF5, *MATa urm1::natNT2 pADH1-6His-Strep-URM1-tADH::URA3 pCYC1-GFP-zap1-C-K871R::LEU2*	this work
ySL_367	DF5, *MATa pCYC1-GFP-zap1-C-C872S::LEU2*	this work
ySL_368	DF5, *MATa urm1::natNT2 pADH1-6His-Strep-URM1-tADH::URA3 pCYC1-GFP-zap1-C-C872S::LEU2*	this work
ySL_415	DF5, *MATa pCYC1-GFP-zap1-C-NLS::LEU2*	this work
ySL_416	DF5, *MATa urm1::natNT2 pADH1-6His-Strep-URM1-tADH::URA3 pCYC1-GFP-zap1-C-NLS::LEU2*	this work
ySL_417	DF5, *MATa pCYC1-GFP-zap1-C-NES::LEU2*	this work

ySL_418	DF5, *MATa urm1::natNT2 pADH1-6His-Strep-URM1-tADH::URA3 pCYC1-GFP-zap1-C-NES::LEU2*	this work
ySL_419	DF5, *MATa pCYC1-GFP-zap1-C-K871R-NLS::LEU2*	this work
ySL_420	DF5, *MATa urm1::natNT2 pADH1-6His-Strep-URM1-tADH::URA3 pCYC1-GFP-zap1-C-K871R-NLS::LEU2*	this work
ySL_421	DF5, *MATa pCYC1-GFP-zap1-C-K871R-NES::LEU2*	this work
ySL_422	DF5, *MATa urm1::natNT2 pADH1-6His-Strep-URM1-tADH::URA3 pCYC1-GFP-zap1-C-K871R-NES::LEU2*	this work
ySL_441	DF5*, MATa urm1::natNT2 pCYC1-GFP-zap1-C-NLS::LEU2*	this work
ySL_443	DF5, *MATa urm1::natNT2 pCYC1-GFP-zap1-C-NES::LEU2*	this work
ySL_445	DF5, *MATa uba4::kanMX6 pCYC1-GFP-zap1-C-NLS::LEU2*	this work
ySL_447	DF5, *MATa uba4::kanMX6 pCYC1-GFP-zap1-C-NES::LEU2*	this work
ySL_452	DF5, *MATa pCYC1-GFP::LEU2*	this work
ySL_455	DF5, *MATa pCYC1-GFP-zap1-C::LEU2*	this work
ySL_457	DF5, *MATa uba4::kanMX6 pCYC1-GFP-zap1-C::LEU2*	this work
ySL_458	DF5, *MATa pCYC1-GFP-zap1-C-K871R::LEU2*	this work
ySL_476	DF5*, MATa cim3-1 pdr5::HIS3MX6 pCYC1-GFP-zap1-C::LEU2*	this work
ySL_508	DF5, *MATa cim3-1 urm1::natNT2 Zap1-HA6::TRP*	this work
ySL_510	DF5*, MATa cim3-1 pCYC1-Zap1-HA6::TRP*	this work
ySL_521	DF5, *MATa natNT2::pGAL1-Urm1 pCYC1-Zap1-6HA::LEU2*	this work
ySL_524	DF5, *MATa doa10::kanMX6 pCYC1-GFP-zap1-C-NES::LEU2*	this work
ySL_525	DF5, *MATa doa10::kanMX6 pCYC1-Zap1-6HA::LEU2*	this work
ySL_526	DF5, *MATa cdc48-3 pCYC1-GFP-zap1-C-NES::LEU2*	this work
ySL_527	DF5, *MATa cdc48-3 pCYC1-ZAP1-6HA::LEU2*	this work

S. cerevisiae vectors

Plasmid type	Name (marker)	Copies/Cell	Reference
Integrative	YIplac211 (URA3) YIplac128 (LEU2)	1	Gietz and Sugino, 1988
2µ	pUG36 (URA3)	50-100	J. H. Hegemann
Yeast two-hybrid	pGAD-C1-3 pGBD-C1-3	50-100	James *et al.*, 1996

S. cerevisiae media and solutions

YPD/YPR/YPG [plates] 1% yeast extract
2% bacto-peptone
2% carbon source (glucose, raffinose or galactose)
[2% agar] sterilized by autoclaving

For selection plates: YPD medium with 2% agar was cooled to 60°C and the respective selection drug was added.

	200 mg/l	geneticine disulphate (G418)
	100 mg/l	nourseothricin (NAT)
	500 mg/l	hygromycin B (Hph)

amino acid drop out mix	800 mg	adenine
	800 mg	uracil
	800 mg	tryptophan
	800 mg	histidine
	800 mg	arginine
	800 mg	methionine
	1200 mg	tyrosine
	2400 mg	leucine
	1200 mg	lysine
	2000 mg	phenylalanine
	8000 mg	threonine
optional:	1200 mg	isoleucine
	6000 mg	valine
	4000 mg	aspartic acid

SC-medium/[plates]	0.67%	yeast nitrogen base
	0.2%	amino acid drop out mix
	2%	carbon source (glucose, raffinose or galactose)
	[2%	agar] sterilized by autoclaving

low zinc medium (LZM)	2x	SC
	20 mM	sodium citrate, pH 4.2
	1 mM	EDTA
	2%	glucose
	adjust volume with ddH_2O	
	sterilized by sterile filtration	

sporulation medium	2% (w/v)	potassium acetate, sterilized by autoclaving
zymolyase 100T solution	0.9 M	sorbitol
	0.1 M	Tris-HCl, pH 8.0
	0.2 M	EDTA, pH 8.0
	50 mM	DTT
	0.5 mg/ml	zymolyase 100T
SORB	100 mM	LiOAc
	10 mM	Tris-HCl, pH 8.0
	1 mM	EDTA, pH 8.0
	1 M	sorbitol
	sterilized by filtration	
PEG	100 mM	LiOAc
	10 mM	Tris-HCl, pH 8.0
	1 mM	EDTA, pH 8.0
	40% (w/v)	PEG-3350
	sterilized by filtration	

Cultivation and storage of *S. cerevisiae*

In general, a fresh single yeast colony was inoculated in YP or SC based medium at 30°C (25°C with heat sensitive strains) overnight. Overnight cultures were generally diluted to 0.1 OD_{600} in a new flask containing fresh medium. Yeast cells were then grown at 30°C under constant shaking until they reach the mid-log phase (OD_{600} 0.6-0.9). Cultures on grown on YP or SC based agar plates were stored at 4°C up to 1-2 months. Conversely, stationary cultures were stored in 15% (v/v) glycerol solutions at -80°C for long-term storage.

Preparations of competent yeast cells

Mid-log phase growing yeast cells were harvested by centrifugation (500 g, 5 min, room temperature), washed with ½ volume of sterile ddH_2O and lastly washed with 1/10 volume SORB. The cells were pelleted again and resuspended in 360 µl

SORB and 50 µl denatured carrier DNA. The competent cells were stored at -80°C.

Transformation of yeast cells

200 ng of circular or 2 µg of linearized plasmid DNA/PCR product was added to 10 µl or 50 µl competent yeast cells, respectively. Six volumes of PEG were added, mixed thoroughly and the cell suspension was incubated at room temperature for 30 min. A final concentration of 10% DMSO was added to the solution prior to heat-shocking the cells at 42°C for 10-20 min. Cells were pelleted by centrifugation (500 g, 3 min, room temperature) and resuspended in 200 µl sterile ddH_2O. If the transformed DNA contains an auxotrophic genetic marker, the transformed cells were directly plated on their respective SC agar plates. For transformed DNA that contain antibiotic resistance markers, transformed cells were incubated for 1-2h in 2 ml liquid YPD medium at 30°C (25°C for heat sensitive strains) prior to plating.

Genomic manipulation by homologous recombination

Integration of DNA into yeast genome was either achieved by introducing a linearized integrative vector or by transforming a PCR DNA fragment in yeast cells. The integrative yeast vectors of the YIplac vector series were used in this study, since they do not contain autonomous replication elements. Consequently, only stably integrated vectors are propagated in yeast. Prior to transformation, YIplac vectors were linearized within their respective auxotrophic markers by introducing a single cut using restriction enzymes. Linearized YIplac plasmids were then integrated into the yeast genome by homologous recombination with the endogenous marker gene.

Deletions, truncations, N-/C-terminal tags, point mutants or fusions were generally introduced by employing a PCR-based strategy, which ensures stable integration into the yeast genome by homologous recombination (Longtine *et al.* 1998, Knop *et al.*, 1999, Janke *et al.*, 2004). For this approach, the PCR products consisted of a selection marker gene and were additionally flanked by 45-55 bp sequences that were homologous to the target sequence. The desired DNA fragments were amplified by PCR, purified using the QIAquick purification PCR kit, transformed

into competent yeast cells and plated on the respective selection medium. The correct recombination event was confirmed by yeast colony PCR.

PCR reaction mixture

100 ng	plasmid DNA
30 µl	10x ThermoPol reaction buffer (NEB)
10.5 µl	dNTP-Mix (10 mM each, NEB)
19.2 µl	forward primer (100 µM)
19.2 µl	reverse primer (100 µM)
2.4 µl	Taq DNA polymerase
2.1 µl	Vent DNA polymerase (NEB)

adjust to a total volume of 300 µl with ddH_2O

Cycling parameters

PCR step	T [°C]	Time	Cycles
Initial denaturation	95/97	3 min	1
Denaturation	94	30 s/1 min	
Annealing	54	30 s	10
68	72	2 min 40 s	
Denaturation	95/97	30 s	
Annealing	54	30 s/1 min	20
68	68	2 min 40 s (+20 s/cycle)	
Final elongation	68	10 min	1
Cooling	4	∞	

Grey: conditions for the amplification of all natNT2-based cassettes

Yeast colony PCR

Genomic alterations such as insertions, deletions, truncations and mutations were identified by the PCR-based yeast colony strategy. A fresh single yeast colony was transferred into a safe-lock reaction tube that contained 20 µl 0.02 M NaOH and acid-washed glass beads (Sigma). The yeast cells were lysed at 95°C for 5 min under vigorous shaking (1400 rpm) and the cell debris was pelleted by centrifugation (16.000 g, 1 min, RT). The supernatant was transferred to a PCR reaction tube and was used as PCR template. Two DNA oligonucleotides were used for the yeast colony PCR that were able to prime upstream/downstream of the altered chromosomal locus (primer 1) as well as within the integrated selection

marker gene (primer 2). The yeast colony PCR was carried out using the PCR reaction mixture and the cycling parameters as described below.

PCR reaction mixture

4.0 µl	yeast solution (template)
5.0 µl	10x ThermoPol reaction buffer (NEB)
1.75 µl	dNTP Mix (10 mM each, Thermo Fisher Scientific)
3.2 µl	primer 1 (10 µM)
3.2 µl	primer 2 (10 µM)
1 µl	50 mM $MgCl_2$
0.4 µl	*Taq* DNA polymerase
32.45 µl	ddH_2O

Cycling parameters

PCR step	T [°C]	Time	Cycles
Initial denaturation	94	5 min	1
Denaturation	94	30 s	
Annealing	55	30 s	30
Elongation	72	1 min/kb	
Final elongation	72	15 min	1
Cooling	4	∞	

Mating of haploid *S. cerevisiae* strains

Equal amounts of freshly streaked haploid yeast strains of opposite mating type (*MAT***a**, *MAT*α) were mixed in 500 µl YPD and incubated at 30°C overnight under constant shaking (200 rpm). Cells were sedimented by centrifugation (500 g, 5 min, RT), resuspended in 100 µl H_2O and plated on respective selection plates to select diploid cells.

Sporulation and tetrad dissection of diploid yeast strains

Fresh diploid colonies were first incubated in 5 ml YPD at 30°C overnight. 800 µl of the overnight culture was harvested by centrifugation (500 g, 5 min, RT), washed four times in 1 ml sporulation medium and incubated in 4 ml sporulation medium at RT for 3-7 days. 10 µl of the culture was mixed with 10 µl zymolyase

100T solution and incubated at RT for 10 min. This mixture was subsequently applied on pre-warmed YPD agar plates, dissected with a micromanipulator (Singer MSM Systems) and grown on YPD plates for 3-3 days at 30°C. Lastly, the tetrads were genotypically examined either by replica plating the cells on selection plates or by their phenotype.

Mating-type analysis of haploid yeast strains

The mating type analysis utilizes the tester strains RC757α and RH448a to identify yeast mating-types, since these strains are hypersensitive to the mating pheromones secreted by both MATa and MATα strains. As a result, tester strains were not able to grow in the proximity of haploid cells with opposite mating type. Consequently, a halo was formed surrounding the replica-plated colony, if said strain displayed the opposite mating type as the tester strain. In principle, the tester strain were resuspended in 50 µl of ddH_2O and mixed with 10 ml of lukewarm YPD containing 1% (w/v) molten agar. The mixture was poured over YPD agar plates. Next, the tetrads were replica plated on the a- and α-tester agar plates and incubated for at 30°C for one or two days.

Analysis of protein-protein interaction using the yeast two-hybrid system (Y2H)

The two-hybrid system was used to identify novel protein-protein interactions in the yeast. Protein-protein interactions were determined by using fusion proteins containing the bait protein fused to the DNA-binding domain (BD) and the prey protein that was fused to the activation domain (AD) of the Gal4 transcription factor. In case the bait interacted with the prey protein, Gal4 BD and AD were brought in proximity, resulting in the reconstitution of a functional Gal4 transcription factor. Essentially, Y2H-specific yeast strains were used which lacked the transcription factor Gal4 and contained the reporter genes GAL1-HIS3 and GAL2-ADE2 that only showed gene expression in presence of a functional Gal4. Initially, full-length ORFs, fragments or mutant variants of proteins were fused to the C-terminus of either the BD or AD of the Gal4 transcription factor and the fusion ORF was inserted into the expression vectors pGBD-C1 and pGAD-C1, respectively.

The plasmids were transformed into competent PJ69-7a cells (Warf) and streaked on SC –Leu –Trp plates at 30°C for 3-3 days. Protein-protein interactions were tested by growing the transformed Y2H strains on SC –Leu –Trp –His and/or on SC –Leu –Trp –Ade agar plates.

Phenotypic analysis of *S. cerevisiae* mutant variants using growth assays

A canonical way to analyze phenotypes of yeast mutant variants was to compare their growth rates with other strains under optimal and suboptimal conditions (e.g. environmental, chemical stressors, etc.). Overnight cultures were harvested during the mid-log growth phase and washed once with 1 ml ddH_2O. A total of 0.5 OD yeast cells (ad 250 µl ddH_2O) were transferred to a 96-well microtiter plate. After four to five 1:5 serial dilutions, the cells were spotted onto the respective agar plates using a sterile 96-pin stamp. Finally, the growth phenotypes of the mutant variants were incubated for several days at different temperatures.

Analysis of protein stability using the cycloheximide chase assay

The protein stability was determined by the cycloheximide chase assay. Cycloheximide is a potent eukaryotic protein synthesis inhibitor that immediately stops *de novo* protein synthesis, which in turn permitted the study of protein degradation over time. Essentially, cells were grown to mid-log phase, harvested by centrifugation (500 g, 5 min, RT) and resuspended in growth medium containing 150 µg/ml of cycloheximide. For each time point, 1 OD of cells were harvested (16.000 g, 1 min, RT) and immediately frozen in liquid nitrogen. Finally, protein extracts were prepared and the protein turnover for the protein of interest was determined by western blotting.

Microsomal preparation

To isolate microsomal fractions, 20 OD log phased cells were sedimented by centrifugation (500 g, 5 min, 4°C), washed once with ice-cold water and resuspended in 1 ml lysis buffer (50 mM Tris-HCl, pH 7.5, 150 mM NaCl, 1 mM EDTA, pH 8.0, EDTA-free protease inhibitors (Roche)). Zirconia/silica beads (ø 0.5

mm, Carl Roth) were added to the cell suspension and the cells were lysed using a multi-tube bead-beater (3x 30 Hz, 1 min, 5 min cooling intervals, 4°C, MM301 Retsch). The reaction tubes containing the cell lysates were perforated with a heated syringe needle and piggybacked into a fresh reaction tube (500 g, 2 min, 4°C). Cell debris was removed by centrifugation (500 g, 10 min, 4°C). The total cell extract (T) contains the soluble fraction (S, cytosolic and nuclear proteins) and the microsomes (P, ER, nuclear envelope and golgi apparatus). To separate the soluble fraction from the microsomal fraction, whole cell extracts were transferred into ultracentrifuge-compatible reaction tubes (microfuge tube polyallomer, Beckman Coulter) and fractionated by ultracentrifugation (100.000 g, 30 min, 4°C, TLA 55 rotor).

Membrane fractionation

To investigate whether the proteins found in the microsomal fraction were either membrane-associated or peripheral membrane proteins, microsomes were enriched as described in microsomal preparation. Microsomal fractions were divided in equal parts and resuspended in lysis buffer either containing 1 M Na_2CO_3, pH 11.3, 500 mM NaCl or 1% SDS. The samples were incubated on ice for 30 min with occasional vortexing and then centrifuged (20.000 g, 30 min, 4°C). After the removal of the supernatant, the pellets were resolubilized in SDS-PAGE sample buffer and analyzed by immunoblotting.

Semi-denaturing purification of ubiquitylated GFP-tagged proteins

To examine ubiquitylated GFP-tagged proteins, 50-200 OD of mid-log phased yeast cells were harvested, lysed by cryogenic grinding and resuspended in lysis buffer (3x volume to 1x OD, 50 mM Tris-HCl, pH 7.5, 150 mM NaCl, 1 mM EDTA, 0.5% Triton X-100, PIC, 10 mM NEM). The cell lysates were piggybacked (500 g, 2 min) to fresh reaction tubes in which the cell debris was sedimented by two centrifugation steps (2655 g, 5 min, 4°C and 15.700 g, 5 min, 4°C). 15 µl pre-equilibrated GFP agarose beads (GFP-Trap_A, Chromotek) were added to the cleared supernatant and incubated for 150 min at 4°C. After removing the supernatant (100 g, 2 min, RT), the beads were washed once with dilution buffer

(10 mM Tris-HCl, pH 7.5, 150 mM NaCl, 0.5 mM EDTA, PIC, 10 mM NEM), thrice with wash buffer 1 (PBS, 8 M urea, 1% SDS) and once with wash buffer 2 (PBS, 1% SDS). The specifically bound proteins were eluted from the agarose beads by the addition of 20 µl SDS-PAGE sample buffer and analyzed by immunoblotting.

Yeast indirect immunofluorescence

Protein subcellular localization was studied by immunofluorescence microscopy. Yeast cells were grown to mid-log phase in SC medium and were fixed by adding a formaldehyde solution (total concentration 0.1 M KPO_4, 4% formaldehyde) to the culture. Cells were incubated for 1h at RT, harvested by centrifugation (500 g, 5 min, 4°C) and washed three times with 1 ml SP buffer (0.1 M KPO_4, pH 6.5, 1.2 M sorbitol). Yeast cells were resuspended in 0.9 ml SPβ buffer (SP containing 20 mM β-mercaptoethanol) and 0.1 ml Zymolyase 100T solution (2.5 mg/ml in SPβ buffer). After an incubation period of 15 to 45 min at 30°C, yeast cell walls were digested. Spheroplasts were kept on ice for 5 min, washed three times with 1 ml cold SP buffer (1.500 g, 5 min) and seeded on polylysine-coated multi-well slides. Cells were permeabilized with methanol (-20°C) for 5 min, followed by incubation with acetone (-20°C) for 30 s. Multi-well slides were air dried for 5 min at room temperature. To prevent unspecific binding of the antibodies, 20 µl of PBS-B (50 mM $NaPO_4$, 150 mM NaCl, pH 7.5, 1% BSA) were added for each multi-slide well and incubated for 1 h at RT. A primary antibody was added (polyclonal rabbit anti-HA Y-11, 1:100 in PBS-B) to each multi-well slide and incubated in a moist chamber at 4°C. Afterwards, cells were washed six times with PBS-B and the fluorescence-labeled secondary antibody (Alexa Fluor 488 goat anti-rabbit IgG) was added for 2 h at RT in a moist chamber. Slides were washed five times with PBS-B and once with PBS-B containing DAPI (0.25 µg/ml DAPI in PBS). The solution was incubated for 30 min at RT in the dark and consequently air dried for 5 min at RT. Finally, a drop of mounting medium (Vectashield, Vector Laboratories) was applied at each well, slides were then covered by a cover slip and lastly sealed with nail polish. Multi-well slides could now be examined under a fluorescence microscope.

5.2.3 Molecular biological techniques

General buffers and solutions

HU sample buffer	8 M	urea
	5%	SDS
	1 mM	EDTA
	1.5%	DTT
	0.04%	bromophenol blue
4x SDS sample buffer	0.25 M	Tris-HCl, pH 6.8
	8%	SDS
	40%	glycerol
	0.04%	bromophenol blue
	5%	β-mercaptoethanol
MOPS buffer	50 mM	MOPS
	50 mM	Tris base
	3.5 mM	SDS
	1 mM	EDTA
Transfer buffer	250 mM	Tris base
	1.92 M	glycine
	0.1%	SDS
	20%	methanol
TBS-T	50 mM	Tris-HCl, pH 7.6
	150 mM	NaCl
	0.1%	Tween 20
TBE buffer 10x	1 M	Tris
	1 M	boric acid
	0.02 M	EDTA

DNA loading buffer 5x	0.5% (w/v)	SDS
	0.1 M	EDTA, pH 8.0
	25%	glycerol
	0.25% (w/v)	orange G

Isolation of plasmid DNA from *E. coli*

A single *E. coli* colony containing the DNA plasmid of interest was inoculated in 5 ml LB medium and incubated for 8-14 h at 37°C under constant shaking. Plasmid preparation kits were used to extract plasmids (Qiaprep Spin Miniprep, Qiagen and AccuPrep Plasmid Mini Extraction Kit, Bioneer).

Isolation of chromosomal DNA from *S. cerevisiae*

To extract chromosomal DNA from *S.* cerevisiae, a yeast DNA purification kit (MasterPure yeast DNA purification, Epicentre) was used. Usually, a total of 1.5 ml overnight yeast culture was used for the chromosomal yeast DNA isolation.

Determining DNA concentration

The DNA concentration was determined by measuring the absorbance at the wavelengths of 260 nm and 280 nm (NanoDrop 1000, Thermo Scientific).

Agarose gel electrophoresis

DNA samples were resuspended with 5x DNA loading buffer, loaded into pockets of 0.7 – 2% agarose gels that contained 0.5 µg/ml ethidium bromide and subjected to gel electrophoresis at 100 V in TBE buffer. A DNA ladder (1 kb Plus DNA ladder, Invitrogen) was used as a size reference. DNA fragments were visualized under UV light.

DNA sequencing

The MPIB core facility and Eurofins Genomics performed all sequencing reaction. The sample concentration usually consisted of 50 - 100 ng/µl for plasmid DNA or 1 – 10 ng/µl for PCR products.

Molecular cloning

Primers that were used for cloning generally consisted of a leader sequence, a restriction site and lastly a hybridization sequence, which was complementary to the template DNA. Generally, a high-fidelity DNA-polymerase (Phusion high-fidelity polymerase, New England Biolabs) was used for PCR-based DNA amplification. The following PCR reaction setup was used:

PCR reaction mixture		
	50-250 ng	template DNA
	10 µl	5x Phusion HF buffer
	1 µl	dNTP Mix (10 mM each, Thermo Fisher Scientific)
	3 µl	primer 1 (10 µM)
	3 µl	primer 2 (10 µM)
	0.5 µl	Phusion DNA polymerase
	31.5 µl	ddH_2O

Cycling parameters

PCR step	T [°C]	Time	Cycles
Initial denaturation	98	1 min	1
Denaturation	98	30 s	30
Annealing	55	30 s	
Elongation	72	30 s /kb	
Final elongation	72	7 min	1
Cooling	4	∞	

PCR products were isolated by gel extraction and were purified by a gel extraction kit (QIAquick gel extraction kit, Qiagen). The PCR products and the vector DNA were sequence-specifically cleaved with their designated restriction enzymes in

accordance to standard protocols and manufacturer's instructions (Sambrook *et al.*, 1989 and New England Biolabs). Optionally, linearized vectors were incubated at 37°C for 1 h with calf intestinal alkaline phosphatase (New England Biolabs) to avoid re-ligation during the DNA ligation reaction. To stop enzymatic activities, insert DNA and linearized vectors were purified on a column (QIAquick PCR purification kit, Qiagen). For the ligation reaction insert vector ratio of 3:1 – 6:1 was used. The ligation reaction was incubated with T4-DNA ligase either for 4 h or over night at 16°C following the manufacturer's instructions (New England Biolabs).

Site-directed mutagenesis

Site-directed mutagenesis was used to introduce specific DNA alterations such as specific substitutions, insertions or deletions in double stranded plasmid DNA (Kunkel, 1985). Principally, this PCR-based method utilizes two complementary oligonucleotide primers, containing the desired mutated nucleotide(s) with 10-15 nt flanking sequences complementary to the template DNA. The template plasmid DNA was amplified with a high-fidelity DNA polymerase (PfuUltra II Fusion HS DNA polymerase, Agilent).

PCR reaction mixture

100 ng	template DNA
5 µl	10x cloned *Pfu* reaction buffer
2.5 µl	dNTP Mix (10 mM each, Thermo Fisher Scientific)
0.5 µl	forward primer (10 µM)
0.5 µl	reverse primer (10 µM)
1 µl	50 mM $MgCl_2$ (NEB)
0.5 µl	PfuUltra II Fusion HS DNA polymerase
39µl	ddH_2O

Cycling parameters

PCR step	T [°C]	Time	Cycles
Initial denaturation	95*/92**	2 min	1
Denaturation	95*/92**	30 s	30
Annealing	60	30 s	

Elongation	72*/68**	1 min/kb* 2 min/kb**	
Final elongation	72*/68**	7 min	1
Cooling	4	∞	
*<10 kb vector DNA or <6 kb genomic DNA		>10 kb vector DNA or >6 kb genomic DNA	

Reverse transcription quantitative PCR (qRT-PCR)

To quantify mRNA expression in yeast a two-step reverse transcription quantitative PCR (qRT-PCR) was applied. First, RNA was extracted from yeast and converted into complementary DNA (cDNA) using a reverse transcriptase. The newly synthesized cDNA served as a template for quantitative real-time PCR. In general, 2 OD of mid-log phased yeast were harvested. RNA was isolated from cells according to the manufacturer's instructions (RNeasy Mini Kit, Qiagen). For the reverse transcription, 1 µg of total RNA was used as a template for the cDNA synthesis. The method was carried out according to the manufacturer's instructions (Transcriptor First Strand cDNA Synthesis Kit, Roche). Thereafter, 18 µl of qRT-PCR master mix containing SYBR Green I Master (LightCycler 480 SYBR Green I Master), primers and H_2O was added into 384 multiwell plates (LightCycler® 480 Multiwell Plate 384) and mixed with 2 µl of 1:5 diluted cDNA samples. Triplicates were made for each reaction and pipetted by a CAS-1200 OCR setup robot (Corbett Lifescience).

PCR reaction mixture		
	10 µl	SYBR Green I Master Mix
	0.12 µl	Primer 1 (100 µM)
	0.12 µl	Primer 2 (100 µM)
	7.76 µl	ddH_2O
	2 µl	cDNA PCR mix (1:5 diluted)

Cycling parameters

PCR step	T [°C]	Time	Cycles
Initial denaturation	95	10 min	1
Denaturation	95	10 s	
Annealing	55	10 s	45
Elongation	72	16 s	
4°C		∞	1

Second derivative maximum method was used to quantify the template cDNA concentrations. As a result, an input sample dilution series for each primer pair was used as a standard (1:1, 1:10, 1:100 and 1:1000). Additionally, to assess the specificity of primer pairs, a melting curve analysis was employed after the amplification step.

Trichloroacetic acid (TCA) protein precipitation

Small-scale, denaturing yeast cell extracts were prepared by TCA protein precipitation. A total of 1 OD yeast cells was pelleted by centrifugation (16.100 g, 1 min) and incubated in 1 ml ice-cold ddH_2O with 150 µl lysis buffer (2M NaOH, 7.5% β-mercaptoethanol) for 15 min on ice. Proteins were then precipitated by the addition of 150 µl 55% TCA and incubated for 15 min on ice. The precipitated material was sedimented by two consecutive centrifugation steps (20.000 g, 15 min, 4°C and 16.000 g, 1 min, RT). Denatured proteins were then resuspended in 100 µl HU sample buffer.

SDS-polyacrylamide gel electrophoresis (SDS-PAGE)

SDS-PAGE was performed in order to separate proteins according to their respective sizes. Pre-cast 4-12% gradient gels (NuPage 4-12% Bis-Tris Protein Gels, Invitrogen) were mainly used for this study, since these gels allowed a good resolution of various sized proteins (10 – 200 kDa). Protein samples were loaded onto the gels and separated by gel electrophoresis was carried out at a constant voltage of 110 V for 2 h using MOPS buffer. Protein sizes were determined by using a pre-stained protein standard marker (Precision Plus Protein All Blue Standards, Bio-Rad Laboratories). Proteins separated by SDS-PAGE were either

stained with Coomassie brilliant blue or transferred to a polyvinylidene fluoride (PVDF) membrane for immunoblotting (see Western blot analysis).

Coomassie staining

To remove SDS from SDS-PAGE gels, which inhibited the staining efficiency Coomassie brilliant blue, gels were washed three times with 100 ml ddH_2O for 10 minutes at RT. Proteins were subjected to an in-gel staining step by incubating it with a Coomassie brilliant blue solution (PageBlue protein staining solution, Thermo Scientific) for 1h (or overnight) at RT. Background staining was removed by washing the gels with 100 ml ddH_2O for 20 min at RT.

Western blot analysis

Western blotting analysis utilizes specific antibodies that allow the visualization of target proteins. Proteins were first separated by SDS-PAGE (see above) and transferred onto PVDF membranes (Immobilon-P, Millipore) using a wet tank blotting system (TE22 Mighty Small Transfer Tank, Hoefer). Protein blotting was achieved in a blotting buffer containing transfer tank at a constant voltage of 70 V for 2 h at 4°C. PVDF membranes were initially blocked for 30 min – 1 h at RT using a blocking buffer (TBST with 5% skim milk powder) and consequently incubated with a primary antibody either for 1 h at RT or overnight at 4°C under constant shaking. The membrane was washed twice with TBST for 5 min at RT, incubated with horseradish peroxidase-conjugated secondary antibody (1:5000, Dianova) diluted in blocking buffer for 1-2 h at RT and washed twice times with TBST for 30 min at RT. Target proteins were detected by chemiluminescence using enhanced chemiluminescence kits (Pierce ECL Western Blotting Substrate and Pierce ECL 2 Western Blotting Substrate, Thermo Fisher Scientific) followed by exposure to light sensitive films (Amersham Hyperfilm ECL, GE Healthcare). Alternatively, a charged-coupled device camera (LAS-3000, Fujifilm) was used for chemiluminescent detection of target proteins.

Purification of ^{HisStrep}Urm1-conjugates from denatured yeast extracts

To identify urmylated conjugates in yeast expressing N-terminally His-tagged Urm1, a denatured Ni-NTA purification was carried out (Hoege *et al.*, 2002; Sacher

et al., 2005). Firstly, 200 OD of log-phased cells were harvested by centrifugation (2500 g, 5 min, 4°C), washed with 50 ml cold PBS, transferred to a 50 ml falcon tube and lysed by incubating the cells with 5 ml of lysis buffer (1.85 M NaOH, 7.5% β-mercaptoethanol) for 15 min on ice. The cell lysate was incubated with 5 ml 55% TCA for 15 min on ice; precipitates were sedimented by centrifugation (8000 g, 20 min, 4°C), washed twice with 5 ml ice-cold acetone. The pellet was air-dried for 10 min at RT, resuspended in buffer A (6 M guanidinium chloride, 100mM NaH2PO4, 10mM Tris-HCl, pH 8.0, 0.5% NP-40) and incubated for 1 h at RT under constant shaking. Insoluble aggregates were removed by centrifugation (20.000 g, 20 min, 4°C), after which the supernatant was transferred to a fresh 15 ml falcon tube. Thereafter, 20 mM imidazole and 50 µl of Ni-NTA agarose beads (Qiagen) were added to the denatured protein extract and incubated over night at 4°C. The protein solution was loaded onto 5 ml a disposable polypropylene column (Qiagen) and the Ni-NTA agarose beads were cleared from the protein extract by gravity-flow. Beads were washed once with 15 ml of washing buffer 1 (buffer A with 20 mM imidazole), 15 ml of washing buffer 2 (buffer A with 20 mM imidazole, pH 6.3), 15 ml of buffer C (8 M urea, 200 mM NaCl, 100 mM Tris-HCl, pH 6.3) with 0.5% NP-40 and finally with 15 ml of buffer C. ^{His}Urm1-conjugates that were bound to the beads were eluted by incubation with 30 µl of SDS sample buffer at 99°C for 10 min. Samples were subsequently subjected to SDS-PAGE and immunoblotting.
For a His/Strep-tag tandem affinity purification of ^{HisStrep}Urm1, Urm1-conjugates were eluted with 15 ml elution buffer (8 M urea, 200 mM NaCl, 50 mM NaH_2PO_4, 100 mM Tris-HCl, pH 6.3, 250 mM imidazole, 1% SDS) and dialyzed against PBS, pH 8.0 at 4°C overnight. 1 ml of strep-tactin slurry (Strep-Tactin Superflow Plus, Qiagen) was added to the dialyzed eluate and incubated for 4 h or overnight at 4°C. The strep-tactin beads were washed three times with 10 bed volumes of PBS. Urm1-conjugates were eluted with 1 ml of 10 mM desthiobiotin, precipitated with 500 µl 55% TCA for 15 min on ice and sedimented by two centrifugation steps (20.000 g, 15 min, 4°C; 20.000 g, 1 min, RT). Precipitates were resuspended in HU buffer, incubated at 65°C for 10 min and analyzed by Western blotting.

Purification of recombinant GST-tagged proteins from *E. coli*

Rosetta (DE3) or Rosetta 2 cells expressing recombinant GST-tagged proteins were resuspended in 30-40 ml lysis buffer (1x PBS, 400 mM NaCl, 5 mM DTT, PIC) and disrupted by a high-pressure homogenizer (3x 40 mbar, EmulsiFlex-C3, Avestin). Lysates were cleared from the insoluble cell material (23.000 g, 20 min, 4°C) and incubated with 800 µl glutathione sepharose slurry (glutathione sepharose 4 Fast Flow, GE Healthcare) for 2 h at 4°C. The suspension was loaded onto a column, which separated the resins from the cell lysate. Resins were washed with 0.5 l lysis buffer and eluted twice with 0.5 ml elution buffer (1x PBS, 400 mM NaCl, 5 mM DTT, 50 mM gluthathione, PIC). The eluate was dialyzed against PBS over night at 4°C, frozen in liquid N_2 and stored at -80°C. For the tandem purification of GST-His-Flag-Urm1, GST purification was carried out as described above. Instead of eluting the glutathione resins with the elution buffer, resins were incubated with 20 U/ml thrombin at 25°C overnight. Resins were sedimented (500 g, 2 min, RT) and 100 µl of Ni-NTA agarose (Qiagen) were incubated with the supernatant for 1h at 25°C. The suspension was loaded onto a column, washed three times with 10 ml Ni-NTA washing buffer (PBS, 20 mM imidazole) and eluted with 1 ml NiNTA elution buffer (PBS, 250 mM imidazole). The elution was subsequently dialyzed against PBS over night at 4°C, frozen in liquid nitrogen and stored at -80°C.

5.3 Mass spectrometry analyses

SILAC-based mass spectrometry

Stable isotope labeling with amino acids in cell culture (SILAC) coupled with MS/MS was employed to detect novel Urm1-conjugates. Auxotrophic yeast mutant variant strains deficient in the biosynthesis of lysine and arginine (*Δlys1 Δarg4*) expressing His- and HA-tagged Urm1 (^{HisHA}Urm1) were grown for at least 10 cell divisions in SC growth media supplemented with either normal or heavy arginine and lysine (Arg^0, Lys^0; Light, Arg^{10}, Lys^8; Heavy, Cambridge Isotope Laboratories). Mid-log phased yeast cells grown in heavy SC media were treated with 10 mM NEM for 1 h at 30°C, harvested and combined with equal amount of untreated cells that were grown in light SC media. For label-swap replication experiments,

cells grown in light SC media were treated with 10 mM NEM for 1 h at 30°C, harvested and combined with equal amount of untreated cells grown in heavy SC media. ^{HisHA}Urm1-conjugates were purified using either denaturing Ni-NTA purification or a denaturing tandem affinity purification (see Purification of ^{HisStrep}Urm1-conjugates from denatured yeast extracts) and separated by SDS-PAGE, stained with Coomassie Blue, excised in ten slices, trypsinized and analyzed by LC-MS/MS at the Biochemistry Core Facility of the Max-Planck Institute of Biochemistry using LTQ-Orbitrap mass spectrometers. Peptides of putative urmylated-conjugates were identified using the MaxQuant software (Cox and Mann, 2008). Search for Urm1 branch motif (TLHGG-ε-K, HGG-ε-K) were carried out either with *urm1-S94R* or *urm1-L96R* mutant variants. These mutants enabled trypsin-dependent cleavage of the C-terminal tail of Urm1 and subsequently the identification of putative urmylation sites.

5.4 Computational analyses

The Saccharomyces Genome Database (www.yeastgenome.org/) and the National Center for Biotechnology Information (www.ncbi.nlm.nih.gov/) were sources for DNA/protein sequences and scientific literature. DNA sequencing analyses and DNA primer design were carried out either with Lasergene 13 (DNASTAR) or with SnapGene Viewer (SnapGene). Protein and DNA sequence alignment was either analyzed with BLAST (blast.ncbi.nlm.nih.gov) or with MultAlin (multalin.toulouse.inra.fr/multalin/). Images obtained either by microscopy or by Western blot quantification were carried out with ImageJ (https://imagej.nih.gov/ij/). Contrast of western blot films was adjusted using Adobe Photoshop CS5.1 (Adobe Systems). For texts, tables, graphs and figures Microsoft Office 2011 (Microsoft Corporation) was used.

6 References

Andersen, J. S., Matic, I., and Vertegaal, A. C. (2009). Identification of SUMO target proteins by quantitative proteomics. Methods Mol. Biol. *497*, 19-31.

Andreini, C., Banci, L., Bertini, I., Rosato, A. (2006). Counting the zinc-proteins encoded in the human genome. J. Proteome Res. *5(1)*, 196-201.

Anjum, R. S., Bray, S. M., Blackwood, J. K., Kilkenny, M. L., Coelho, M. A., Foster, B. M., Li, S., Howard, J. A., Pellegrini, L., Albers, S. V., Deery, M. J., and Robinson, N. P. (2015). Involvement of a eukaryotic-like ubiquitin-related modifier in the proteasome pathway of the archaeon *Sulfolobus acidocaldarius*. Nat. Commun. *6*, 8163.

Arnold, L., Höckner, S., and Seufert, W. (2015). Insights into the cellular mechanism of the yeast ubiquitin ligase APC/C-Cdh1 from the analysis of in vivo degrons. Mol. Biol. Cell. *26(5)*, 843–858.

Avci, D., Fuchs, S., Schrul, B., Fukumori, A., Breker, M., Frumkin, I., Chen, C. Y., Biniossek, M. L., Kremmer, E., Schilling, O., Steiner, H., Schuldiner, M., and Lemberg, M. K. (2014). Mol Cell. *56(5)*, 630-640.

Bachmair A., Finley D., Varshavsky A. (1986). *In vivo* half-life of a protein is a function of its amino-terminal residue. Science *234 (4773)*, 179-186.

Baker, R. T., Board, P. G. (1987). The human ubiquitin gene family: structure of a gene and pseudogenes from the Ub B subfamily. Nucleic Acids Res. *15*, 443–463.

Begley, T. P., Xi, J., Kinsland, C., Taylor, S. and McLafferty (1999). The enzymology of sulfur activation during thiamin and biotin biosynthesis. F. Curr. Opin. Chem. Biol. *3*, 623–629.

Bennett, E.J., Bence, N.F., Rajadas, J., and Kopito, R.R. (2005). Global impairment of the ubiquitin-proteasome system by nuclear or cytoplasmic protein aggregates precedes inclusion body formation. Mol. Cell *17*, 351–365.

Bird, A., Evans-Galea, M. V., Blankman, E., Zhao, H., Luo, H., Winge, D. R., and Eide, D. J. (2000). Mapping the DNA Binding Domain of the Zap1 Zinc-Responsive Transcriptional Activator. J. Biol. Chem. *275(21)*, 16160-16166.

Bird, A. J., Zhao, H., Luo, H., Jensen, L. T., Srinivasan, C., Evans-Galea, M., Winge, D. R., and Eide, D. J. (2000). A dual role for zinc fingers in both DNA binding and zinc sensing by the Zap1 transcriptional activator. EMBO J. *19*, 3704 –3713.

Bird, A. J., Swierczek, S., Qiao, W., Eide, D. J., and Winge, D. R. (2006). Zinc Metalloregulation of the Zinc Finger Pair Domain. J. Biol. Chem. *281*, 25326 – 25335.

Bird, A. J., McCall, K., Kramer, M., Blankman, E., Winge, D. R.,and Eide, D. J. (2003). Zinc fingers can act as Zn2+ sensors to regulate transcriptional activation domain function. EMBO J. *22*, 5137–5146.

Bird, A. J. (2015). Cellular sensing and transport of metal ions: implications in micronutrient homeostasis. J. Nut. Biochem. *26*, 1103–1115.

Bjork, G. R., Huang, B., Persson, O. P., and Bystrom, A. S. (2007). A conserved modified wobble nucleoside (mcm^5s^2U) in lysyl-tRNA is required for viability in yeast. RNA *13*, 1245–1255.

Böttcher, B., Palige, K., Jacobsen, I. L., Hube, B., and Brunke, S. (2015). Csr1/Zap1 Maintains Zinc Homeostasis and Influences Virulence in Candida dubliniensis but Is Not Coupled to Morphogenesis. Eukaryot Cell. *14(7)*, 661–670.

Broadley, M. R., White, P. J., Hammond, J. P., Zelko I., and Lux A. (2007). Zinc in plants. New Phytologist. *173 (4)*, 677–702.

Brugnera, E., Georgiev, O., Radtke, F., Heuchel, R., Baker, E., Sutherland, G. R., and Schaffner, W. (1994). Cloning, chromosomal mapping and characterization of the human metal-regulatory transcription factor MTF-1. Nucleic Acids Res. *22(15)*, 3167–3173.

Burroughs, A. M., Iyer, L. M., and Aravind, L. (2009). Natural history of the E1-like superfamily: implication for adenylation, sulfur transfer and ubiquitin conjugation. Proteins *75(4)*, 895–910.

Cadima-Couto, I., Freitas-Vieira, A., Nowarski, R., Britan-Rosich, E., Kotler, M., Goncalves, J. (2009). Ubiquitin-fusion as a strategy to modulate protein half-life: A3G antiviral activity revisited. Virology. *393(2)*, 286-94.

Catic, A, and Ploegh, H. L. (2005). Ubiquitin – conserved protein or selfish gene? Trends in Biochemical Sciences *30(11)*, 600–604.

Chalfie M., Euskirchen G., Ward W. W., Prasher D. C. (1994). Green fluorescent protein as a marker for gene expression. Science *263*, 802–805.

Chau, V., Tobias, J. W., Bachmair, A., Marriott, D., Ecker, D.J., Gonda, D. K., and Varshavsky, A. (1989). A multiubiquitin chain is confined to specific lysine in a targeted short-lived protein. Science *243*, 1576-1583.

Chen, P., Johnson, P., Sommer, T., Jentsch, S., and Hochstrasser, M. (1993). Multiple ubiquitin-conjugating enzymes participate in the in vivo degradation of the yeast MAT alpha 2 repressor. Cell *74*, 357–369.

Chen, C., Tuck, S., and Bystrom, A. S. (2009). Defects in tRNA modification associated with neurological and developmental dysfunctions in *Caenorhabditis elegans* elongator mutants. PLoS Genet. *5(7)*, e1000561.

Choi, S., and Bird, A. J. (2014). Zinc'ing sensibly: controlling zinc homeostasis at the transcriptional level. Metallomics *6*, 1198-1215.

Chong, Y.T., Koh, J. L., Friesen, H., Duffy, S. K., Cox, M. J., Moses, A., Moffat, J., Boone, C., and Andrews, B. J. (2015). Yeast Proteome Dynamics from Single Cell Imaging and Automated Analysis. Cell *161(6)*, 1413-1424.

Chowdhury M. M., Dosche C., Löhmannsröben H.-G., and Leimkühler S. (2012). Dual Role of the Molybdenum Cofactor Biosynthesis Protein MOCS3 in tRNA Thiolation and Molybdenum Cofactor Biosynthesis in Humans. J. Biol. Chem. *287*, 17297-17307.

Costanzo M., Baryshnikova A., Bellay J., Kim Y., Spear E. D., Sevier C. S., Ding H., Koh J. L., Toufighi K., Mostafavi S., Prinz J., Onge R. P. St., VanderSluis B., Makhnevych T., Vizeacoumar F. J., Alizadeh S., Bahr S., Brost R. L., Chen Y., Cokol M., Deshpande R., Li Z., Lin Z. Y., Liang W., Marback M., Paw J., San Luis B. J., Shuteriqi E., Tong A. H., van Dyk N., Wallace I. M., Whitney J. A., Weirauch M. T., Zhong G., Zhu H., Houry W. A., Brudno M., Ragibizadeh S., Papp B., Pal C., Roth F. P., Giaever G., Nislow C., Troyanskaya O. G., Bussey H., Bader G. D., Gingras A. C., Morris Q. D., Kim P. M., Kaiser C. A., Myers C. L., Andrews B. J., and Boone C. (2010). The Genetic Landscape of a Cell. Science *5964*(327), 425-431.

Dean, R. T., Fu, S., Stocker, R., and Davies, M. J. (1997). Biochemistry and pathology of radical-mediated protein oxidation. Biochem. J. *324 (Pt 1)*, 1-18.

Eide, D. J. (2011). The oxidative stress of zinc deficiency. Metallomics *3*, 1124-1129.

Koh J. L., Chong Y. T., Friesen H., Moses A., Boone C., Andrews B. J., and Moffat J. (2015). CYCLoPs: A Comprehensive Database Constructed from Automated Analysis of Protein Abundance and Subcellular Localization Patterns in Saccharomyces cerevisiae. G3 (Bethesda) *5(6)*,1223-1232.

Chen Z. J., and Sun, L. J. (2009). Nonproteolytic functions of ubiquitin in cell signaling. Mol. Cell. *33(3)*, 275-286.

Choi, S., and Bird, A. J. (2014). Zinc'ing sensibly: controlling zinc homeostasis at the transcriptional level. Metallomics *6*, 1198-1215.

Chong, Y. T., Koh, J. L., Friesen, H., Duffy, K., Cox, M. J., Moses, A., Moffat, J., Boone, C., and Andrews, B. J. (2015). Yeast Proteome Dynamics from Single Cell Imaging and Automated Analysis. Cell *161(6)*, 1413-1424.

Cox, K. H., Kulkarni, A., Tate, J. J., and Cooper, T.G. (2004). Gln3 phosphorylation and intracellular localization in nutrient limitation and starvation differ from those generated by rapamycin inhibition of Tor 1/2 in *Saccharomyces cerevisiae*. J. Biol. Chem. *279*, 10270–10278.

Cox, J., and Mann, M. (2008). MaxQuant enables high peptide identification rates, individualized p.p.b.-range mass accuracies and proteome-wide protein quantification. Nat. Biotechnol. *26*, 1367-1372.

Damon, J. R., Pincus, D., and Ploegh, H. L. (2015). tRNA thiolation links translation to stress responses in *Saccharomyces cerevisiae*. Mol. Biol. Cell *26(2)*, 270-282

Deng, M., and Hochstrasser, M. (2006). Spatially regulated ubiquitin ligation by an ER/nuclear membrane ligase. Nature *443 (7113)*, 827–831.

De Nicola, R., Hazelwood, L. A., DeHulster, E. A., Walsh, M. C., Knijnenburg, T. A., Reinders, M. J., Walker, G. M., Pronk, J. T., Daran, J. M., and Daran-Lapujade, P. (2007). Physiological and transcriptional responses of Saccharomyces cerevisiae to zinc limitation in chemostat cultures. Appl. Environ. Microbiol. *73*, 7680 –7692.

Desterro, J. M., Rodriguez, M. S. & Hay, R. T. (1998). SUMO-1 modification of IkappaBalpha inhibits NF-kappaB activation. Mol. Cell *2*, 233-239

Dewez, M., Bauer, F., Dieu, M., Raes, M., Vandenhaute, J., and Hermand, D. (2008). The conserved Wobble uridine tRNA thiolase Ctu1-Ctu2 is required to maintain genome integrity. Proc. Natl. Acad. Sci. USA *105(14)*, 5459-5464.

Eide, D. J. (2003). Review Multiple regulatory mechanisms maintain zinc homeostasis in Saccharomyces cerevisiae. J Nutr. *133(5 Suppl 1)*, 1532S-1535S.

El Yacoubi, B., Bailly, M., and de Crécy-Lagard, V. (2012). Biosynthesis and function of posttranscriptional modification of transfer RNAs. Annu. Rev. Genet. *46*, 69–95.

Fan, J. B., Arimoto, K. I., Motamedchaboki, K., Yan, M., Wolf D. A., and Zhang, DE. (2015). Identification and characterization of a novel ISG15-ubiquitin mixed chain and its role in regulating protein homeostasis. Scientific Reports *5(1)*, 425-436.

Fichtner, L., Jablonowski, D., Schierhorn, A., Kitamoto, H. K., Stark, M. J., and Schaffrath, R. (2003). Elongator's toxin-target (TOT) function is nuclear localization sequence dependent and suppressed by post-translational modification. Mol Microbiol. *49(5)*, 1297-1307.

Finley, D., Ozkaynak, E., and Varshavsky, A. (1987). The yeast polyubiquitin gene is essential for resistance to high temperatures, starvation, and other stresses. Cell *48*, 1035-1046.

Finley, D., Sadis, S., Monia, B. P., Boucher, P., Ecker, D. J., Crooke, S. T., and Chau, V. (1994). Inhibition of proteolysis and cell cycle progression in a multiubiquitination-deficient yeast mutant. Mol. Cell. Biol. *14*, 5501-5509.

Frey, A. G., Bird, A. J., Evans-Galea, M. V., Blankman, E., Winge, D. R., and Eide D. J. (2011). Zinc-regulated DNA binding of the yeast Zap1 zinc-responsive activator. PLoS ONE *6(7)*, e22535.

Fukada, T., Yamasaki, S., Nishida, K., Murakami, M. and Hirano, T. (2011). Zinc homeostasis and signaling in health and diseases Zinc signaling. J. Biol. Inorg. Chem. *16(7)*, 1123–1134.

Furukawa, K., Mizushima, N., Noda, T., and Ohsumi, Y. (2000). A protein conjugation system in yeast with homology to biosynthetic enzyme reaction of prokaryotes. J. Biol. Chem. *275(11)*, 7462–7465.

Gaither, L. A., and Eide D. J. (2001). 2 Eukaryotic zinc transporters and their regulation. BioMetals *14*, 251–270.

Geoffroy, MC., and Hay, R. T. (2009). An additional role for SUMO in ubiquitin-mediated proteolysis. Nature Reviews Mol. Cell Biol. *10*, 564-568.

Ghaemmaghami, S., Huh, W. K., Bower, K., Howson, R. W., Belle, A., Dephoure, N., O'Shea, E. K., and Weissman, J. S. (2003). Global analysis of protein expression in yeast. Nature *425(6959)*, 737-741.

Ghislain, M., Udvardy, A., and Mann, C. (1993). S. cerevisiae 26S protease mutants arrest cell division in G2/metaphase. Nature *366*, 358-362.

Gietz, R.D., and Sugino, A. (1988). New yeast-Escherichia coli shuttle vectors constructed with in vitro mutagenized yeast genes lacking six-base pair restriction sites. Gene *74*, 527-534.

Gilon, T., Chomsky, O., and Kulka, R. G. (1998). Degradation signals for ubiquitin system proteolysis in Saccharomyces cerevisiae. EMBO J. *17*, 2759–2766.

Goehring, A. S., Rivers, D. M., and Sprague, G. F., Jr. (2003). Attachment of the ubiquitin-related protein Urm1p to the antioxidant protein Ahp1p. Eukaryot Cell *2*, 930–936.

Goehring, A. S., Rivers, D. M., Sprague, G. F., Jr. (2003). Urmylation: A ubiquitin-like pathway that functions during invasive growth and budding in yeast. Mol. Biol. Cell *14*, 4329–4341.

Gong, L., Ji, W. K., Hu, X. H., Hu, W. F., Tanga, X.-C., Huang, Z.-C., Li, L., Liu, M., Xiang, S.-H., Wu, E., Woodward, Z., Liu, Y.-Z., Nguyena, Q. D., and Li. D. W.-C. (2014). Sumoylation differentially regulates Sp1 to control cell differentiation. Proc. Natl. Acad. Sci. USA *111*, 5574–5579.

Grant, C. M., Quinn, K. A., and Dawes, I. W. Differential protein S-thiolation of glyceraldehyde-3-phosphate dehydrogenase isoenzymes influences sensitivity to oxidative stress. (1999). Mol. Cell Biol. *19(4)*, 2650-2656.

Gregory, J. D. (1955). The stability of N-ethylmaleimide and its reaction with sulfhydryl groups. J. Am. Chem. Soc. *77*, 3922–3923.

Herbig A., Bird A. J., Swierczek S., McCall K., Mooney M., Wu C. Y., Winge D. R., Eide D. J. (2005). Zap1 activation domain 1 and its role in controlling gene expression in response to cellular zinc status. Mol. Microbiol. *57*, 834–846

Hambidge, K. M. and Krebs, N. F. (2007). Zinc deficiency: a special challenge. J. Nutr. *137(4)*, 1101–1105.

Hamer, D. H. (1986). Metallothionein. Ann. Rev. Biochem. *55*, 913-951.

Ho, E., and Ames, B. N. (2002). Low intracellular zinc induces oxidative DNA damage, disrupts p53, Nfkappa B, and AP1 DNA binding, and affects DNA repair in a rat glioma cell line. Proc. Natl. Acad. Sci. U. S. A. *99(26)*, 16770–5.

Ho E. (2004). Zinc deficiency, DNA damage and cancer risk. J. Nutr. Biochem. *15*, 572 – 578.

Hochstrasser, M. (2000). Evolution and function of ubiquitin-like protein-conjugation systems. Nat. Cell Biol. *2*, E153 - E157.

Hochstrasser, M. (2009). Origin and function of ubiquitin-like proteins. Nature *458*, 422-429.

Hochstrasser, M., Ellison, M. J., Chau, V., and Varshavsky, A. (1991). The short-lived MAT alpha 2 transcriptional regulator is ubiquitinated in vivo Proc. Natl. Acad. Sci. U. S. A *88*, 4606–4610.

Hochstrasser, M., and Varshavsky, A. (1990). In vivo degradation of a transcriptional regulator: the yeast alpha 2 repressor. Cell 61, 697–708.

Hoege, C., Pfander, B., Moldovan, G.L., Pyrowolakis, G., and Jentsch, S. (2002). RAD6- dependent DNA repair is linked to modification of PCNA by ubiquitin and SUMO. Nature *419*, 135-141.

Hofmann, K. & Stoffel, W. (1993). TMbase - A database of membrane spanning proteins segments. Biol. Chem. Hoppe-Seyler *374*,166.

Hopper, A.K. (2013). Transfer RNA post-transcriptional processing, turnover, and subcellular dynamics in the yeast Saccharomyces cerevisiae. Genetics *194*, 43–67.

Horton, P., Park, K. J., Obayashi, T., Fujita, N., Harada, H., Adams-Collier, C. J., and Nakai, K. (2007). WoLF PSORT: protein localization predictor. Nucleic. Acids. Res. *35 (suppl_2)*, W585-W587.

Huang, B., Lu, J., and Bystrom, A. S. (2008). A genome-wide screen identifies genes required for formation of the wobble nucleoside 5-methoxycarbonylmethyl-2-thiouridine in *Saccharomyces cerevisiae*. RNA *14(10)*, 2183-2194.

Humbard, M. A., Miranda, H. V., Lim, J.-M., Krause, D. J., Pritz, J. R., Zhou, G., Chen, S, Wells, L., and Maupin-Furlow, J. A. (2010). Ubiquitin-like small archaeal modifier proteins (SAMPs) in *Haloferax volcanii*. Nature *463*, 54–60.

Husnjak, K., Elsasser, S., Zhang, N., Chen, X., Randles, L., Shi, Y., Hofmann, K., Walters, K. J., Finley, D., and Dikic, I. (2008). Proteasome subunit Rpn13 is a novel ubiquitin receptor. Nature *453*, 481–488.

Iyer, L. M., Burroughs, A. M., and Aravind, L. (2006). The prokaryotic antecedents of the ubiquitin-signaling system and the early evolution of ubiquitin-like beta-grasp domains. Genome Biol. *7(7)*, R60.

Jablonowski, D., Zink, S., Mehlgarten, C., Daum, G., and Schaffrath R. (2006). tRNAGlu wobble uridine methylation by Trm9 identifies Elongator's key role for zymocin-induced cell death in yeast. Mol. Microbiol. *59(2)*, 677-88.

Jackman, J. E., Alfonzo, J. D. (2013). Transfer RNA modifications: Nature's combinatorial chemistry playground. Wiley Interdiscip. Rev. RNA. *4*, 35–48.

James, P., Halladay, J., and Craig, E.A. (1996). Genomic libraries and a host strain designed for highly efficient two-hybrid selection in yeast. Genetics *144*, 1425-1436.

Janke, C., Magiera, M. M., Rathfelder, N., Taxis, C., Reber, S., Maekawa, H., Moreno-Borchart, A., Doenges, G., Schwob, E., Schiebel, E., et al. (2004). A versatile toolbox for PCR-based tagging of yeast genes: new fluorescent proteins, more markers and promoter substitution cassettes. Yeast *21*, 947-962.

Jarosz, M., Olbert, M., Wyszogrodzka, G., Młyniec, K., and Librowski, T. Antioxidant and anti-inflammatory effects of zinc. Zinc-dependent NF-κB signaling. (2017). Inflammopharmacology *25(1)*, 11-24.

Jeong, J. S., Kwon, S. J., Kang, S. W., Rhee, S. G., and Kim, K. (1999). Purification and characterization of a second type thioredoxin peroxidase (type II TPx) from *Saccharomyces cerevisiae*. Biochemistry *38*, 776–783.

Johansson, M. J. O., Esberg, A., Huang, B., Björk, G. R., and Byström, A. S. (2008). Eukaryotic wobble uridine modifications promote a functionally redundant decoding system. Mol. Cell. Biol. *28*, 3301–3312.

Johnson, C., Van Antwerp, D., and Hope, T. J. (1999). An N-terminal nuclear export signal is required for the nucleocytoplasmic shuttling of IκBα. EMBO J. *18(23)*, 6682-6693.

Jüdes, A., Bruch, A., Klassen, R., Helm, M., and Schaffrath, R. (2016). Sulfur transfer and activation by ubiquitin-like modifier system Uba4•Urm1 link protein urmylation and tRNA thiolation in yeast. Microbial. Cell *3(11)*, 554 – 564.

Kawamata, T., Horie, T., Matsunami, M., Sasaki, M., and Ohsumi Y. (2017). Zinc starvation induces autophagy in yeast. J. Biol. Chem. *292(20)*, 8520-8530

Kerscher, O., Felberbaum, R., and Hochstrasser, M. (2006). Modification of proteins by ubiquitin and ubiquitin-like proteins. Annu. Rev. Cell. Dev. Biol. *22*, 159–180.

Kim, M. J., Kil, M., Jung, J. H. and Kim, J. (2008). Roles of zinc-responsive transcription factor Csr1 in filamentous growth of the pathogenic yeast Candida albicans. J. Microbiol. Biotechnol. *18*, 242–247.

Krepinsky, K., and Leimkühler, S. (2007). Site-directed mutagenesis of the active site loop of the rhodanese-like domain of the human molybdopterin synthase sulfurase MOCS3. FEBS Journal *274*, 2778–2787.

Krezel, A., and Maret, W. (2007). Dual nanomolar and picomolar Zn(II) binding properties of metallothionein. J. Am. Chem. Soc. *129(35)*, 10911-10921.

Knop, M., Siegers, K., Pereira, G., Zachariae, W., Winsor, B., Nasmyth, K., and Schiebel, E. (1999). Epitope tagging of yeast genes using a PCR-based strategy: more tags and improved practical routines. Yeast *15*, 963-972.

Khoshnood, B., Dacklin, I., and Grabbe, C. (2016). Urm1: an essential regulator of JNK signaling and oxidative stress in Drosophila melanogaster. Cell. Mol. Life Sci. *73(9)*, 1939-1954.

Koh, J. L., Chong, Y. T., Friesen, H., Moses, A., Boone, C., Andrews, B. J., Moffat, J. (2015). CYCLoPs: A Comprehensive Database Constructed from Automated Analysis of Protein Abundance and Subcellular Localization Patterns in *Saccharomyces cerevisiae.* G3 (Bethesda) *5(6)*, 1223-32.

Kosugi, S., Hasebe, M., Tomita, M., and Yanagawa, H. (2009). Systematic identification of yeast cell cycle-dependent nucleocytoplasmic shuttling proteins by prediction of composite motifs. Proc. Natl. Acad. Sci. USA *106*, 10171-10176.

Kunkel, T. A. (1985) Rapid and efficient site-specific mutagenesis without phenotypic selection. Proc. Natl. Acad. Sci. U. S. A. *82,* 488-492.

Lake, M. W., Wuebbens, M. M., Rajagopalan, K. V., and Schindelin, H. (2001). Mechanism of ubiquitin activation revealed by the structure of a bacterial MoeB-MoaD complex. Nature *414*, 325–329.

Laxman, S., Sutter, B. M., Wu, X., Kumar, S., Guo, X., Trudgian, D. C., Mirazei, H., and Tu, B. P. (2013). Sulfur Amino Acids Regulate Translational Capacity and Metabolic Homeostasis through Modulation of tRNA Thiolation. Cell *154(2)*, 416–429.

Lee, J., Spector, D., Godon, C., Labarre, J., and Toledano, M. B. (1999). A new antioxidant with alkyl hydroperoxide defense properties in yeast. J. Biol. Chem. *274*, 4537–4544.

Lehmann, C., Begley, T. P., and Ealick, S. E. (2006). Structure of the Escherichia coli ThiS-ThiF complex, a key component of the sulfur transfer system in thiamin biosynthesis. Biochemistry *45(1)*, 11-19.

Leidecker, O., Matic, I., Mahata, B., Pion, E. & Xirodimas, D. P. (2012). The ubiquitin E1 enzyme Ube1 mediates NEDD8 activation under diverse stress conditions. Cell Cycle *11*, 1142–1150.

Leidel, S., Pedrioli, P. G., Bucher, T., Brost, R., Costanzo, M., Schmidt, A., Aebersold, R., Boone, C., Hofmann, K. and Peter, M. (2009). Ubiquitin-related modifier Urm1 acts as a sulphur carrier in thiolation of eukaryotic transfer RNA. Nature *458*, 228–232.

Leimkühler, S., Wuebbens, M. M., and Rajagopalan, K. V. (2001). Characterization of Escherichia coli MoeB and Its Involvement in the Activation of Molybdopterin Synthase for the Biosynthesis of the Molybdenum Cofactor. J. Biol. Chem. *276*, 34695–34701.

Li, X., Zhao, X., Fang, Y., Jiang, X., Duong, T., Fan, C., Huang C. C., and Kain S. R. (1998). Generation of Destabilized Green Fluorescent Protein as a Transcription Reporter. J. Biol. Chem. *273*, 34970- 34975.

Lindert, U., Cramer, M., Meuli, M., Georgiev, O., and Schaffner, W. (2009). Metal-responsive transcription factor 1 (MTF-1) activity is regulated by a nonconventional nuclear localization signal and a metal-responsive transactivation domain. Mol. Cell. Biol. *29(23)*, 6283-6293.

Longtine, M. S., McKenzie, A., 3rd, Demarini, D. J., Shah, N. G., Wach, A., Brachat, A., Philippsen, P., and Pringle, J. R. (1998). Additional modules for versatile and economical PCR-based gene deletion and modification in Saccharomyces cerevisiae. Yeast *14*, 953-961.

Lu, J., Huang, B., Esberg, A., Johansson, M. J. O., and Byström, A. S. (2005). The *Kluyveromyces lactis* γ-toxin targets tRNA anticodons. *RNA. 11(11)*, 1648–1654.

Lüders, J., Pyrowolakis, G., Jentsch, S. (2003). The ubiquitin-like protein HUB1 forms SDS-resistant complexes with cellular proteins in the absence of ATP. EMBO Rep. *4(12)*, 1169-1174.

Luo, S., and Levine, R. L. (2008). Methionine in proteins defends against oxidative stress. FASEB J. *23(2)*, 464-472.

Lyons, T. J., Gasch, A. P., Gaither, L. A., Botstein, D., Brown, P. O., and Eide, D. J. (2000). Genome-wide characterization of the Zap1p zinc-responsive regulon in yeast. Proc. Natl. Acad. Sci. U. S. A. *97*, 7957–7962.

MacDiarmid, C. W., Gaither, L. A., and Eide D. J. (2000). Zinc transporters that regulate vacuolar zinc storage in *Saccharomyces cerevisiae*. EMBO J. *19*, 2845-2855.

MacDiarmid, C. W., Milanick, M. A., and Eide D. J. (2003). Induction of the ZRC1 Metal Tolerance Gene in Zinc-limited Yeast Confers Resistance to Zinc Shock. J. Biol. Chem. *278*, 15065–15072.

MacDiarmid, C. W., Taggart, J., Kerdsomboon, K., Kubisiak, M., Panascharoen, S., Schelble, K., and Eide D. J. (2013). Peroxiredoxin chaperone activity is critical for protein homeostasis in zinc-deficient yeast. J. Biol. Chem. *288(43)*, 31313-31327.

Machnicka, M. A., Milanowska, K., Osman Oglou, O., Purta, E., Kurkowska, M., Olchowik, A., Januszewski, W., Kalinowski, S., Dunin-Horkawicz, S., Rother, K.M., Helm, M., Bujnicki, J. M., and Grosjean, H. (2013). MODOMICS: A database of RNA modification pathways—2013 update. Nucleic Acids Res. *41*, D262–D267.

Mann, M. (2006). Functional and quantitative proteomics using SILAC. Nat. Rev. Mol. Cell Biol. *7*, 952-958.

Maine, G. N., Li, H., Zaidi, I. W., Basrur, V., Elenitoba-Johnson, K. S. J., and Burstein, E. (2010). A bimolecular affinity purification method under denaturing conditions for rapid isolation of a ubiquitinated protein for mass spectrometry analysis. Nat. Protoc. *5(8)*, 1447-1459.

Malakhov, M. P., Mattern, M. R., Malakhova, O. A., Drinker, M., Weeks, S. D., and Butt, T. R. (2004). SUMO fusions and SUMO-specific protease for efficient expression and purification of proteins. J. Struct. Funct. Genomics *5*, 75–86.

Marelja, Z., Stocklein, W., Nimtz, M., and Leimkühler ,S. (2008). A novel role for human Nfs1 in the cytoplasm: Nfs1 acts as a sulfur donor for MOCS3, a protein involved in molybdenum cofactor biosynthesis. J. Biol. Chem. *283*, 25178–25185.

Matic, I., Hay, R. T. (2012). Detection and quantitation of SUMO chains by mass spectrometry. Methods Mol. Biol. *832*, 239-247.

Matic, I., van Hagen, M., Schimmel, J., Macek, B., Ogg, S. C., Tatham, M. H., Hay, R. T., Lamond, A. I., Mann, M., and Vertegaal, A. C. (2008). In vivo identification of human small ubiquitin-like modifier polymerization sites by high accuracy mass spectrometry and an *in vitro* to *in vivo* strategy. Mol. Cell Proteomics *7(1)*, 132-144.

Matic, I., Schimmel, J., Hendriks, I. A., van Santen, M. A., van de Rijke, F., van Dam, H., Gnad, F., Mann, M., and Vertegaal, A.C.O. (2010). Site-Specific Identification of SUMO-2 Targets in Cells Reveals an Inverted SUMOylation Motif and a Hydrophobic Cluster SUMOylation Motif. Mol. Cell *39*, 641-652.

Matthies, A., Rajagopalan, K. V., Mendel, R. R., and Leimkühler, S. (2004). Evidence for the physiological role of a rhodanese-like protein for the biosynthesis of the molybdenum cofactor in humans. Proc. Natl. Acad. Sci. USA *101*, 5946–5951.

Matthies, A., Nimtz, M., and Leimkühler, S. (2005). Molybdenum cofactor biosynthesis in humans: identification of a persulfide group in the rhodanese-like domain of MOCS3 by mass spectrometry. Biochemistry *44*, 7912-7920

Maupin-Furlow, J. A. (2013). Ubiquitin-like proteins and their roles in archaea. Trends Microbiol. *21(1)*, 31-38.

Mendel, R. R., Schwarz, G. (2002). Biosynthesis and molecular biology of the molybdenum cofactor (Moco). Met. Ions Biol. Syst. *39*, 317-368.

Miyabe, S., Izawa, S., and Inoue, Y. (2000). Expression of ZRC1 coding for suppressor of zinc toxicity is induced by zinc-starvation stress in Zap1-dependent fashion in *Saccharomyces cerevisiae*. Biochem. Biophys. Res. Commun. *276(3)*, 879-884.

Moldovan, G. L., Pfander, B., and Jentsch, S. (2006). PCNA controls establishment of sister chromatid cohesion during S phase. Mol. Cell *23*, 723-732.

Moldovan, G. L., Pfander, B., and Jentsch, S. (2007). PCNA, the Maestro of the Replication Fork. Cell *129(4)*, 665-679.

Moradas-Ferreira, P., Costa, V., Piper, P., and Mager, W. (1996). The molecular defences against reactive oxygen species in yeast. Mol. Microbiol. *19*, 651-658.

Moreno, M. A. , Ibrahim-Granet, O., Vicentefranqueira, R., Amich, J., Ave, P., Leal, F., Latge, J. P. and Calera, J. A. (2007). The regulation of zinc homeostasis by the ZafA transcriptional activator is essential for *Aspergillus fumigatus* virulence. Mol. Microbiol., 2007, 64, 1182–1197

Nakai, Y., Nakai, M., and Hayashi, H. (2008). Thio-modification of yeast cytosolic tRNA requires a ubiquitin-related system that resembles bacterial sulfur transfer systems. J. Biol. Chem. *283(41)*, 27469-76.

Nedialkova, D. D., and Leidel, S. A. (2015). Optimization of codon translation rates via tRNA modifications maintains proteome integrity. Cell *161(7)*, 1606–1618.

Netzer, N,, Goodenbour, J. M., David, A., Dittmar, K. A., Jones, R. B., Schneider, J. R., Boone, D., Eves, E. M., Rosner, M. R., Gibbs, J. S., Embry, A., Dolan, B., Das, S., Hickman, H. D., Berglund, P., Bennink, J. R., Yewdell, J. W., and Pan, T. Innate immune and chemically triggered oxidative stress modifies translational fidelity. Nature *462(7272)*, 522-526.

Nijman, S. M., Luna-Vargas, M. P., Velds, A., Brummelkamp, T. R., Dirac, A. M., Sixma, T. K., and Bernards, R. (2005). A genomic and functional inventory of deubiquitinating enzymes. Cell *123*, 773-786.

Noma, A., Sakaguchi, Y., and Suzuki, T. (2009). Mechanistic characterization of the sulfur-relay system for eukaryotic 2-thiouridine biogenesis at tRNA wobble positions. Nucleic Acids Res. *37*, 1335–1352.

North, M., Steffen, J., Loguinov, A. V., Zimmerman, G. R., Vulpe, C. D., and Eide, D. J. (2012). Genome-wide functional profiling identifies genes and processes important for zinc-limited growth of *Saccharomyces cerevisiae*. PLoS Genet. *8*, e1002699.

Ong, S. E., Blagoev, B., Kratchmarova, I., Kristensen, D.B., Steen, H., Pandey, A., and Mann, M. (2002). Stable isotope labeling by amino acids in cell culture, SILAC, as a simple and accurate approach to expression proteomics. Mol. Cell Proteomics *1*, 376-386.

Ong, S. E., Kratchmarova, I., and Mann, M. (2003). Properties of 13C-substituted arginine in stable isotope labeling by amino acids in cell culture (SILAC). J Proteome Res. *2*, 173–181.

Oteiza, P. I., Clegg, M. S., Zago, M. P., and Keen, C. L. (2000). Zinc deficiency induces oxidative stress and AP-1 activation in 3T3 cells. Free Radical Biol. Med. *28(7)*, 1091–9.

Ozkaynak, E., Finley, D., Solomon, M. J., and Varshavsky, A. (1987). The yeast ubiquitin genes: a family of natural gene fusions. EMBO J. *6*, 1429–1439.

Palmiter, R. D., and S. D. Findley. (1995). Cloning and functional characterization of a mammalian zinc transporter that confers resistance to zinc. EMBO J. *14*, 639–649.

Park, S. S., Wu, W. W., Zhou, Y., Shen, R. F., Martin, B., Maudsley, S. Effective correction of experimental errors in quantitative proteomics using stable isotope labeling by amino acids in cell culture (SILAC). J. Proteomics. *75(12)*, 3720-3732.

Pfander, B., Moldovan, G. L., Sacher, M., Hoege, C., and Jentsch, S. (2005). SUMO-modified PCNA recruits Srs2 to prevent recombination during S-phase. Nature *436*, 428-433.

Pitterle, D. M., Johnson, J. L., and Rajagopalan, K. V. (1993*). In vitro* synthesis of molybdopterin from precursor Z using purified converting factor. J. Biol. Chem. *268*, 13506-13509.

Powell, S. R. (2000). The antioxidant properties of zinc. J. Nutr. *130(5S Suppl)*, 1447S-1454S.

Pedrioli, P. G., Leidel, S., and Hofmann, K. (2008). Urm1 at the crossroad of modifications. EMBO reports *9*, 1196-1202.

Pickart, C. M. (2001). Ubiquitin enters the new millennium. Mol. Cell *8*, 499- 504.

Plum, L. M., Rink, L., and Haase, H. (2010). The Essential Toxin: Impact of Zinc on Human Health. Int. J. Environ. Res. Public Health. *7(4)*, 1342–1365.

Prakash, A., Bharti, K., Majeed, A. B. (2015). Zinc: indications in brain disorders. Fundam. Clin. Pharmacol. *29(2)*, 131–149.

Prasad, A. (2008). Zinc in Human Health: Effect of Zinc on Immune Cells. Mol. Med. *14(5-6)*, 353–357.

Psakhye I., and Jentsch S. (2012). Protein group modification and synergy in the SUMO pathway as exemplified in DNA repair. Cell *151(4)*, 807-820.

Qiao, W., Mooney, M., Bird, A. J., Winge, D. R., and Eide, D. J. (2006). Zinc binding to a regulatory zinc-sensing domain monitored in vivo by using FRET. Proc. Natl. Acad. Sci. U. S. A. *103*, 8674–8679.

Rajagopalan, K. V. (1997). Biosynthesis and processing of the molybdenum cofactors. Biochemical Society Transactions *25 (3),* 757-761.

Rape, M. (2010). Assembly of K11-Linked Ubiquitin Chains by the Anaphase-Promoting Complex. Subcellular Biochemistry Ch. Conjugation and Deconjugation of Ubiquitin Family Modifiers *54*, 107-115.

Ravid, T., Kreft, S. G., and Hochstrasser, M. (2006). Membrane and soluble substrates of the Doa10 ubiquitin ligase are degraded by distinct pathways. EMBO J. *25(3)*, 533–543.

Reyes-Turcu, F. E., Ventii, K. H., and Wilkinson, K. D. (2009). Regulation and cellular roles of ubiquitin-specific deubiquitinating enzymes. Annu. Rev. Biochem *78*, 363-397.

Rezgui, V. A., Tyagi, K., Ranjan, N., Konevega, A. L., Mittelstaet, J., Rodnina, M. V., Peter, M., Pedrioli, P. G. (2013). tRNA tKUUU, tQUUG, and tEUUC wobble position modifications fine-tune protein translation by promoting ribosome A-site binding. Proc. Natl. Acad. Sci. USA. *110(30)*, 12289-94.

Rubio-Texeira, M. (2007). Urmylation controls Nil1p and Gln3p-dependent expression of nitrogen-catabolite repressed genes in Saccharomyces cerevisiae. FEBS Lett. *581(3)*, 541-550.

Rudolph, M. J., Wuebbens, M. M., Rajagopalan, K. V., and Schindelin, H. (2001). Crystal structure of molybdopterin synthase and its evolutionary relationship to ubiquitin activation. Nat. Struct. Biol. *8*, 42–46.

Rutherford, J. C., and Bird, A. J. (2004). Metal-Responsive Transcription Factors That Regulate Iron, Zinc, and Copper Homeostasis in Eukaryotic Cells. Eukaryot. Cell. *3(1)*, 1–13.

Sacher, M., Pfander, B., and Jentsch, S. (2005). Identification of SUMO-protein conjugates. Methods Enzymol *399*, 392-404.

Sambrook, J., Fritsch, E. F., and Maniatis, T. (1989). Molecular Cloning, Cold Spring Harbor Laboratory Press, NY).

Schlieker, C. D., Van der Veen, A. G., Damon, J. R., Spooner, E., and Ploegh, H. L. (2008). A functional proteomics approach links the ubiquitin-related modifier Urm1 to a tRNA modification pathway. Proc. Natl. Acad. Sci. USA *105(47)*, 18255-18260.

Schmitz, J., Chowdhury, M. M., Hanzelmann, P., Nimtz, M., Lee, E. Y., Schindelin, H., and Leimkühler, S. (2008). The sulfurtransferase activity of Uba4 presents a link between ubiquitin-like protein conjugation and activation of sulfur carrier proteins. Biochemistry *47*, 6479-6489.

Schneider, O., Fogaca, S., Kmetzsch, L., Schrank, A., Vainstein, M. H. and Staats, C. C. (2012). Zap1 regulates zinc homeostasis and modulates virulence in *Cryptococcus gattii*. PLoS One *7*, e43773.

Schorpp, K. K. (2010). Charakterisierung des Urm1-Konjugations-Systems. Dissertation, LMU München: Faculty of Biology.

Schuppe-Koistinen, I., Moldeus, P., Bergman, T., and Cot- greave, L. A. (1994). S-thiolation of human endothelial cell glyceraldehyde-3-phosphate dehydrogenase after hydrogen per- oxide treatment. Eur. J. Biochem. *221*, 1033–1037.

Singh, R. K., Zerath, S., Kleifeld, O., Scheffner, M., Glickman, M. H., Fushman, D. (2012). Recognition and cleavage of related to ubiquitin 1 (Rub1) and Rub1-ubiquitin chains by components of the ubiquitin-proteasome system. Mol. Cell Proteomics *11*, 1595–1611.

Slekar, K. H., Kosman, D. J., and Culotta, V. C. (1996). The yeast copper/zinc superoxide dismutase and the pentose phosphate pathway play overlapping roles in oxidative stress protection. J. Biol. Chem. *271(46)*, 28831-28836.

Spence, J., Sadis, S., Haas, A. L., Finley, D. (1995). A ubiquitin mutant with specific defects in DNA repair and multiubiquitination. Mol. Cell Biol. *15(3)*, 1265-73.

Spragg, R. G., Hinshaw, D. B., Hyslopp, P. A., Schraufstätter, I. U., and Cochrane, C. G. (1985). Alterations in adenosine triphosphate and energy charge in cultured endothelial and P388D1 cells after oxidant injury. J. Clin. Invest. *76*, 1471–1476.

Stadtman, E. R., and Berlett, B. S. (1997). Reactive oxygen-mediated protein oxidation in aging and disease. Chem. Res. Toxicol. *10*, 485-494.

Stamler, J. S., Simon, D. I., Osborne, J. A., Mullins, N. E., Jaraki, O., Michel, T., Singel, D. J., and Loscalzo, J. (1992). S-Nitrosylation of proteins with nitric oxide: synthesis and characterization of biologically active compounds. Proc. Natl. Acad. Sci. USA *89*, 444–448.

Steinacher, R., and Schär, P. (2005). Functionality of Human Thymine DNA Glycosylase Requires SUMO-Regulated Changes in Protein Conformation. Functionality of human thymine DNA glycosylase requires SUMO-regulated changes in protein conformation. Curr. Biol. *15*, 616–623.

Sugarman, B. (1983). Zinc and infection. Rev. Infect. Dis. *5(1)*, 137-147.

Tagwerker, C., Flick, K., Cui, M., Guerrero, C., Dou, Y., Auer, B., Baldi, P., Huang, L., and Kaiser, P.A. (2006). A tandem affinity tag for two-step purification under fully denaturing conditions: application in ubiquitin profiling and protein complex identification combined with *in vivo* cross-linking. Mol. Cell Proteomics *8*, 366–378.

Taylor, S. V., Kelleher, N. L., Kinsland, C., Chiu, H.-J., Costello, C. A., Backstrom, A. D., McLafferty, F. W., and Begley, T. P. (1998). Thiamin biosynthesis in Escherichia coli. Identification of ThiS thiocarboxylate as the immediate sulfur donor in the thiazole formation. J. Biol. Chem. *273*, 16555–16560.

Thompson, D. M., and Parker, R. (2009). The RNase Rny1p cleaves tRNAs and promotes cell death during oxidative stress in *Saccharomyces cerevisiae*. J. Cell. Biol. *185(1)*, 43-50.

Tükenmez, H., Xu, H., Esberg, A., and Byström, A. S. (2015). The role of wobble uridine modifications in +1 translational frameshifting in eukaryotes. Nucleic Acids Research *43(19)*, 9489–9499.

Vashist, S., and Ng, D. T. Misfolded proteins are sorted by a sequential checkpoint mechanism of ER quality control. (2004). J. Cell. Biol.*165 (1)*, 41–52.

van der Veen, A. G., Schorpp, K., Schlieker, C., Buti, L., Damon, J. R., Spooner, E., Ploegh, H. L., and Jentsch, S. (2011). Role of the ubiquitin-like protein Urm1 as a noncanonical lysine-directed protein modifier. Proc. Natl. Acad. Sci. USA *108(5)*, 1763–1770.

Wang, C., Xi, J., Begley, T. P., and Nicholson, L. K. (2001). Solution structure of ThiS and implications for the evolutionary roots of ubiquitin. Nat. Struct. Biol. *8*, 47–51.

Wang, Z., Feng, L. S., Matskevich, V., Venkataraman, K., Parasuram, P., and Laity, J. H. (2006). Solution structure of a Zap1 zinc-responsive domain provides insights into metalloregulatory transcriptional repression in Saccharomyces cerevisiae. J. Mol. Biol. *357*, 1167–1183

Wang, F., Liu, M., Qiu, R., and Ji, C. (2011). The dual role of ubiquitin-like protein Urm1 as a protein modifier and sulfur carrier. Protein Cell *2(8)*, 612-619.

Wang, Z., Li, H., Guan, W., Ling, H., Wang, Z., Mu, T., Shuler, F. D., and Fang, X. (2010). Human SUMO fusion systems enhance protein expression and solubility. Protein Expr Purif. *73(2)*, 203-8.

Waters, B. M., and Eide, D. J. (2002). Combinatorial Control of Yeast FET4 Gene Expression by Iron, Zinc, and Oxygen. J. Biol. Chem. *277*, 33749–33757.

Wiborg, O., Pedersen, M. S., Wind, A., Berglund, L. E., Marcker, K. A., and Vuust, J. (1985). The human ubiquitin multigene family: some genes contain multiple directly repeated ubiquitin coding sequences. EMBO J. *4*, 755–759.

Wilkinson, K. D. (1997). Regulation of ubiquitin-dependent processes by deubiquitinating enzymes. FASEB J. *11*, 1245-1256.

Wu, C. Y., Bird, A. J., Winge, D. R., and Eide, D. J. (2007). Regulation of the Yeast TSA1 Peroxiredoxin by ZAP1 Is an Adaptive Response to the Oxidative Stress of Zinc Deficiency. J. Biol. Chem. *282*, 2184 –2195.

Wu, C. Y., Bird, A. J., Chung, L. M., Newton, M. A., Winge, D.R., and Eide, D. J. (2008). Differential control of Zap1-regulated genes in response to zinc deficiency in *Saccharomyces cerevisiae*. BMC Genomics *9*, 370.

Wu, C. Y., Roje, S., Sandoval, F. J., Bird, A. J., Winge, D. R., and Eide, D. J. (2009). Repression of sulfate assimilation is an adaptive response of yeast to the oxidative stress of zinc deficiency. J. Biol. Chem. *284(40)*, 27544–27556.

Xi, J., Ge, Y., Kinsland, C., McLafferty, F. W., and Begley, T. P. (2001). Biosynthesis of the thiazole moiety of thiamin in Escherichia coli: identification of an acyldisulfide-linked protein-protein conjugate that is functionally analogous to the ubiquitin/E1 complex. Proc. Natl. Acad. Sci. USA *98(15)*, 8513-8518.

Xu, J., Zhang, J., Wang, L., Zhou, J., Huang, H., Wu, J., Zhong, Y., and Shi, Y. (2006). Solution structure of Urm1 and its implications for the origin of protein modifiers. Proc. Natl. Acad. Sci. USA *103(31)*, 11625-11630.

Xu, P., Duong, D. M., Seyfried, N. T., Cheng, D., Xie, Y., Robert, J., Rush, J., Hochstrasser, M., Finley, D., and Peng, J. (2009). Quantitative proteomics reveals the function of unconventional ubiquitin chains in proteasomal degradation. Cell *137*, 133–145.

Yamaguchi-Iwai, Y., Ueta, R., Fukunaka, A., Sasaki, R. (2002). Subcellular localization of Aft1 transcription factor responds to iron status in Saccharomyces cerevisiae. J. Biol. Chem. *277(21)*, 18914-18918.

Yu, J., and Zhou C.-Z. (2008). Crystal structure of the dimeric Urm1 from the yeast Saccharomyces cerevisiae. Proteins *71(2)*, 1050-5.

Zhao, H., and Eide D. J. (1996). The yeast ZRT1 gene encodes the zinc transporter protein of a high-affinity uptake system induced by zinc limitation. Proc. Natl. Acad. Sci. U. S. A. *93(6)*, 2454–2458.

Zhao, H., and Eide D. J. (1996). The ZRT2 Gene Encodes the Low Affinity Zinc Transporter in *Saccharomyces cerevisiae*. J. Biol.Chem. *271*, 23203-23210.

Zhao, H., and Eide D. J. (1997). Zap1p, a metalloregulatory protein involved in zinc-responsive transcriptional regulation in Saccharomyces cerevisiae. Mol. Cell. Biol. *17(9)*, 5044-5052.

Zhao, H., Butler, E., Rodgers, J., Spizzo, T., Duesterhoeft, S., and Eide, D. (1998). Regulation of zinc homeostasis in yeast by binding of the ZAP1 transcriptional activator to zinc-responsive promoter elements. J. Biol. Chem. *273*, 28713–28720.

7 Abbreviations

%	percent
°C	celsius
µ	micro (x10-6)
µg	microgram
µl	microliter
2µ	multi-copy vectors
aa	amino acid
AAA	ATPases associated with various cellular activities
AD	transactivation domain
ATP	adenosine 5-triphosphate
BD	Gal4 DNA binding domain
bp	base pairs
BSA	bovine serum albumin
CCD	camera charged-coupled device camera
cDNA	complimentary DNA
CEN	centromeric (low copy vectors)
CHX	cycloheximide
C-terminal	carboxyl-terminal
C-terminus	carboxyl terminus
DAPI	4',6-diamidino-2-phenylindole
DBD	DNA-binding domain
DMSO	dimethylsulfoxide
DNA	deoxyribonucleic acid
dNTP	deoxy nucleoside triphosphate
DTT	dithiothreitol
DUB	deubiquitylating
E	glutamate
E1	ubiquitin activation enzyme
E2	ubiquitin conjugation enzyme
E3	ubiquitin ligase
E4	polyubiquitylation factor

EDTA	ethylenediaminetetraacidic acid
ELP	elongation protein
ER	endoplasmic reticulum
ERAD	ER-associated degradation
F	farad
g	gram
g	gravitational constant ($6.6742x10^{-11}$ N m^2 kg^{-2})
Gal	galactosidase
GFP	green fluorescence protein
GG	double glycine
Gln	glutamine
Glu	gluatamate
h	hour
H_2O_2	hydrogen peroxide
HA	human influenza hemagglutinin
Ig	immunoglobulin
IP	immunoprecipitation
IPTG	Isopropyl β-D-1-thiogalactopyranoside
K	kilo ($x10^3$)
J	Joule
K	lysine
kan	kanamycin
kb	kilo base pairs
kDa	kilo dalton
LB	Luria-Bertani
LC-MS/MS	liquid chromatography tandem mass spectrometry
Lys	lysine
LZM	limited zinc medium
M	molar
m	milli ($x10^{-3}$)
MAT	mating type
mcm^5U_{34}	5-methylcarboxymethyluridine modification at U_{34}

min	minutes
MoCo	Molybdenum cofactor
MOPS	3-N-Morpholinopropane sulfonic acid
mRNA	messenger RNA
MW	molecular weight
MS	mass spectrometry
MS/MS	tandem mass spectrometry
n	nano ($x10^{-9}$)
NEM	N-ethylmaleimide
NH_2OH	hydroxylamine
Ni-NTA	nickel–nitrilotriacetic acid
nm	nanometer
nt	nucleotide
ADP	adenosine 5-diphosphate N-terminal amino-terminal
N-terminal	amino terminal
N-terminus	amino terminus
OD	optical density
ORF	open reading frame
PAGE	polyacrylamide gel electrophoresis
PBS	phosphate-buffered saline
PCR	polymerase chain reaction
PEG	polyethylene glycol
PIC	protease inhibitor cocktail
PMSF	phenylmethylsulphonyl fluoride
PTM	post-translational modification
PVDF	polyvinylidene fluoride
Q	glutamine
qRT-PCR	reverse transcription quantitative PCR
RNA	ribonucleic acid
rpm	rounds per minute
ROS	reactive oxygen species
RT	room temperature

RT-qPCR	reverse transcriptase quantitative polymerase chain reaction
RLD	rhodanese-like domain
s	seconds
S	sedimentation coefficient (Svedberg)
SAMP	small archaeal ubiquitin-like modifier protein
SC	synthetic complete
SDS	sodium dodecylsulfate
SILAC	stable isotope labeling with amino acids in cell culture
s^2U_{34}	thio-modification of U_{34}
SUMO	small ubiquitin-like modifier
TAP	tandem affinity purification
TBE	Tris/borate/EDTA buffer
t-BOOH	tert-butyl hydroperoxide
TBS	Tris-buffered saline
TCA	trichloro acidic acid
TEMED	N,N,N',N'-tetramethylethylenediamin
Tris	Tris(hydroxymethyl)aminomethane
tRNA	transfer RNA
U	unit
U_{34}	wobble uridine at 34^{th} position in tRNA
Ub	ubiquitin
UBA	ubiquitin associated
UBC	ubiquitin-conjugating enzyme
UBD	ubiquitin-binding domain
UBL	ubiquitin-like protein
ULP	ubiquitin-like processing enzyme
UPS	ubiquitin/proteasome system
Urm1	ubiquitin-related modifier 1
UV	ultraviolet light
V	volt
v/v	volume per volume
w/v	weight per volume

WT	wild type
YPD	yeast bactopeptone dextrose medium
Y2H	yeast-two hybrid
ZF	zinc finger
Zn	zinc
ZRE	zinc-responsive element
Ω	ohm

Acknowledgements

I would like to express my sincere gratitude to late my PhD supervisor Stefan Jentsch for his support and guidance in professional and personal matters. It was an honor meeting him and will be dearly missed as brilliant scientist and as a friend.

Moreover, I would like to thank my PhD supervisor Daniel Krappmann, who kindly accepted me as his PhD student and Prof. Dr. Angelika Böttger as my co-referee. I would also like to thank all the members of the thesis committee, who cordially agreed to referee my thesis.

I would also thank Kenji, Lucas, Tim and Boris for critical reading of this thesis. In particular, I would like to express my sincere gratitude Boris and Kenji for their tremendous support in the last months of my thesis. I am grateful to Cyril Boulègue for his great support in the mass spectrometry analyses throughout my work. In addition I would like to thank Dirk, Jochen, Sven, Ulla, Klara and Massimo for their great help in the lab and outside the lab. In addition, I would like to thank Kenji for his guidance in the beginning of my PhD. Jörg, Tim, Alex, Ben, Claudio, Frank, Ivan, Flo, Sven, Jochen, Dirk, Ivan, Matias and Annamaria for the great atmosphere in the lab.

I would like to thank my mum and Greg for their endless support throughout my life. Finally, I would like to thank Barbara for your unwaveringly support and endless patience.

Curriculum Vitae

Personal Data

Name	Sean Tzu-Hsiang Lin

Education

08/2010 – 12/2017	**PhD studies** at the Max Planck Institute of Biochemistry, Department of Molecular Cell Biology, Germany PhD thesis: *"Role of the ubiquitin-like protein Urm1 as a protein modifier"* Supervisor: Prof. Dr. S. Jentsch, MPI of Biochemistry, Martinsried
10/2007 – 03/2010	**Diploma** in Biology, Heinrich-Heine Universität Düsseldorf, Germany
03/2009 – 12/2009	Diploma thesis: "Identifikation und Charakterisierung von Ftm-Domänen-spezifischen Interaktionspartnern" Supervisor: Prof. Dr. U. Rüther, Animal Developmental and Molecular Biology, Heinrich-Heine Universität, Düsseldorf, Germany
10/2005 – 08/2007	**Intermediate diploma** in Biology at Heinrich-Heine Universität Düsseldorf, Germany